The Dissertation Committee for Michael Pikulski Certifies that this is the approved version of the following dissertation:

Characterization and Isomer Differentiation of Glycosides and Oligosaccharides Using Chemical Derivatization with Quadrupole Ion Trap Mass Spectrometry

Committee:

Jennifer S. Brodbelt, Supervisor

James A. Holcombe

David A. Vanden Bout

Kimberly Kline

Bob G. Sanders

Characterization and Isomer Differentiation of Glycosides and Oligosaccharides Using Chemical Derivatization with Quadrupole Ion Trap Mass Spectrometry

by

Michael Pikulski, B.S.; M.S.

Dissertation

Presented to the Faculty of the Graduate School of

The University of Texas at Austin

in Partial Fulfillment

of the Requirements

for the Degree of

Doctor of Philosophy

The University of Texas at Austin

December 2007

Dedication

This work is dedicated to my father,

Bernard Michael Pikulski

Characterization and Isomer Differentiation of Glycosides and Oligosaccharides Using Chemical Derivatization with Quadrupole Ion Trap Mass Spectrometry

Publication No._____

Michael Pikulski, Ph.D.

The University of Texas at Austin, 2007

Supervisor: Jennifer S. Brodbelt

Several innovative tandem mass spectrometric strategies have been developed for the structural determination and isomer differentiation of glycosides and oligosaccharides. Specifically, collisionally activated dissociation (CAD) and infrared multiphoton dissociation (IRMPD) are used in conjunction with derivatization methods designed to exploit variations in binding energies or attach chromophores. These include metal complexation incorporating modified neutral auxiliary ligands and covalent derivatization involving site-specific reactions.

The elucidation of flavonoid isomers is accomplished by electrospray ionization tandem mass spectrometry (ESI-MS/MS) via formation and CAD of metal/flavonoid complexes containing an auxiliary ligand. Addition of a metal salt and a suitable neutral auxiliary ligand to flavonoids in solution results in the formation of [M(II) (flavonoid-H) ligand]$^+$ complexes by ESI which, upon collisional activated dissociation, often result in more distinctive fragmentation patterns than observed for conventional protonated or deprotonated flavonoids. We compare and explore the use of alternative pyridyl ligands, with electron-releasing substituents including 4,7-diphenyl-1,10-phenanthroline. Using this technique, three groups of flavonoid glycoside isomers are differentiated, including glycosides of apigenin, quercetin and luteolin.

A tunable ESI-MS/MS strategy for differentiation of flavone and flavanone diglycoside isomers based on metal complexation with auxiliary ligands that have electron-withdrawing substituents is reported. A series of auxiliary ligands with electron-withdrawing substituents was synthesized in order to tailor the relative metal binding affinities of the ligands and thus directly influence the stabilities, and consequently the dissociation pathways, of the complexes. Upon collisionally activated dissociation, the complexes yield fragmentation patterns in which the abundances of key diagnostic ions are enhanced, thus facilitating isomer differentiation.

A strategy for increasing the efficiency of IRMPD in a quadrupole ion trap (QIT) based on another metal complexation strategy is described. Two IR-active ligands (IRALs) that have an IR-active phosphonate functional groups were synthesized. The IR-active groups were therefore incorporated into the analyte complexes via metal complexation. We demonstrate this new IRMPD approach for the structural characterization of flavonoids. The fragment ions obtained by IRMPD are similar to those obtained by CAD and allow facile isomer differentiation of flavonoids. Fourier

transform infrared absorption attenuated total reflectance (FTIR-ATR) and energy-variable CAD experiments indicate that the high IRMPD efficiencies stem from the very large IR absorptivities of the IR-active ligands.

A simplified method for determining the sequence and branching of oligosaccharides using IRMPD in a QIT is described. An IR-active boronic acid (IRABA) reagent was synthesized and subsequently used to derivatize the oligosaccharides prior to IRMPD analysis. The IRABA ligand is designed to both enhance the efficiency of the derivatization reaction and to facilitate the photon absorption process. The resulting IRMPD spectra display oligosaccharide fragments that are formed from primarily one type of diagnostic cleavage, thus making sequencing straightforward. The presence of sequential fragment ions, a phenomenon of IRMPD, permit the comprehensive sequencing of the oligosaccharides studied in a single stage of activation. The approach is demonstrated for two series of oligosaccharides, the lacto-N-fucopentaoses (LNFPs) and the lacto-N-difucohexaoses (LNDFHs).

Table of Contents

Chapter 1: Introduction

1.1 INTRODUCTION

Carbohydrates are often attached to biologically important compounds including phytochemicals, lipids, peptides and proteins.[1-6] The carbohydrate segment of the resulting glycoconjugates often affects the tertiary structure and activity of these compounds, thus participating in both architectural and biorecognitive roles. For example, the position and type of single sugar moieties has been shown to dramatically affect the uptake and activity of glycosylated flavonoids in rats.[7, 8] In addition, the carbohydrate portions of protein and lipid glycoconjugates specifically contribute to the resulting conformations, the reactivities, and chemical role in numerous biological processes. Oligosaccharides are known to play roles in cell-cell signaling, cellular differentiation, regulation of biochemical pathways, viral replication, parasitic infection, immune response and inflammation.[9-15.]

Glycoconjugates have two major segments known as the aglycon (the non-sugar part of the molecule) and the glycan (sugar-containing part). While the aglycon may be almost any chemical structure, naturally occurring glycans most commonly consist of the monosaccharide units depicted in Figure 1-1.

Complete structural analysis of the glycan portions is complex since they are often highly branched and have several different linkage types between their fundamental monosaccharide units. Some of the simplest glycoconjugates may have only one or two monosaccharide units attached but more complicated types may have as many as 200.

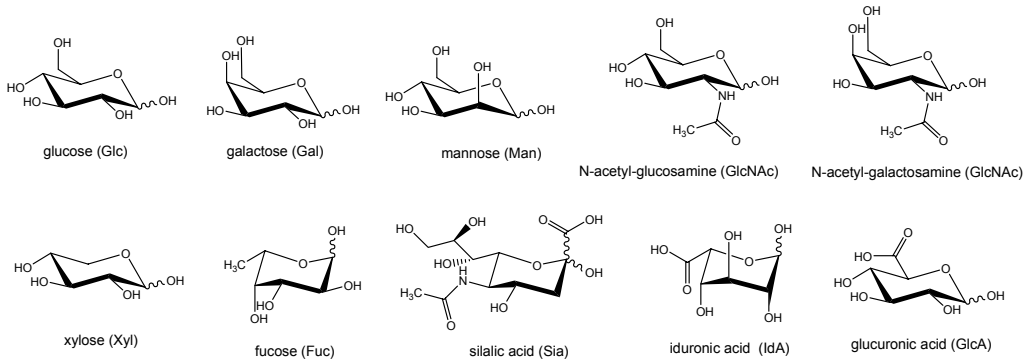

Figure 1-1. The biologically important monosaccharide units.

As depicted in Figure 1-1, even a simple monosaccharide such as glucose has four chiral centers and the identity of a sugar is largely dependent upon the stereochemistry of these carbon atoms, with the exception of carbon-1 (see Figure 1-2). The cyclic forms of saccharides give rise to two different configurations, alpha and beta, that are determined by the position of the hydroxyl group at carbon-1. This carbon is known as the anomeric carbon and the two different forms are anomers of each other. When two sugars are joined to form a glycosidic bond, the anomeric carbon (carbon-1) is often part of the linkage and the anomeric configuration is one of the important determinations to be made in the analysis of oligosaccharides.

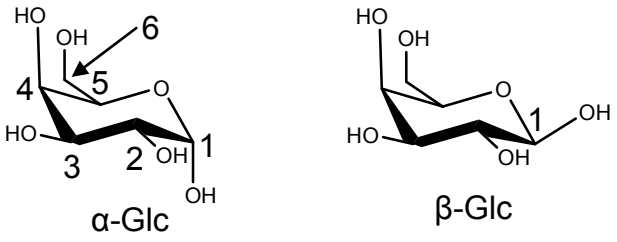

Figure 1-2. The two glucose anomers, α-Glc and β-Glc, with the carbon atoms numbered.

Another important determination to be made in the analysis of oligosaccharides is the particular linkage between monosaccharide units. One monosaccharide unit may react with another releasing a water molecule and forming a glycosidic bond. The linkage often involves the hydroxyl group attached to the anomeric carbon and any of the other carbon atoms on the adjoining monosaccharide. For example, two glucose units may be attached between the hydroxyl group of carbon-1 and the hydroxyl group of carbon-4, or between the hydroxyl group of carbon-1 and the hydroxyl group of carbon-6, each producing two different diglucosides. These linkages are clearly shown in chemical structures and the detailed names of oligosaccharides. An oligosaccharide whose characterization is described in Chapter 6 is shown in Figure 1-3. To describe the type of glycosidic bonds formed, the format includes the anomeric configuration of carbon-1, the carbon number of the first sugar and the carbon number of the second sugar separated by an arrow (Figure 1-3).

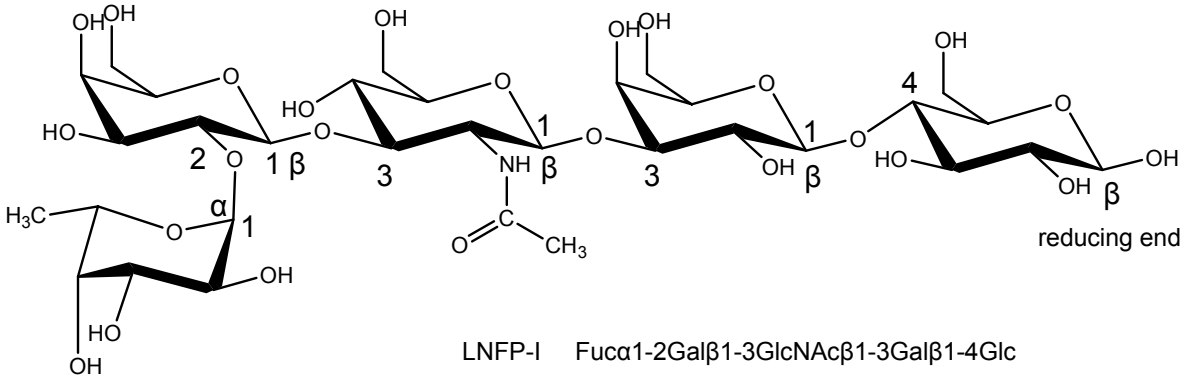

Figure 1-3. Structure of LNFP-I, detailing the anomeric configurations and linkages in the structure.

One example of a class of compounds that commonly have only one or two monosaccharide units in their glycosidic forms is the flavonoids, phytochemicals touted

for their health benefits.[16-21] Because of this relative simplicity, the glycan portion is usually analyzed attached to the aglycon. Prior to the more modern liquid chromatography/mass spectrometry (LC/MS) techniques such as those mentioned in Chapters 3 and 4, the structural analysis of flavonoid glycosides has necessitated extraction from kilograms of plant material followed by preparative LC purification to obtain milligram quantities of purified material sufficient for NMR analyses. An abundant number of preparative HPLC techniques have been developed for the isolation and purification of flavonoid glycosides.[22, 23] The detailed structural analysis of the carbohydrate portions by NMR involves the use of the more complicated two-dimensional techniques. Flavonoid glycosides have also been characterized using mass spectrometry; however, until the 1990s, techniques were limited to electron impact ionization (EI), chemical ionization (CI) and fast atom bombardment (FAB) ionization. More recently, softer ionization methods have been coupled with tandem mass spectrometry to augment the structural information obtained using mass spectrometry and they are becoming established tools.[24, 25] Recent reviews by Stobiecki[25] and Cuyckens & Claeys[24] describe much of this work. Two innovative strategies employing metal complexation are described in Chapters 3 and 4 of this dissertation.

For the analysis of more complex glycoconjugates, the glycan portion is often first chemically or enzymatically cleaved from the aglycon for characterization of the resulting oligosaccharides.[26-28] Glycoproteins and glycopeptides are examples of biologically important compounds that often fall into this category. The most popular enzyme for cleavage from proteins and peptides is PNGase (protein N-glycanase) for the cleavage of N-linked glycans. Compounds commonly used for chemical cleavage include hydrazine for N-linked glycans and sodium borohydride for O-linked glycans. Following cleavage of the glycan portion, the resulting oligosaccharides are then

characterized independent of the aglycon. Oligosaccharides are in many ways more structurally complex than other biologically important molecules such as proteins and nucleic acids in that they are often highly branched and have several different linkage types between their fundamental monosaccharide units. In fact, for a single hexasaccharide, there are 10^{12} possible isomers.[29] This results in a great number of structural possibilities that make characterization of oligosaccharides a challenging task.

Following cleavage of the oligosaccharides, a chromatographic profile must be obtained to enable purification of the components since even one glycosylation site may yield a complex mixture of glycans. The individual oligosaccharides are then commonly analyzed for sequence, linkage types and anomeric configuration of each glycosidic bond using enzymatic analyses, high performance liquid chromatography (HPLC), lectin-specific binding, NMR and mass spectrometry.[3, 26, 27]

Enzymatic analysis is commonly used to determine the presence or absence of a particular monosaccharide, glycosidic bond or motif in an oligosaccharide. In more elaborate schemes, they may be used to determine sequence information. Enzymes that cleave glycosidic bonds with a great degree of specificity are used (e.g., only cleave a particular anomeric configuration and linkage type of one monosaccharide). Numerous enzymes are sold commercially and examples include Galactosidase from *Streptococcus pneumoniae* that cleave Gal β1-4 linkages and Mannosidase from *Helix pomatia* that cleave Man β1-4 linkages.[30, 31] After these specific enzymatic cleavages, the resulting oligosaccharides are then evaluated to determine the presence of the monosaccharide unit or glycosidic bond in question. To sequence an oligosaccharide, the technique requires several enzymes used in succession. The amount of material required is dependent upon how many sequential analyses are performed and the method of detection used. To make more sense of the resulting oligosaccharides following enzymatic cleavage, the original

oligosaccharides being analyzed are commonly modified at the reducing end with a fluorescent tag that is used as a fixed reference point that can be monitored chromatographically.[32-35] The tag is usually added via reductive amination and typically involves the addition of an aromatic amine.[36-38] Examples include 8-aminonapthalene-1,3,6-trisulfonic acid (ANTS) and 7-aminomethylcoumarin (AMC). The derivatization procedure involves the heating of the oligosaccharide in acidic solvent with excess of the derivatization reagent and a reducing agent such as sodium borohydride (typical times range from 15 mins – 2 hours). The excess reagents are then typically removed using solid phase extraction (SPE). Sometimes a purification step is also required before the reduction step. While the fluorescent tag enables sensitive detection of eluting oligosaccharides, some of the most valuable information can be obtained by coupling the chromatograph to a mass spectrometer. Obtaining the masses of the eluting oligosaccharides enables a mapping strategy to be used. Depending upon the specific glycosidases and the type of chromatography used, information such as the number of monosaccharide residues removed, the skeletal structure and the linkage type of particular residues may be obtained.

In one study, Lai and Her successfully used specific enzymes to differentiate between α1-3 and α1-6 core-fucosylated glycans in bee venom.[39] The oligosaccharides were released from phospholipase A_2 (PLA) with peptide-N-glycanase A (PNGase A) and peptide-N-glycanase F (PNGase F) and labeled by reductive amination with p-aminobenzoic acid ethyl ester (ABEE). The derivatized products were then separated chromatographically using reversed phase HPLC and monitored using UV and ESI-MS. Isobaric oligosaccharides containing both of the fucose residues being studied were identified and differentiated since α1-3 fucosylation cleavage is prevented by PNGase F.[9] By using the two enzymes it was determined that were no differences in the anomeric

configuration and linkages involving these fucose moieties in the PLA oligosaccharides in the venom of bees.

In another study, Qian *et al*.[40] used an array of specific enzymes, HPLC and mass spectrometry to analyze oligosaccharides in cetuximab, a therapeutic antibody used for cancer. The oligosaccharides were released using PNGase F and were then derivatized with the fluorescent tag anthranilic acid via reductive amination. The tagged oligosaccharides were then purified using SPE. Next, normal phase HPLC was used to fractionate the oligosaccharides which were then concentrated for analysis and subjected to an array of different combinations of five specific glycosidases. The digested oligosaccharides were then desalted by dialysis and analyzed using MALDI-TOF MS and MS/MS. The full scan spectra yielded a species profile of the oligosaccharides that was used in conjunction with the MS/MS data to identify 21 distinct oligosaccharide structures and in some cases obtained complete sequence information.

Another strategy utilizes lectins, proteins that bind to oligosaccharides with a high degree of specificity, for structural determination. They may bind to specific monosaccharide units or structural motifs. Lectins may be used for column fractionation of oligosaccharides after release from glycoproteins[27, 41] or in microarrays for more specific glycoprofiling of fractionated oligosaccharides and more recently whole glycoconjugates or even whole cells,[42-45] although the analysis of glycoproteins and cells is more applicable to detecting only changes in glycosylation. The most common experiment involves the use of lectins with binding specificity for a particular disaccharide unit or larger structural motif that are used to test for the presence of that unit in an unknown, often as a mode of separation. One of the most popular methods for immobilizing lectins for column chromatography is the linkage of lectins to agarose gel using a cyanogen bromide method[46, 47] with a linear polyacrylic hydrazide spacer[48] for

increased column stability and performance. One example of a lectin used for immobilized affinity chromatography is *Aleuria aurantia lectin* (AAL) from mushrooms.[49] The lectin is commercially available in a recombinant form produced by *E. coli* with the same properties[50] and may be used to determine the presence or absence of an α-Fuc residue at a particular position in the core of an oligosaccharide and may therefore be separated from their nonfucosylated derivatives. In one procedure, radioactive oligosaccharides are dissolved in buffer and loaded on the column and allowed to stand for 30 mins.[51] Chromatography is then initiated at a flow rate of 12 mL/hr and 1 mL fractions are collected and the radioactivity measured. Only oligosaccharides with a non-fucosylated core pass through the column without interaction. Addition of L-fucose to the column is required to elute the oligosaccharides with a fucosylated core. Another variation involves the affinity chromatography of oligosaccharides labeled with a fluorescent tag which eliminates the need for radioactive samples.

In one study, Madrid *et al*. used a series of lectins and enzymatic analyses to characterize N- and O-linked oligosaccharides in human goblet cells.[52] Interactions between the oligosaccharides and lectins, and the presence of particular mono- and disaccharides was determined using a lectin staining procedure and microscopy. The oligosaccharides were released from some proteins and this data was compared to the data obtained for the corresponding glycoconjugates. It was determined that there was masking of the data for unreleased oligosaccharides. The presence of specific monosaccharide and disaccharide units, in some cases including linkage information was determined.

NMR provides a vast amount of information about the structures of oligosaccharides including linkage types and anomeric configuration; however it requires

milligram quantities of purified sample.[53, 54] If there is sufficient sample, it is often the first type of analysis performed since it is a nondestructive technique. Overall, one-dimensional NMR methods are not sufficient for stereochemical information of oligosaccharides and there is no systematic method for structural determination because of its limitations. ^{1}H NMR Nuclear Overhauser effect (NOE) experiments can help to determine linkage and sequence; however, there is substantial overlap of multiplets in an important region of the spectra that results in ambiguity of assignments. ^{13}C NMR spectra have few overlapping lines; however, the chemical shift differences of the ring carbons are small and difficult to assign. Two-dimensional NMR, where both the x- and y-axes contain chemical shift information, has helped to overcome several of these difficulties. For example, two-dimensional shift correlation spectroscopy (COSY) enables the identification of all the protons in a sugar residue. Briefly, an anomeric proton resonance is assigned and spins are correlated in a stepwise manner around the ring. For identification of the sugars, vicinal coupling constants of all ring protons is also needed. Other useful two-dimensional techniques include total correlation spectroscopy (TOCSY), relayed correlation spectroscopy (RELAY) and Homonuclear Hartmann-Hahn spectroscopy (HOHAHA). To characterize an oligosaccharide using NMR often requires a combination of NMR experiments, most of which require a great deal of technical expertise to analyze. In one study, Vanhaecke *et al*. used five different NMR techniques to fully characterize lychnose, a tetrasaccharide produced by *Stellaria media*.[55] In another study, Urai, *et al*. used seven different NMR techniques to characterize an oligosaccharide produced by a marine bacterium.[56]

Mass spectrometry is another powerful instrumental technique that provides detailed information about oligosaccharides.[57-61] In addition to revealing the exact mass of an unknown oligosaccharide, it can be used for compositional information. In fact, the

most popular method for linkage determination is a methylation derivatization in conjunction with mass spectrometry.[62] There are a number of established methylation procedures; however, because of the high consumption of sample for this derivatization technique (methylation, glycosidic cleavage and derivatization followed by sample cleanup), alternative techniques for linkage determination are desirable. Mass spectrometry has also been widely used in conjunction with enzymatic analysis, as mentioned previously in the paragraph discussing enzymatic analyses. Soft ionization techniques such as fast atom bombardment (FAB), matrix assisted laser desorption ionization (MALDI) and electrospray ionization (ESI) are the preferred methods since they do not lead to fragmentation of the molecular ion.[57-60, 63-65] Of these, ESI has been the most popular because of its amenability to HPLC. Low-energy activation methods can then be used to fragment the molecular ion in a controlled fashion and promote cleavage at primarily glycosidic bonds, thus providing sequence information.[64-71] Additionally, in some types of instruments, a fragment ion may be selected for further analysis (MS^n).[58, 64, 65, 67, 71, 72] A significant amount of research has been dedicated to the analysis of oligosaccharides, and Zaia has published a recent review.[60]

A systematic nomenclature for the fragmentation of oligosaccharides that was developed by Domon and Costello[36] has become established and a diagram is shown in Figure 1-4. Ions that have the charge retained at the reducing end are designated X, Y, and Z. They are labeled using the format ${}^{k,l}X_j$, Y_j and Z_j, where j is the number of the bond broken starting with 0, and k and l indicate the bonds broken from cross-ring cleavages of the sugar. Ions that have the charge retained at the non-reducing end are designated A, B, and C. They are labeled using the format ${}^{g,h}A_i$, B_i and C_i, where i is the number of the bond broken, counting from the terminal sugar beginning with 1, and g and h indicate cross-ring cleavages of the sugar. For branched oligosaccharides, an additional

notation is included that indicates the branch. They are labeled with Greek letters starting at the largest branch and ending with the smallest branch.

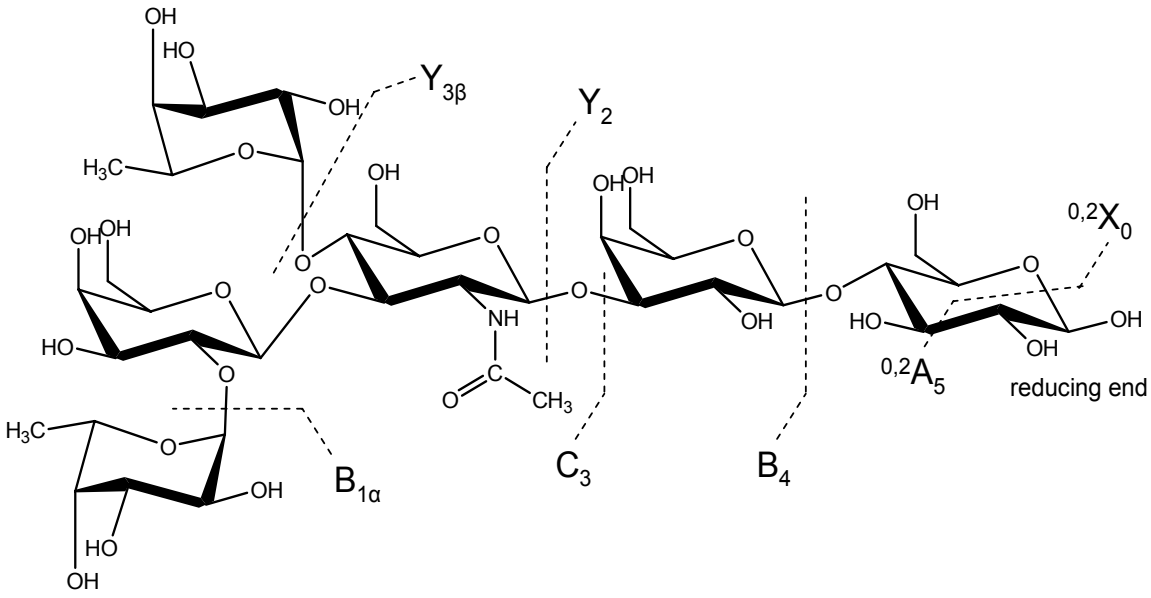

Figure 1-4. Example of nomenclature for oligosaccharide fragment ions.

Mass spectrometers that have the capability of trapping ions such as the QIT and Fourier transform ion trap mass spectrometer (FTICR) are ideal for elaborate structural analysis since they are designed for multiple stages of ion isolation, activation and mass analysis (several stages of tandem mass spectrometry, or MS^n). Because of its affordability, ruggedness, ease of use and small size, the QIT has been the most popular of the trapping instruments. For these reasons, the work presented in this dissertation describes novel methods for the analysis of glycosides and glycans utilizing tandem mass spectrometry in the QIT. In addition to analysis of the conventional positive and negative ions formed, several unique methods of chemical derivatization are described that

dramatically enhance the characterization and isomer differentiation of the model compounds studied.

Chapters 5 and 6 compare and contrast tandem mass spectral data obtained from collisionally activated dissociation (CAD) and infrared multiphoton dissociation (IRMPD). There are several advantages to using IRMPD over CAD in an ion trap, and they are pointed out in the following sections and throughout this dissertation. Since the use of IRMPD and its advantages are correlated with the operation of the ion trap, this is discussed in the following sections.

1.2 THE QUADRUPOLE ION TRAP MASS SPECTROMETER

1.2.1 Ion Formation and Injection

Historically, several different ionization sources have been used in conjunction with the QIT including electron ionization (EI), chemical ionization (CI), matrix assisted laser desorption ionization (MALDI) and electrospray ionization (ESI). For the research presented in this dissertation, ESI was the source used for the work presented. The advantages of using ESI rather than the other common ionization sources are presented at the beginning of each chapter, detailed for each specific analyte type. ESI is the most versatile of the techniques largely due to its amenability to high performance liquid chromatography (HPLC). Moreover, ESI is a soft ionization process that does not cause decomposition of analytes. As a result, tandem mass spectrometry can be utilized to study the structure of the intact analyte ions.

The first use of ESI with a mass spectrometer was reported by Fenn *et al.*[73] Since ESI requires little sample preparation and operates at atmospheric pressure, it is comparatively inexpensive and easy to operate since sample changes are made outside of the vacuum chamber. For ESI, a solution of the analyte is pumped through a needle to

which a high voltage is applied. Typical experimental conditions for this process are 10 μM analyte solutions pumped at 5 μL/min with a needle voltage of ~4 – 4.5 kV. Positive ions are formed by applying a positive voltage to the electrospray needle, and negative ions are formed by applying a negative voltage.

Charged droplets are formed at the needle tip and a potential difference between the needle and the front plate of the mass spectrometer guides charged droplets into the front aperture of the mass spectrometer into a heated capillary (Figure 1.3). Upon exit from the needle and continuing to inside the heated capillary, the charged droplets are reduced to desolvated ions. After formation of desolvated ions, they are guided into the entrance endcap of the ion trap through a series of focusing lenses.

Several theories involving the electrospray mechanism have been proposed, and there are two major models for the production of desolvated ions known as the charged residue model and the ion evaporation model.[74-77] As the highly charged droplets undergo desolvation and fission events (Coulombic explosions), they become smaller and smaller due to greater charge repulsion. It is in the latest stages of the production of the desolvated ions where the two models differ. The charged residue model focuses on the evaporation of the last solvent molecules so that the analyte is left desolvated and carries the charge from the final droplet. The ion evaporation model focuses on expulsion of the charged analyte from the smaller droplets due to the great Coulombic repulsions formed. There is evidence for both of these models and the electrospray process is probably best described as a combination of the two.

1.2.2 The Quadrupole Ion Trap

The core of a QITMS consists of two endcap electrodes and a central ring electrode that define the trapping area (Figure 1-5). The ions formed in the source region are guided into the trapping area through holes in the entrance endcap electrode. An ac

voltage with a frequency in the rf, known as the trapping voltage (V), is applied to the ring electrode and the endcap electrodes are held at ground. This creates a trapping field for ions. The periodic motion of the ions in this trapping field is related to the V applied and is called the secular frequency. Ion motion in the direction of the ring electrode is called the radial direction (r_0) and ion motion in direction of the endcap electrodes is called the axial direction (z_0). QITs are operated with a background He gas in the 10^{-3} Torr range. The purpose of this gas is to cool the ions and keep them closer to the center of the trap, resulting in the most optimal resolution and sensitivity during mass analysis.[78]

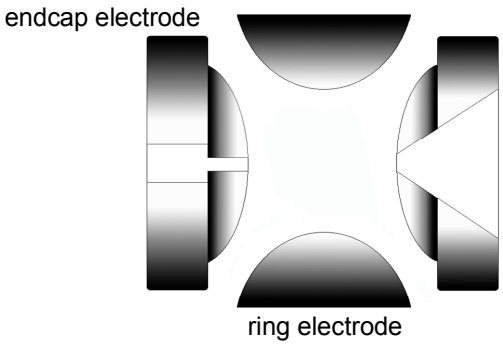

Figure 1-5. Diagram of the quadrupole ion trap (QIT).

1.2.3 Tandem Mass Spectrometry

Tandem mass spectrometry is one of the most powerful techniques to obtain structural information about a compound. The most common experiment involves the formation of an intact ion using a soft ionization source, isolation of the intact ion from the other species that may be formed in the source using an ion ejection technique, activation (fragmentation) of the intact ion and finally detection of the product ions formed. A fragment ion of interest may be further isolated and activated, known as MS/MS/MS or MS^3. The process may be repeated as long as the ion population is sufficient (MS^n).[79] Multiple stages of MS often reveal enough information for

determination of a fragmentation pathway that may better elucidate the structural details of a compound. For the research presented in this dissertation, two methods of activation, collisionally activated dissociation (CAD) and infrared multiphoton dissociation (IRMPD), are used in a quadrupole ion trap instrument and are compared for glycosides (flavonoid diglycosides) and glycans (oligosaccharides).

1.2.3.1 Collisionally Activated Dissociation (CAD)

The goal of CAD is to increase the internal energies of ions through collisions with the background He gas which ultimately results in dissociation. CAD is a well established technique in the QIT.[80-83] When CAD is performed, ions at the m/z of interest are isolated and then their kinetic energies are excited by application of an ac voltage across the endcap electrodes at the frequency of the ions' motion. When excited, the ions undergo collisions with the neutral background He gas. During the collisions, there is a conversion of kinetic energy to internal energy. Multiple collisions result in an increase in internal energy that is great enough to break bonds in the isolated ions (approximately 5-10 eV). Typically hundreds of low energy collisions occur resulting in a range of energy deposition and allowing several competing dissociation processes. A drawback is that the ion population may also be reduced by scattering during collision.

For successful CAD it is necessary to increase the kinetic energy of the ions for energetic collisions without causing ejection from the trap. Increasing the rf trapping voltage results in a more efficient trapping efficiency and allows for a significant increase in the supplementary voltage applied to the endcaps, yielding higher energy deposition during CAD. However, increasing the rf trapping voltage also raises the so-called low mass cutoff in which low m/z ions cannot be trapped. Thus, there is a compromise between ion stability, the low mass cutoff, and energy deposition during CAD. Usually the rf trapping voltage is set so the low mass cutoff is approximately one-third the mass

of the parent ion, giving a reasonable tradeoff between satisfactory energy deposition and loss of low m/z information.

1.2.3.2 Infrared Multiphoton Dissociation (IRMPD)

IRMPD is a technique in which the internal energies of the isolated ions are increased by absorption of low energy photons.[84] In this case, the ions absorb many photons until the internal energy is increased to a point where dissociation takes place.[85] Therefore, like CAD, IRMPD results in low energy fragmentation pathways. Because IRMPD does not require the use of a collision gas, it has been very successful as an alternative to CAD in FTICR mass spectrometers.[86-94]

IRMPD is emerging as a versatile ion activation method for QITs.[95-113] There are clear advantages to IRMPD over CAD in a QIT that include elimination of the low mass cutoff, no ion losses due to scattering and the formation of secondary fragment ions. Since IRMPD does not require the resonant excitation that CAD does, it is not necessary to increase the rf trapping voltages and thus the low mass cutoff problem is eliminated. Therefore, lower mass fragment ions that were lost in CAD may be observed and may provide valuable structural information. Also, since IRMPD is not a collision based technique, the ion losses from scattering after collision with the bath gas are not an issue, resulting in higher overall ion populations. Since IR absorption is a non-selective process, primary fragment ions may also absorb IR photons, gain energy, and dissociate into secondary fragment ions. The result is that primary and secondary ions are observed from one stage of dissociation. While these fragment ions occasionally complicate the spectra, they often provide additional structural information without the requirement of multiple stages of activation.

Since the QIT operates at a higher pressure compared to the FTICR, a problem associated with IRMPD is collisional cooling with the bath gas after irradiation with

photons. Collisional cooling often occurs at a faster rate than absorption of photons resulting in efficient dissociation. This shortcoming has been compensated for by heating the bath gas,[105, 114] using CAD-assisted IRMPD,[108] using a pulsed gas introduction method,[107] or optimization of the bath gas pressure between the accumulation and dissociation timeframes.[109] However, the performance of the QIT is compromised. It has been shown by a few groups that the IRMPD efficiencies of compounds containing phosphate functional groups are superior to that of non-phosphorylated compounds.[90, 96-98, 115] In some of the research presented in this dissertation, similar IR-active functional groups have been deliberately attached to analytes using chemical derivatization to increase their IRMPD efficiencies.

1.3 OVERVIEW OF CHAPTERS

Chapter 2 describes the experimental parameters for the research presented in this dissertation. The instrumentation used is described and sample preparation details are provided.

Chapters 3 and 4 describe the isomer differentiation of flavonoid diglycosides using a metal complexation strategy with an emphasis on characterization of the glycan moiety. In addition to the metal, the methods employ the complexation of a neutral pyridyl auxiliary ligand. In Chapter 3 the ligands are modified electron-releasing functional groups and in Chapter 4 the ligands are modified electron-withdrawing functional groups.

Chapter 5 presents the modification of analytes with neutral auxiliary ligands that have IR-active functional groups to increase the efficiency of photon absorption by IRMPD. The metal complexation strategy with flavonoid diglycosides is used as a model for the method.

Chapter 6 explores a chemical derivatization strategy for oligosaccharides by using a reagent with an IR-active group to increase the photon absorption efficiency. A modified boronic acid is used to derivatize oligosaccharides and the method is used for isomer differentiation and sequencing of the analytes.

Chapter 7 presents the synthetic methods employed for ligands with electron-withdrawing groups in Chapter 4 and IR-active functional groups in Chapter 5. In addition, the synthesis of the modified boronic acid used in Chapter 6 is described.

1.4 REFERENCES

1. Fukuda, M.; Hindsgaul, O. *Molecular and Cellular Glycobiology*; Oxford University Press: Oxford, 2000.

2. Hermann, K. *J. Food Technol.* **1976**, *11*, 433-448.

3. Varki, A.; Cummings, R.; Esko, J.; Freeze, H.; Hart, G.; Marth, J. *Essentials of Glycobiology*, First ed.; Cold Spring Harbor Laboratory Press: Cold Spring Harbor, NY, 1999.

4. Kobata, A. In *Biology of Carbohydrates*; Ginsburg, V., Robbins, P. W., Eds.; Wiley: New York, 1984; Vol. 2, pp 87-162.

5. Rademacher, T. W.; Parekh, R. B. *Annu. Rev. Biochem.* **1988**, *57*, 785-838.

6. Wink, M. *Functions of Plant Secondary Metabolites and their Exploitation in Biotechnology*; Sheffield Press, 1999.

7. Murota, K.; Mitsukuni, Y.; Ichikawa, M.; Tsushida, T.; Miyamoto, S.; Terao, J. *J. Agric. Food Chem.* **2004**, *52*, 1907-1912.

8. Arts, I.; Sesink, A.; Faassen-Peters, M.; Hollman, P. *Br. J. Nutr.* **2004**, *91*, 841-847.

9. Varki, A. *Glycobiology* **1993**, *3*, 97-130.

10. Linhardt, R. J.; Toida, T. *Acc. Chem. Res.* **2004**, *37*, 431-438.

11. Fannon, M.; Forsten, K. E.; Nugent, M. A. *Biochemistry* **2000**, *39*, 1434-1445.

12. Wu, Z. L.; Zhang, L.; Yabe, T.; Kuberan, B.; Beeler, D. L.; Love, A.; Rosenberg, R. D. *J. Biol. Chem.* **2003**, *278*, 17121-17129.

13. Dwek, R. A. *Chemical Reviews* **1996**, *96*, 683-720.

14. Kukuruzinska, M. A.; Lennon, K. *Crit. Rev. Oral. Biol. Med.* **1998**, *9*, 415-448.

15. Helenus, A.; Aebi, M. *Science* **2001**, *291*, 2364-2369.

16. Bors, W. H.; Michel, C. In *Flavonoids in Health and Disease*; Rice-Evans, C. A., Ed.; Marcel Dekker: New York, 1998, pp 111-136.

17. Hertog, M. G. L. *Arch. Int. Med.* **1995**, *155*, 1184-1184.

18. Knekt, P.; Jarvinen, R.; Reunanen, A.; Maatela, J. *British Medical Journal* **1996**, *312*, 478-481.

19. Pietta, P. *Flavonoids in Medicinal Plants*; Marcel Dekker: New York, 1998.

20. RiceEvans, C. A.; Miller, N. J. *Biochem. Soc. Trans.* **1996**, *24*, 790-795.

21. RiceEvans, C. A.; Miller, N. J.; Paganga, G. *Free Radical Biol. Med.* **1996**, *21*, 417-417.

22. Harborne, J. B.; Mabry, T. J. *The Flavonoids: Advances in Research*, 1 ed.; Chapman and Hall: New York, 1982.

23. Harborne, J. B. *The Flavonoids - Advances in Research since 1986*; Chapman and Hall: London, 1994.

24. Cuyckens, H.; Claeys, M. *J. Mass Spectrom.* **2004**, *39*, 461-461.

25. Stobiecki, M. *Phytochemistry* **2000**, *54*, 237-256.

26. Fukuda, M.; Kobata, A. *Glycobiology A Practical Approach*; Oxford University Press: Oxford, 1993.

27. Taylor, M. E.; Drickamer, K. *Introduction to Glycobiology*; Oxford University Press: Oxford, 2003.

28. Patel, T. P.; Parekh, R. B. *Methods Enzymol.* **1994**, *230*, 57-66.

29. Laine, R. A. *Glycobiology* **1994**, *4*, 759-767.

30. Sutton, C. W.; O'Neill, J. A.; Cottrell, J. S. *Anal. Biochem.* **1994**, *218*, 34-46.

31. Kobata, A. *Anal. Biochem.* **1979**, *100*, 1-14.

32. Yamamoto, K.; Hamase, K.; Zaitsu, K. *J. Chromatogr. A* **2003**, *1004*, 99-106.

33. Anumula, K. R. *Anal. Biochem.* **1994**, *220*, 275-283.

34. Royle, L.; Mattu, T. S.; Hart, E.; Langridge, J. I.; Merry, A. H.; Murphy, N.; Harvey, D. J.; Dwek, R. A.; Rudd, P. M. *Anal. Biochem.* **2002**, *304*, 70-90.

35. Hase, H. *Methods Enzymol.* **1994**, *230*, 225-237.

36. Domon, B.; Mueller, D. R.; Richter, W. J. *Org. Mass Spectrom.* **1994**, *29*, 713-719.

37. Kim, Y. S.; Liu, J.; Han, X. J.; Pervin, A.; Linhardt, R. J. *J. Chromatogr. Sci.* **1995**, *33*, 162-167.

38. Harvey, D. J. *J. Am. Soc. Mass Spectrom.* **2000**, *11*, 900-915.

39. Lai, C.-C.; Her, G.-R. *J. Chromatogr. B* **2001**, *766*, 243-250.

40. Qian, J.; Liu, T.; Yang, L.; Daus, A.; Crowley, R.; Zhou, Q. *Anal. Biochem.* **2007**, *364*, 8-18.

41. Osawa, T.; Tsuji, T. *Annu. Rev. Biochem.* **1987**, *56*, 21-42.

42. Angeloni, S.; Ridet, J. L.; Kusy, N.; Gao, H.; Crevoisier, F.; Guinchard, S.; Kochar, S.; Sigrist, H.; Sprenger, N. *Glycobiology* **2005**, *15*, 31-41.

43. Zheng, T.; Peelen, D.; Smith, L. M. *J. Am. Chem. Soc.* **2005**, *127*, 9982-9983.

44. Kuno, A.; Uchiyaa, N.; Koseki-Kuno, S.; Ebe, Y.; Takashima, S.; Yamada, M.; Hirabayashi, J. *Nature Methods* **2005**, 851-856.

45. Pilobello, K. T.; Krishnamoorthy, L.; Slawek, D.; Mahal, L. K. *ChemBioChem* **2005**, *6*, 985-989.

46. Cuatrecasas, P.; Anfinsen, C. B. *Methods Enzymol.* **1971**, *22*, 345-378.

47. Porath, J. *Methods Enzymol.* **1974**, *34*, 13-30.

48. Wilcheck, M.; Miron, T. *Methods Enzymol.* **1974**, *34*, 72-76.

49. Kochibe, N.; Furukawa, K. *Biochemistry* **1980**, *19*, 2841-2846.

50. Fukumori, N.; Takeuchi, T.; Hagiwara, H.; Ohbayashi, T.; Endo, N.; Kuhibe, U.; Nagata, U.; Kobata, A. *Journal of Biochemistry* **1990**, *107*, 190-196.

51. Endo, T. *J. Chromatogr. A* **1996**, *720*, 251-261.

52. Madrid, J. F.; Aparicio, R.; Saez, F. J.; Hernandez, F. *Histochem. J.* **2000**, *32*, 281-289.

53. Agrawal, P. K. *Phytochemistry* **1992**, *31*, 3307-3330.

54. Duus, J. O.; Gotfredsen, C. H.; Bock, K. *Chemical Reviews* **2000**, *100*, 4589-4614.

55. Vanhaecke, M.; Ende, W. V.; Laere, A. V.; Herdewijn, P.; Lescrinier, E. *Carbohydr. Res.* **2006**, *341*, 2744-2750.

56. Urai, M.; Yoshizaki, H.; Anzai, H.; Ogihara, J.; Iwabuchi, N.; Harayama, S.; Sunairi, M.; Nakajima, M. *Carbohydr. Res.* **2007**, *342*, 933-942.

57. Dwek, R. A. *Annu. Rev. Biochem.* **1993**, *62*, 65-100.

58. Fernandez, L. E. M. *Carbohydr. Polym.* **2007**, *68*, 797-807.

59. Harvey, D. J. *Mass Spectrom. Rev.* **1999**, *18*, 349-451.

60. Zaia, J. *Mass Spectrom. Rev.* **2003**, *23*, 161-227.

61. Park, Y.; Lebrilla, C. B. *Mass Spectrom. Rev.* **2005**, *24*, 232-264.

62. Ciucanu, I. *Anal. Chim. Acta* **2006**, *576*, 147-155.

63. Suzuki, Y.; Suzuki, M.; Ito, E.; Ishii, H.; Miseki, K.; Suzuki, A. *Glycoconjugate Journal* **2005**, *22*, 427-431.

64. Pfenninger, A.; Karas, M.; Finke, B.; Stahl, B. *J. Am. Soc. Mass Spectrom.* **2002**, *13*, 1331-1340.

65. Pfenninger, A.; Karas, M.; Finke, B.; Stahl, B. *J. Am. Soc. Mass Spectrom.* **2002**, *13*, 1341-1348.

66. Lancaster, K. S.; An, H. J.; Li, B.; Lebrilla, C. B. *Anal. Chem.* **2006**, *78*, 4990-4997.

67. Park, Y.; Lebrilla, C. B. *Mass Spectrom. Rev.* **2005**, *24*, 232-264.

68. Penn, S. G.; Cancilla, M. T.; Lebrilla, C. B. *Anal. Chem.* **1996**, *68*, 2331-2339.

69. Chai, W.; Piskarev, V.; Lawson, A. M. *Anal. Chem.* **2001**, *73*, 651-657.

70. Weiskopf, A. S.; Vouros, P.; Harvey, D. J. *Anal. Chem.* **1998**, *70*, 4441-4447.

71. Konig, S.; Leary, J. A. *J. Am. Soc. Mass Spectrom.* **1998**, *9*, 1125-1134.

72. Leavell, M. D.; Leary, J. A. *J. Am. Soc. Mass Spectrom.* **2001**, *12*, 528-536.

73. Yamashita, M.; Fenn, J. B. *J. Phys. Chem.* **1984**, *88*, 4451-4459.

74. Wilm, M.; Mann, M. *Int. J. Mass Spectrom. Ion Processes* **1994**, *136*, 167-180.

75. VanBerkel, G. J.; Zhou, F. *Anal. Chem.* **1995**, *67*, 2916-2923.

76. Gaskell, S. J. *J. Mass Spectrom.* **1997**, *32*, 677-688.

77. Fenn, J. B.; Mann, M.; Meng, C. K.; Wong, S. F.; Whitehouse, C. M. *Mass Spectrom. Rev.* **1990**, *9*, 37-70.

78. Stafford, G. C. J.; Kelley, P. E.; Syka, J. E. P.; Reynolds, W. E.; Todd, J. F. J. *Int. J. Mass Spectrom. Ion Processes* **1984**, *88*, 97-111.

79. Louris, J. N.; Brodbelt-Lustig, J. S.; Cooks, R. G.; Glish, G. L.; VanBerkel, G. J.; McLuckey, S. A. *Int. J. Mass Spectrom. Ion Processes* **1990**, *96*, 117-137.

80. McLuckey, S. A. *J. Am. Soc. Mass Spectrom.* **1992**, *3*, 599-614.

81. Louris, J. N.; Cooks, R. G.; Syka, J. E. P.; Kelley, P. E.; Stafford, G. C. J.; Todd, J. F. J. *Anal. Chem.* **1987**, *59*, 1677-1685.

82. Charles, M. J.; McLuckey, S. A.; Glish, G. L. *J. Am. Soc. Mass Spectrom.* **1994**, *5*, 1031-1041.

83. Williams, J. D.; Cooks, R. G.; Syka, J. E. P.; Hemberger, P. H.; Nogar, N. S. *J. Am. Soc. Mass Spectrom.* **1993**, *4*, 792-797.

84. Bomse, D. S.; Woodin, R. L.; Beauchamp, J. L. *J. Am. Chem. Soc.* **1979**, *101*, 5503-5512.

85. Little, D. P.; Speir, J. P.; Senko, M. W.; O'Connor, P. B.; McLaffery, F. W. *Anal. Chem.* **1994**, *66*, 2809-2815.

86. Goldberg, D.; Bern, M.; Li, B. S.; Lebrilla, C. B. *J. Proteome Res.* **2006**, *5*, 1429-1434.

87. Little, D. P.; Speir, J. P.; Senko, M. W.; Oconnor, P. B.; Mclafferty, F. W. *Anal. Chem.* **1994**, *66*, 2809-2815.

88. Meng, F. Y.; Cargile, B. J.; Patrie, S. M.; Johnson, J. R.; McLoughlin, S. M.; Kelleher, N. L. *Anal. Chem.* **2002**, *74*, 2923-2929.

89. Sannes-Lowery, K. A.; Hofstadler, S. A. *J. Am. Soc. Mass Spectrom.* **2003**, *14*, 825-833.

90. Flora, J. W.; Muddiman, D. C. *Anal. Chem.* **2001**, *73*, 3305-3311.

91. Cooper, H. J.; Heath, J. K.; Jaffray, E.; Hay, R. T.; Lam, T. T.; Marshall, A. G. *Anal. Chem.* **2004**, *76*, 6982-6988.

92. Lancaster, K. S.; Hyun Joo, A.; Bensheng, L.; Lebrilla, C. B. *Anal. Chem.* **2006**, *78*, 4990-4997.

93. Xie, Y.; Lebrilla, C. B. *Anal. Chem.* **2003**, *75*, 1590-1598.

94. Zhang, J.; Schubothe, K.; Bensheng, L.; Russell, S.; Lebrilla, C. B. *Anal. Chem.* **2005**, *77*, 208-214.

95. Wilson, J. J.; Brodbelt, J. S. *Anal. Chem.* **2006**, *78*, 6855-6862.

96. Crowe, M. C.; Brodbelt, J. S.; Goolsby, B. J.; Hergenrother, P. *J. Am. Soc. Mass Spectrom.* **2002**, *13*, 630-649.

97. Crowe, M. C.; Brodbelt, J. S. *J. Am. Soc. Mass Spectrom.* **2004**, *15*, 1581-1592.

98. Crowe, M. C.; Brodbelt, J. S. *Anal. Chem.* **2005**, *77*, 5726-5734.

99. Keller, K. M.; Brodbelt, J. S. *Anal. Biochem.* **2004**, *326*, 200-210.

100. Goolsby, B. J.; Brodbelt, J. S. *J. Mass Spectrom.* **1998**, *33*, 705-712.

101. Goolsby, B. J.; Brodbelt, J. S. *J. Mass Spectrom.* **2000**, *35*, 1011-1024.

102. Goolsby, B. J.; Brodbelt, J. S. *Anal. Chem.* **2001**, *73*, 1270-1276.

103. Shen, J.; Brodbelt, J. S. *Analyst* **2000**, *125*, 641-650.

104. Vartanian, V. H.; Goolsby, B.; Brodbelt, J. S. *J. Am. Soc. Mass Spectrom.* **1998**, *9*, 1089-1098.

105. Payne, A. H.; Glish, G. L. *Anal. Chem.* **2001**, *73*, 3542-3548.

106. Black, D. M. P., A.H.; Glish, G.L. *J. Am. Soc. Mass Spectrom.* **2006**, *17*, 932-938.

107. Boue, S. M.; Stephenson, J. L.; Yost, R. A. *Rapid Commun. Mass Spectrom.* **2000**, *14*, 1391-1397.

108. Hashimoto, Y.; Hasegawa, H.; Yoshinari, K.; Waki, I. *Anal. Chem.* **2003**, *75*, 420-425.

109. Hashimoto, Y.; Hasegawa, H.; Waki, L. *Rapid Commun. Mass Spectrom.* **2004**, *18*, 2255-2259.

110. Stephenson, J. L.; Booth, M. M.; Shalosky, J. A.; Eyler, J. R.; Yost, R. A. *J. Am. Soc. Mass Spectrom.* **1994**, *5*, 886-893.

111. Drader, J. J.; Hannis, J. C.; Hofstadler, S. A. *Anal. Chem.* **2003**, *75*, 3669-3674.

112. Colorado, A.; Shen, J. X. X.; Vartanian, V. H.; Brodbelt, J. *Anal. Chem.* **1996**, *68*, 4033-4043.

113. Pikulski, M.; Wilson, J. J.; Aguilar, A.; Brodbelt, J. S. *Anal. Chem.* **2006**, *78*, 8512-8517.

114. Racine, A. H.; Payne, A. H.; Remes, P. M.; Glish, G. L. *Anal. Chem.* **2006**, *78*, 4609-4614.

115. Flora, J. W.; Muddiman, D. C. *J. Am. Chem. Soc.* **2002**, *124*, 6546-6547.

Chapter 2: Experimental

2.1 MASS SPECTROMETRY

Electrospray ionization (ESI) coupled with a quadrupole ion trap (QIT) mass spectrometer was used for the experiments described in Chapters 3-6. Two different ESI-QIT-MS instruments were used.

For ESI, a solution of the analyte is pumped through a needle to which a high voltage is applied, typically 4 – 4.5 kV. Positive ions are formed by applying a positive voltage to the electrospray needle, and negative ions are formed by applying a negative voltage. Charged droplets are formed at the needle tip and a potential difference between the needle and the front plate of the mass spectrometer guides charged droplets into the mass spectrometer where they undergo desolvation and are guided into the QIT. The details of this process are provided in Chapter 1. ESI is a soft ionization process that does not cause decomposition of analytes. As a result, tandem mass spectrometry can be utilized to study the structure of the intact analyte ions.

Two techniques known as collisionally activated dissociation (CAD) and infrared multiphoton dissociation (IRMPD) were used in the QITs. CAD is an activation technique that involves the increase of the internal energies of the ions through collisions with the background helium gas which ultimately results in dissociation. During the collisions, there is a conversion of kinetic energy to internal energy. Hundreds of collisions results in an increase in internal energy that is great enough to break the lowest energy bonds between atoms in the ions. The details of the process are described further in Chapter 1. A drawback to the technique is that the ion population may also be reduced by scattering during collision, thereby reducing sensitivity of the fragment ions formed.

IRMPD is a technique in which the internal energies of the isolated ions are increased by absorption of low energy photons. In this case, the ions absorb many photons until the internal energy is increased to a point where dissociation takes place. Because IRMPD does not require the use of a collision gas, the ion losses from scattering after collision with the bath gas are not an issue, resulting in higher overall ion populations. Since IR absorption is a non-selective process, primary fragment ions may also absorb IR photons, gain energy, and dissociate into secondary fragment ions. The result is that primary and secondary ions are observed from one stage of dissociation.

2.1.1 Finnigan LCQ-Duo Ion Trap Mass Spectrometer

ESI-MS CAD experiments were performed using a Finnigan LCQ-Duo QIT mass spectrometer using the Xcalibur (Finnigan, San Jose, CA) software package and the electrospray source. During ESI, the pressure in the ion trap with helium added was nominally 1.9 x 10^{-5} Torr, measured by the ionization gauge. The electrospray voltage used was typically +4.5 kV in the positive ion mode experiments and -4.0 kV in the negative ion mode experiments. The heated capillary was set to 150-100 °C. Solutions were typically 1.0 – 2.0 x 10^{-5} M in analyte and were infused using a syringe pump (Harvard Apparatus, Holliston, MA) at flow rates from 2-10 μL/min. The lens and octapole voltages, sheath gas flow rate and capillary voltage were optimized for maximum intensity of the ion of interest.

2.1.2 Finnigan LCQ Deca XP Ion Trap Mass Spectrometer

ESI-MS CAD and IRMPD experiments were performed using a Finnigan LCQ-Duo QIT mass spectrometer using the Xcalibur (Finnigan, San Jose, CA) software package and the electrospray source. IRMPD experiments were performed using a Synrad Model 48-5 50-W continuous wave CO_2 laser. The vacuum manifold of the

instrument was modified to permit mounting of a CF viewport flange with a ZnSe window to permit passage of radiation into the instrument.[1] The port was aligned with a 5-mm hole drilled into the ring electrode to permit irradiation of the QIT trapping volume. The laser was gated at the appropriate point in the scan function controlled by software TTL triggers. The electrospray voltage used was typically +4.5 kV in the positive ion mode experiments and -4.0 kV in the negative ion mode experiments. The heated capillary was set to 150-100 °C. Solutions were typically 1.0 – 2.0 x 10^{-5} M in analyte and were infused using a syringe pump (Harvard Apparatus, Holliston, MA) at flow rates from 2-10 μL/min. The lens and octapole voltages, sheath gas flow rate and capillary voltage were optimized for maximum intensity of the ion of interest. During ESI, the pressure in the ion trap with helium added was nominally 2.7 – 2.8 x 10^{-5} Torr, measured by an ionization gauge external to the ion trap. Irradiation times were typically 5 – 25 ms at 50 W and were adjusted to tune sequential fragmentation in several experiments.

2.2 MOLECULAR MODELING

The molecular modeling studies were performed using the CAChe Worksystem Pro (Beaverton, OR) and Gaussian '03 (Pittsburgh, PA) software packages. Preoptimization and generation of coordinates was performed with CAChe Worksystem Pro using MM3/AM1. Final optimizations were performed with the Gaussian '03 software package at the B3LYP/6-31G* level.

2.3 FOURIER TRANSFORM INFRARED SPECTROSCOPY

FTIR analysis was performed using a Thermo Mattson (Madison, WI) Infinity Gold FTIR equipped with a Spectra-Tech Thermal ARK module, and ATR accessory.

2.4 NUCLEAR MAGNETIC RESONANCE SPECTROSCOPY

NMR experiments were performed using a Varian 400 MHz instrument (Varian Inc., Pal Alto, CA).

2.5 CHEMICALS

Apigenin, vitexin, apigenin-7-glucoside, isorhoifolin, rhoifolin, isovitexin, quercetin, luteolin, quercitrin, kaempferol-3-glucoside, luteolin-4'-glucoside, luteolin-7-glucoside, orientin, neodiosmin and narirutin were purchased from Indofine (Somerville, NJ). Fortunellin, linarin, poncirin and didymin were purchased from Extrasynthese (Genay, France). Naringin, neohesperidin, hesperidin, 2,2'-bipyridine, 4,7-diphenyl-1,10-phenanthroline, 1,10-phenanthroline, 2,2':6',2"-terpyridine, 4,4'-dimethyl-2,2'-bipyridine, 6,6'-dibromo-2,2'-bipyridine, 4,4'-dimethyl-2,2'-bipyridine, 5-nitro-1,10-phenanthroline, $CoBr_2$, $NiBr_2$, $CuBr_2$, CsF_2 and LNDFH-Ib were purchased from Sigma-Aldrich (Milwaukee, WI). LNFP-I, II, III, V, LNDFH Ia and II and DSLNT were purchased from V-Labs (Covington, LA). Diethyl(aminomethyl)phosphonate oxalate was purchased from Acros Organics (Belgium). Glacial acetic acid, 30% hydrogen peroxide, fuming sulfuric acid, fuming nitric acid, acetyl bromide, phosphorus tribromide, diisopropylamine, butyllithium, chlorotrimethylsilane, hexabromoethane, sodium chloride, thionyl chloride, bromine, diethyl phosphite, triethyl phosphite, sodium borohydride, ammonium hydroxide, methanol, dichloromethane, chloroform, ethyl acetate, tetrahydrofuran, petroleum ether, N,N-dimethylformamide, hexanes and 2-formylphenylboronic acid were purchased from Fisher (Somerville, NJ). Tetrakis(triphenylphosphine)Palladium(0) was purchased from Strem Chemicals (Newburyport, MA).

2.7 REFERENCES

1. Wilson, J. J.; Brodbelt, J. S. *Anal. Chem.* **2006**, *78*, 6855-6862.

Chapter 3: Differentiation of Flavonoid Glycoside Isomers By Using Metal Complexation and Electrospray Ionization Mass Spectrometry

3.1 OVERVIEW

The elucidation of flavonoid isomers is accomplished by electrospray ionization tandem mass spectrometry (ESI-MS/MS) via formation and collisional activated dissociation (CAD) of metal/flavonoid complexes containing an auxiliary ligand. Addition of a metal salt and a suitable neutral auxiliary ligand to flavonoids in solution results in the formation of [M(II) (flavonoid-H) ligand]$^+$ complexes by ESI which, upon collisional activated dissociation, often result in more distinctive fragmentation patterns than observed for conventional protonated or deprotonated flavonoids. Previously, 2,2'-bipyridine was used as an auxiliary ligand, and now we compare and explore the use of alternative pyridyl ligands, including 4,7-diphenyl-1,10-phenanthroline. Using this technique, three groups of flavonoid glycoside isomers are differentiated, including glycosides of apigenin, quercetin and luteolin.

3.2 INTRODUCTION

Flavonoids are polyphenolic phytochemicals which occur in edible fruits and vegetables. They have been reported to act as antioxidants,[1] antimicrobials,[2] free radical scavengers,[1] metal chelators,[1] and anti-viral and anti-bacterial agents.[3] Since they are a ubiquitous part of the human diet, their effect on human health is of interest. Flavonoids are known to have medicinal and chemopreventive activities in humans.[4-7] For example, a diet rich in flavonoids has shown to have an inverse relationship with heart disease.[8-10]

There is a basic structure which is common to all flavonoids; however, there is a great diversity of flavonoids due to different hydroxylation and glycosylation positions. Most flavonoids exist as glycosides in plant sources, and many only differ by the nature

of the aglycon, and/or by the glycosylation site, the sequence, and the interglycosidic linkages of the glycan portion. The biological activities of flavonoids are affected by these subtle structural differences.[11] Therefore, there is a critical need for the development of analytical methods to elucidate structurally similar compounds.

A number of mass spectrometric techniques have been used to study the structures of flavonoids.[12] Electron ionization (EI) has been used to evaluate the fragmentation pathways of some aglycons[13] and for limited structural studies of glycosides. However, derivatization was required to make the flavonoids sufficiently volatile for EI and in some cases did not result in meaningful fragmentation patterns.[14-17] Fast atom bombardment (FAB) and liquid secondary ion mass spectrometry (LSIMS) have been used extensively.[18-36] In addition, thermospray[37-39] and atmospheric pressure chemical ionization (APCI)[40-41] have been used for several applications involving the analysis of flavonoids. Most recent, electrospray ionization (ESI) has become a popular choice.[40-49] For example, the positive ESI mode was used to identify and quantitate flavonoids in soya flours and baby foods,[43] and in hops and beer.[48] Also, the negative ESI mode was used to identify and quantitate flavonoids in tea extracts[44] and plants such as *Passiflora incarnate.*[47]

Tandem mass spectrometry has been used to elucidate many of these compounds.[23-24,31-36,44-47,50-52] For example, CAD of deprotonated flavonoid glycosides commonly results in loss of the sugars (formation of Y_0^- and Y_1^- ions). CAD of deprotonated flavonoid-O-glycosides allows distinction of rutinosides (1→6 disaccharides) from neohesperidosides (1→2 disaccharides) based on the greater abundance of the Y_1^- ions for the neohesperidosides compared to the rutinosides.[50] However, unique fragment ions were not observed for each isomer in all cases, so some identifications were based on differences in abundances of fragment ions of the same m/z

values. In addition, CAD of protonated flavonoid-C-glycosides allowed the differentiation between 6-C and 8-C glycosides.[51] However, the isomeric distinctions generally relied on the relative abundances of common product ions in the MS/MS spectra for some compounds, and diagnostic product ions were only observed in the MS/MS/MS spectra. Hvattum et al. used CAD to evaluate the formation of radical fragment ions from deprotonated flavonoid glycosides by loss of neutral sugar radicals.[52] The radical fragmentation processes were related to the number of hydroxyl substituents on the B ring of the flavonoid, in addition to the type and position of the sugar substituent. It was surmised that the radical loss of the 3-O-sugar substituent was enhanced by the presence of multiple hydroxyl groups on the B ring due to the electron-donating properties of the hydroxyl groups, thus weakening the glycosidic bonds.

Due to their acidic functional groups, protonation of flavonoid glycosides is inefficient, often resulting in weak positive ESI mass spectra. In some cases, the fragmentation patterns of protonated flavonoids do not differentiate similar compounds or isomers. Although deprotonation results in more intense mass spectra in the negative ESI mode, the fragmentation patterns again frequently do not differentiate similar compounds or isomers. Metal complexation is an alternative ionization mode which has been explored in the Brodbelt group in the past.[53-58] It has been observed that metal complexation can both increase ion intensity and alter fragmentation pathways, resulting in many more structurally distinctive fragment ions. Dramatic increases in intensities of some flavonoids[56] have been observed with the use of copper, nickel or cobalt, along with 2,2'-bipyridine or 1,10-phenanthroline as an auxiliary ligand. In this chapter, the differentiation of three series of flavonoid glycosides with the use of 2,2'-bipyridine (bpy) and 4,7-diphenyl-1,10-phenanthroline (dpphen), a new auxiliary ligand, is shown. Although some of these compounds have been differentiated in the positive ion mode

based on differences in the relative intensities of specific fragment ions[50-51] and in the negative ion mode based on low intensity fragment ions formed upon CAD,[50] in this chapter isomers are differentiated via more intense, distinctive ions in the CAD spectra.

Two classes of flavonoids, flavones and flavonols, are considered in this chapter. The use of metal complexation for differentiation within these two classes of flavonoids is extended and expanded. The differentiation of glycosides of apigenins, commonly found in olive oil,[59] orange juice,[60] celery,[61] and garlic[62] is accomplished (Figure 3-1, Group I); in addition to glycosides of kaempferol, commonly found in lettuce,[64] green beans,[65] and grapes,[66] glycosides of quercetin, commonly found in onions,[63] kale,[64] lettuce,[64] and green beans[65] and glycosides of luteolin, commonly found in broccoli,[62] carrots,[62] and celery (Figure 3-1, Group II).[62]

3.3 EXPERIMENTAL

Experiments were performed with a Finnigan LCQ Duo quadrupole ion trap mass spectrometer equipped with an electrospray ionization source. The flow rate of the solutions was 5 μL min^{-1}. The lens and octapole voltages, sheath gas flow rate and capillary voltage were optimized for maximum intensity of the ion of interest. The capillary temperature was 200 °C. The interface pressure, measured with the convectron gauge at the skimmer cone, was normally 0.9 Torr. The pressure in the ion trap with helium added was nominally 1.9 x 10^{-5} Torr, measured by the ionization gauge. The spectra were acquired with ion injection times of 5 ms and an average of 10 microscans.

Group Ia (MW=432)

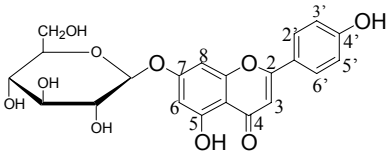

apigenin-7-glucoside

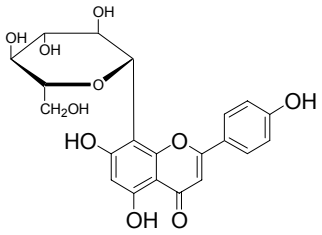

vitexin

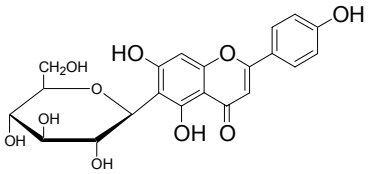

isovitexin

Group Ib (MW=578)

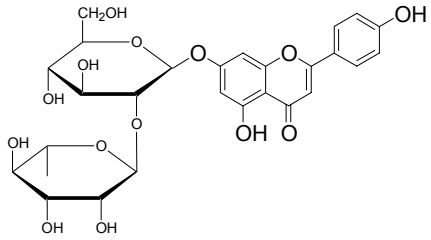

rhoifolin (1→2)

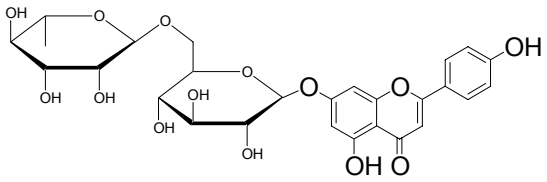

isorhoifolin (1→6)

Group II (MW=448)

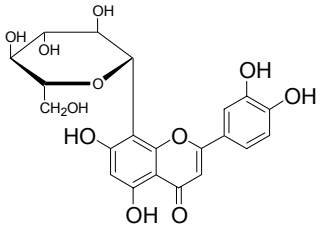

orientin

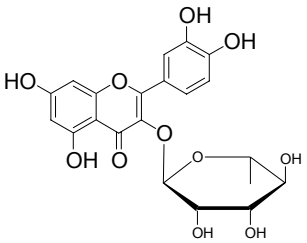

quercitrin

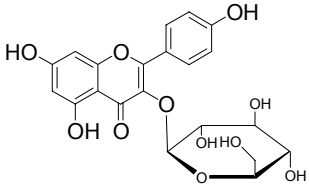

kaempferol-3-glucoside

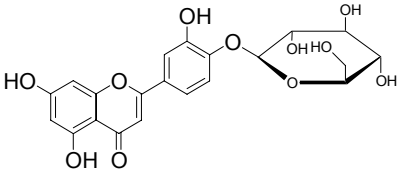

luteolin-4'-glucoside

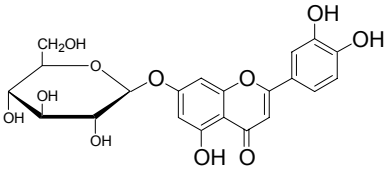

luteolin-7-glucoside

Figure 3-1. Structures of flavonoids studied, with molecular weights in parentheses.

In the negative ESI mode, the ion corresponding to $[L-H]^-$ was optimized, where L is the flavonoid. In the positive ESI mode, when solutions of flavonoid/metal/auxiliary ligand were used, the ion corresponding to $[M(II)\ (L-H)\ A]^+$ was optimized, where M is the metal and A is the auxiliary ligand. During MS/MS experiments, these parent ions were isolated and the CAD voltage was adjusted so that the parent ion intensity decreased to 20% of the base peak.

Stock solutions of 4.0×10^{-4} M metal salt/methanol and 4.0×10^{-4} M auxiliary ligand/methanol were used to create the analytical solutions. Solutions containing a flavonoid, a metal salt, and an auxiliary ligand were ~1:1:1 at 1.0×10^{-5} M. The analytical solutions used for the negative ESI experiments were 1.0×10^{-5} M flavonoid in methanol. The flavonoids apigenin, vitexin, apigenin-7-glucoside, isorhoifolin, rhoifolin, isovitexin, quercetin, luteolin, quercitrin, kaempferol-3-glucoside, luteolin-4'-glucoside, luteolin-7-glucoside and orientin were purchased from Indofine (Somerville, NJ). 2,2'-Bipyridine, 4,7-diphenyl-1,10-phenanthroline, 1,10-phenanthroline, 2,2':6',2"-terpyridine, 4,4'-dimethyl-2,2'-bipyridine, $CoBr_2$, $NiBr_2$, and $CuBr_2$ were purchased from Aldrich (Milwaukee, WI). The HPLC grade methanol was purchased from EM Science (Gibbstown, NJ). All materials were used without further purification.

The nomenclature for glycoconjugates proposed by Domon and Costello[67] is used to describe the fragmentation pathways for O-glycosides and the neutral losses for C-glycosides. Fragments from a terminal sugar unit are labeled using ${}^{g,h}A_i$, B_i and C_i, where i is the number of the bond broken, counting from the terminal sugar beginning with 1, and g and h are the cross-ring cleavages of the sugar. Fragments which include the aglycon are labeled ${}^{k,l}X_j$, Y_j and Z_j, where j is the number of the bond broken, counting from the aglycon beginning with 0, and k and l are the cross-ring cleavages of the sugar.

3.4 RESULTS AND DISCUSSION

3.4.1 Negative Ion Mode

Since the negative ESI mode has been so widely used for mass spectrometric analysis of flavonoids, we have compared the relative ionization efficiencies and diagnostic utility of the CAD spectra for deprotonated flavonoids to those obtained for the metal complexes in this chapter. The spectra collected in the negative ion mode were clean with intense ions due to the efficiency of deprotonation of the flavonoids. The spectra were dominated by $[L-H]^-$ ions, the ion selected for the CAD studies. Also observed were $[L\ (L-H)]^-$ ions; dissociation of these dimer species yielded $[L-H]^-$ ions. The following sections describe the CAD results for the deprotonated flavonoids of the three sets of isomers in order to establish benchmarks for the degree of differentiation.

3.4.1.1 Group Ia Differentiation: Apigenin-7-glucoside, Vitexin and Isovitexin (MW 432)

The CAD mass spectra of the Group Ia flavonoids are shown in Figure 3-2, and the MS^n data for the Group I flavonoids in the negative ESI mode is summarized in Table 3-1. Upon CAD of the deprotonated flavonoids, the O-bonded glucoside, apigenin-7-glucoside, is easily differentiated from the C-bonded isomers, isovitexin and vitexin, because deprotonated apigenin-7-glucoside dissociates primarily by loss of the glucose residue (Glc) (-162 Da) resulting in the Y_0^- ion at m/z 269 (Figure 3-2a). Likewise, both of the C-bonded glucosides, vitexin and isovitexin, are easily differentiated from apigenin-7-glucoside because the deprotonated species dissociate by losses of 120 Da and 90 Da due to cross-ring sugar cleavages (corresponding to $^{0,2}X_0^+$ and $^{0,3}X_0^+$, respectively, Figure 3-2b and c). Cross-ring cleavages are commonly observed in the dissociation of saccharides,[67-71] and this type of process is also observed for the C-bonded glycosides[18,23] since the typical rearrangements across the oxygen glycosidic bond do not take place.

However, the CAD spectra of deprotonated vitexin and isovitexin do not have significant diagnostic ions which differentiate them from each other in the negative ESI mode, nor can the intensities of the two major fragment ions (with identical mass-to-charge values for each isomer) be used to reliably distinguish and quantify the two flavonoids in mixtures.

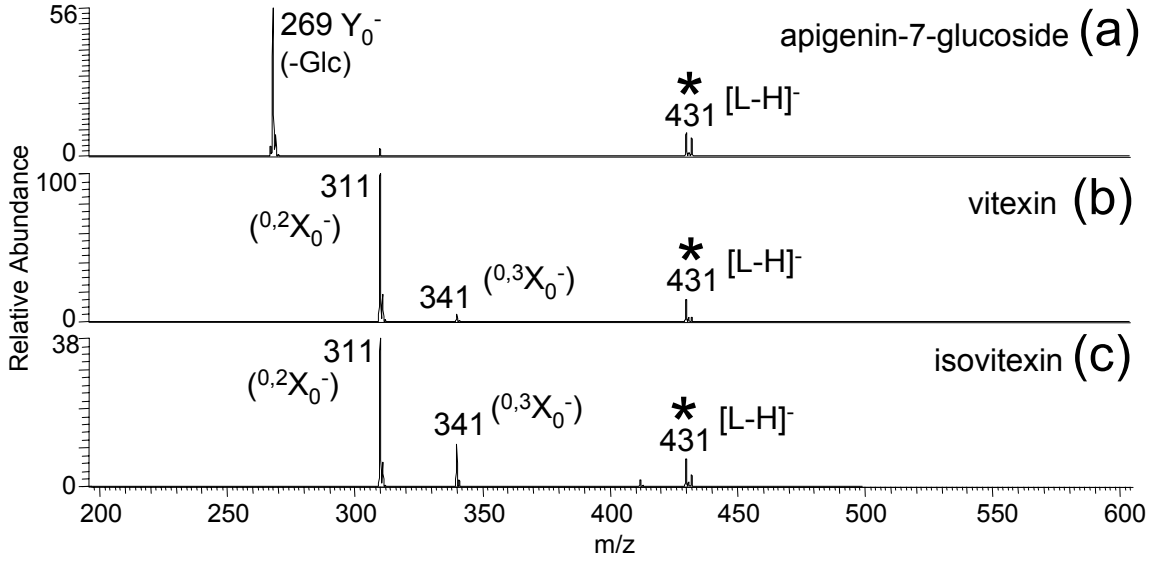

Figure 3-2. CAD spectra for deprotonated flavonoids from Group Ia. The parent ions are labeled with asterisks.

A second stage of ion isolation and activation (i.e. MS/MS/MS) undertaken on the major fragment ion at m/z 311 (seen in Figure 3-2b and 2c) results exclusively in the loss of CO for both vitexin and isovitexin, so even MS^n does not sufficiently differentiate these two compounds. This lack of isomer differentiation is a good example of why other ionization modes that might create different types of precursor ions with more distinctive dissociation properties should be explored.

Table 3-1. MS^n spectra of deprotonated Group I flavonoids.

		MS/MS[1]			MS/MS/MS[1]		
	m/z	m/z	Loss	%	m/z	Loss	%
apigenin-7-glucoside	431	269	162	100	225	44	100
					197	72	36
					120	149	28
		311	120	6			
vitexin	431	311	120	100	283	28	100
		341	90	6			
isovitexin	431	311	120	100	283	28	100
		341	90	28	323	18	100
					269	72	8
					311	30	6
rhoifolin	577	269	308	100	225	44	100
		413	164	4			
		311	266	3			
		431	146	3			
		457	120	2			
		371	206	2			
isorhoifolin	577	269	308	100	225	44	100

[1]MS/MS and MS/MS/MS data correspond to their parent ions (labeled m/z) on the left. The standard deviations of the fragment ion intensities are typically +/- 5%.

3.4.1.2 Group Ib Differentiation: Rhoifolin and Isorhoifolin (MW 578)

Both deprotonated rhoifolin and isorhoifolin dissociate primarily by loss of the disaccharide, resulting in the Y_0^- ion at m/z 269 (Figure 3-3a and b). Although these two isomers in theory may be differentiated by the occurrence of several unique losses from deprotonated rhoifolin (formation of ions at m/z 311, 371, 431, and 457)[50] these ions are less than 5% relative intensity in the CAD spectra and could fall below limits of detection in more complex samples. Further fragmentation of the Y_0^- ion results in the loss of CO_2

for each isomer. Thus, CAD of deprotonated rhoifolin and isorhoifolin does not differentiate these isomers with confidence.

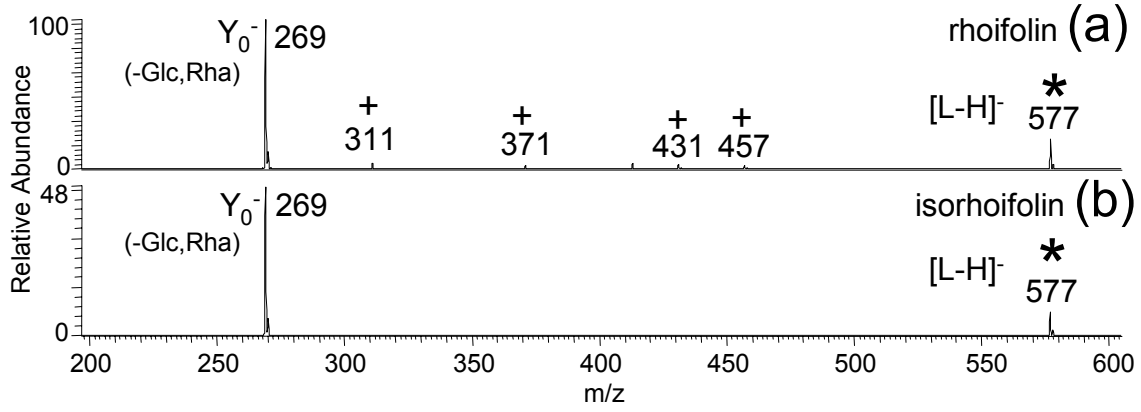

Figure 3-3. CAD spectra for deprotonated flavonoids from Group Ib. The parent ions are labeled with asterisks. The + symbols represent previously identified low-intensity ions which could fall below limits of detection in more complex samples.

3.4.1.3 Group II Differentiation (MW 448)

The CAD mass spectra for the five deprotonated flavonoids in Group II are shown in Figure 3-4, and the MS^n data is summarized in Table 3-2. Deprotonated orientin, the C-bonded isomer, is easily differentiated from the others by the losses of 120 Da and 90 Da due to cross-ring cleavages (Figure 3-4a), which are observed for some of the Group Ia flavonoids. In addition, deprotonated quercitrin is distinguished from the others because of the unique loss of the terminal rhamnose residue (Rha) (-146 Da), resulting in the Y_0^- ion at m/z 301 (Figure 3-4b). The deprotonated flavonoids of the remaining three isomers, the O-glucosides, each dissociate by loss of their terminal Glc (-162 Da, formation of m/z 285) (Figure 3-4c, d and e). In addition to the prominent loss of Glc, deprotonated kaempferol-3-glucoside undergoes an even more pronounced radical loss of the sugar, presumably via a homolytic bond cleavage[52] at the 3-O-glucose bond which

results in the ion at m/z 284. Note that this type of process also occurs for deprotonated quercitrin (leading to the Y_o^- ion at m/z 300), although to a much lesser extent.

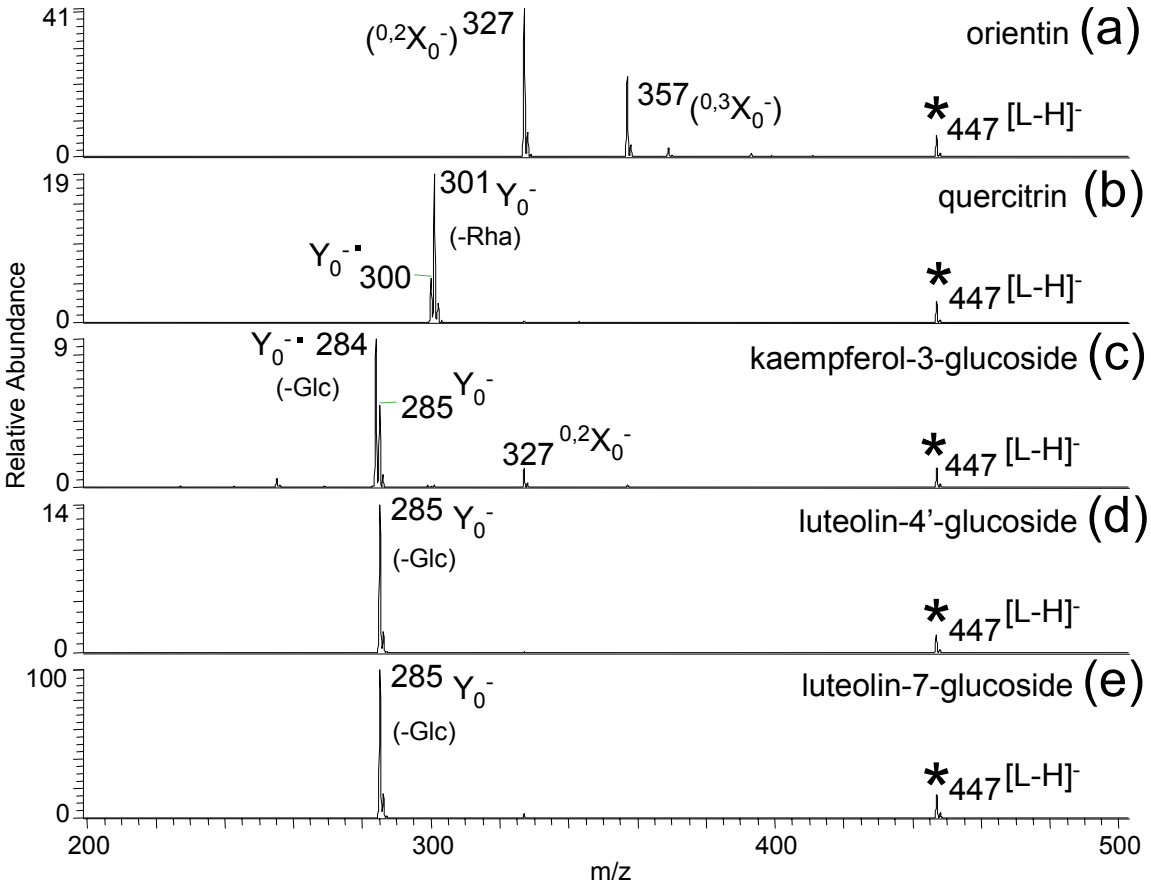

Figure 3-4. CAD spectra for deprotonated flavonoids from Group II. The parent ions are labeled with asterisks.

These two isomers both have their sugars attached at the 3 position. The radical ion pathway was only observed for 3-substituted flavonoid glycosides and not for the 7-glucoside, luteolin7-glucoside, as has been reported.[52] The exact structure of the radical $Y_o^{-\cdot}$ ion at m/z 284 is difficult to define because there are several possible sites of deprotonation of the flavonoids, and thus a variety of reasonable initial precursor

structures and final product structures can be drawn and in which the resulting oxygen radical site can be stabilized via resonance.

Table 3-2. MS^n spectra of deprotonated Group II flavonoids.

		MS/MS[1]			MS/MS/MS[1]		
	m/z	m/z	Loss	%	m/z	Loss	%
orientin	447	327	120	100			
		357	90	54			
quercitrin	447	301	146	100			
		300	147	26			
kaempferol-3-glucoside	447	284	163	100	255	29	100
					256	28	32
					227	57	6
		285	162	53			
		327	120	14			
luteolin-4'-glucoside	447	285	162	100	241	44	100
					199	86	82
					243	42	59
					217	68	51
					175	110	40
					242	43	27
					257	28	22
					151	134	21
					213	72	20
					218	67	18
					223	62	15
					267	18	10
luteolin-7-glucoside	447	285	162	100	241	44	100
					199	86	77
					217	68	69
					243	42	67
					175	110	60
					213	72	26
					257	28	24
					242	43	21
					151	134	21
					267	18	17

[1]MS/MS and MS/MS/MS data correspond to their parent ions (labeled m/z) on the left. The standard deviations of the fragment ion intensities are typically +/- 5%.

The remaining two isomers, deprotonated luteolin-4'-glucoside and luteolin-7-glucoside, are not differentiated by CAD nor by MS^3 spectra. While the fragmentation of the primary fragment ion (m/z 285) is extensive in the MS^3 spectra obtained for deprotonated luteolin-4'-glucoside and luteolin-7-glucoside (see Table 3-2), the ions are similar and do not unequivocally distinguish these two isomers in the negative ion mode. Most of the secondary fragmentation pathways involve losses of CO, CO_2 and H_2O from the selected primary fragment ion (m/z 285). For example, both of the MS/MS/MS spectra are dominated by a loss of 44, the loss of CO_2, from m/z 285.

3.4.2 Metal Complexation

Due to the unsatisfactory differentiation of the flavonoid isomers based on CAD mass spectra of the deprotonated flavonoids, metal complexation was explored as an alternative way to ionize the flavonoids and create different types of parent structures. Due to our previous studies in this area,[53-58] 2,2'-bipyridine was selected as the first auxiliary ligand and $CoBr_2$ was used as the metal salt. For the flavonoids, acidic sites that may be deprotonated in solution and are adjacent to a second binding site (i.e. another oxygen atom) are the likely chelation sites for the metal ions. Using luteolin-7-glucoside as an example, the metal binding site may be between the carbonyl functionality and a deprotonated hydroxyl at the 5 position (Figure 3-5a), or between adjacent hydroxyls on the B ring, one being deprotonated (Figure 3-5b), or even involve the sugar moiety (Figure 3-5c). The structures shown in Figure 3-5 are just a subset of reasonable possibilities, and the ESI process may generate a mixture of these metal complexes. Complexes of the type $[M(II)\ (L - H)\ A]^+$ where M is the metal, A is the auxiliary ligand, and L is the flavonoid, were produced for copper, cobalt, and nickel, and all of these complexes were more intense than the deprotonated flavonoids. While the copper and nickel complexes were more intense than the cobalt complexes, the latter

produced ions which enabled differentiation of the isomers upon CAD. Thus, $CoBr_2$ was used for the remainder of the study, and only the CAD spectra of the [Co(II) (flavonoid – H) 2,2'-bipyridine]$^+$ complexes were evaluated for the isomers.

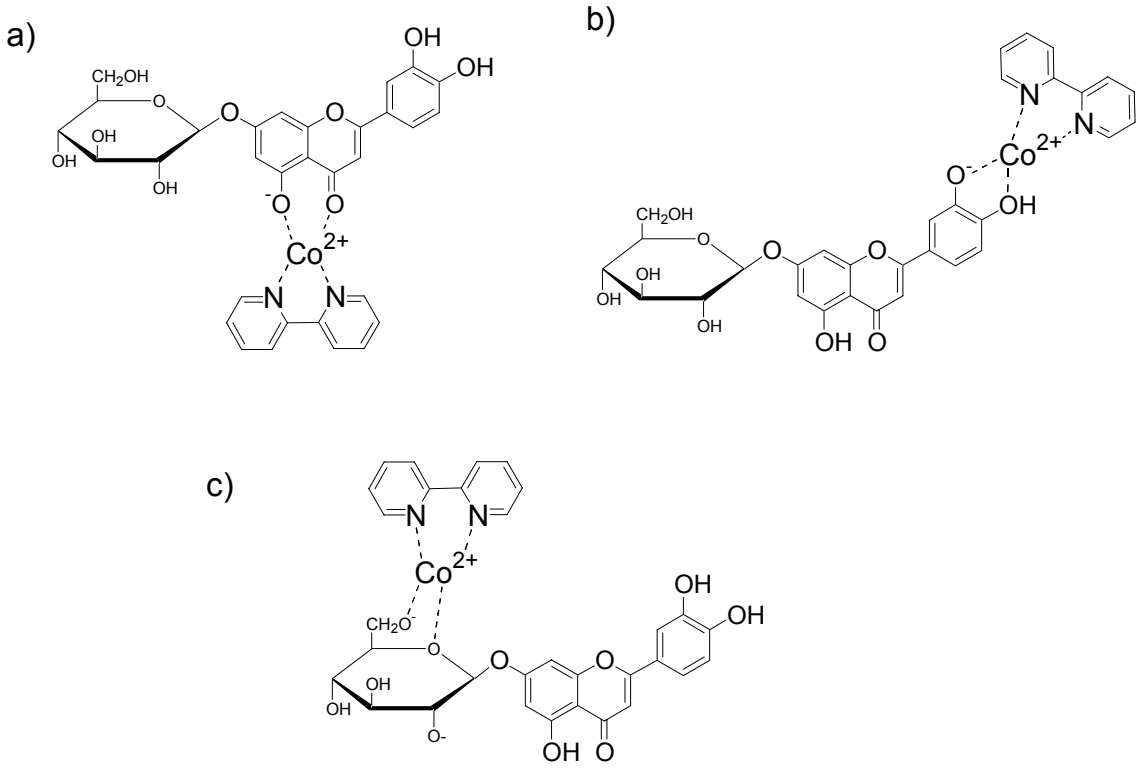

Figure 3-5. Proposed structures for [Co(II) (L-H) bpy]$^+$ complexes.

3.4.3 Complexation with Cobalt and 2,2'-Bipyridine

Upon ESI of solutions containing one flavonoid, a cobalt salt, and 2,2'-bipyridine, ions observed in these spectra included [Co(II) (L - H) 2 x bpy]$^+$ and [Co(II) (L - H) bpy]$^+$, with the latter being about five times more intense than the former. In addition, there were minor product ions due to in-source fragmentation of the sugar for the O-bonded isomers, such as the loss of terminal Rha or the entire disaccharide. The [Co(II) (L – H) bpy]$^+$ complexes formed were generally an order of magnitude more intense than

the $[L - H]^-$ ions formed in the negative ion mode. In addition to this improvement in sensitivity, the CAD fragmentation patterns were generally richer and more distinctive than those observed for the negative ion mode.

3.4.3.1 Group Ia Differentiation: Apigenin-7-glucoside, Vitexin and Isovitexin (MW 432)

The CAD spectra of the $[Co(II) (L – H) bpy]^+$ complexes are illustrated in Figure 3-6 for the group Ia isomers. The CAD spectrum for the apigenin-7-glucoside complex is distinctive from the other two isomers in that there is only one major ion (Y_0^+complex, m/z 484) due to the loss of Glc (Figure 3-6a). In addition, there is a low intensity ion due to the loss of the aglycon moiety at m/z 376. The loss of the entire aglycon moiety from the complex means that the cobalt ion and 2,2'-bipyridine are coordinated only to the sugar moiety in the resulting product ion, suggesting that the initial structure proposed in Figure 3-5c may be operative or that the cobalt/2,2'-bipyridine moiety may migrate from the aglycon to the saccharide upon collisional activation of the complex.

The $[Co(II) (L – H) bpy]^+$ complex of vitexin also undergoes the loss of the Glc upon CAD which is common for the O-glycosides but was not expected for a C-bonded glycoside. The losses of 120 Da and 90 Da due to cross-ring cleavages are also dominant (Figure 3-6b). In addition, the vitexin complex dissociates by several other pathways, including the loss of 150 Da ($^{0,1}X_0^+$), a similar neutral loss to which has been reported in the positive ion mode,[23] and the loss of one or two molecules of water. While the $[Co(II) (L – H) bpy]^+$ complexes of isovitexin also undergo two of the same cross-ring cleavages as does the vitexin isomer, resulting in losses of 90 Da and 120 Da (Figure 3-6c), the losses from Glc, 150 Da and 108 Da are unique for the isovitexin complex. The latter loss of 108 Da was the same as one of the neutral losses also observed in the positive ion mode[23] and was proposed to be due to elimination of 90 Da in conjunction with water.

Thus, comparison of the CAD spectra in Figure 3-2b and 3-2c to those seen in Figure 3-6b and 3-6c confirms that isovitexin and vitexin are more effectively differentiated based on the results for the metal complexes.

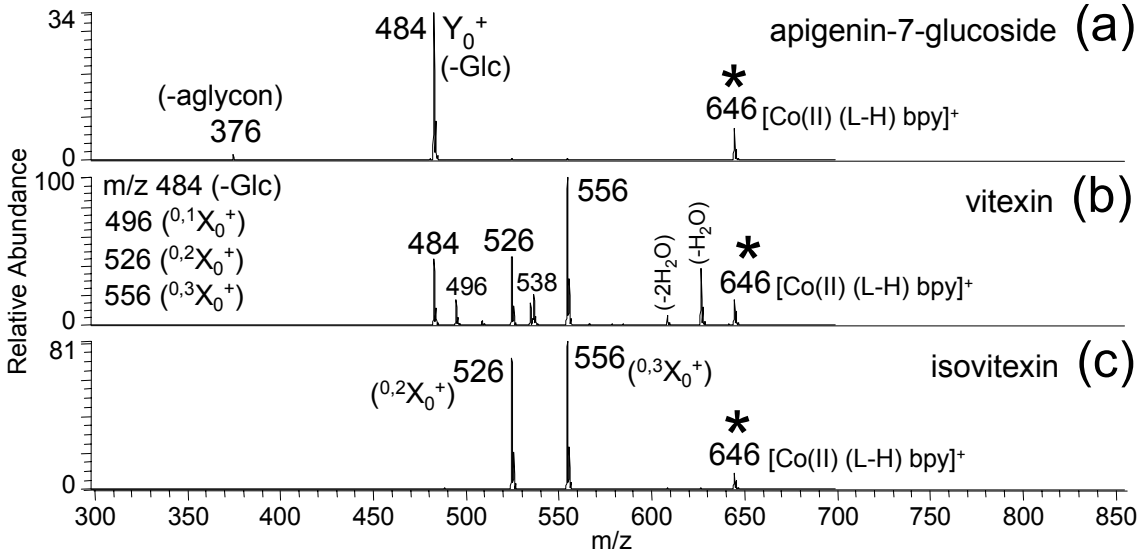

Figure 3-6. CAD spectra of $[Co(II) (L-H) bpy]^+$ complexes of Group Ia flavonoids. The parent ions are labeled with asterisks.

Due to the diverse array of fragmentation pathways for the $[Co(II) (L - H) bpy]^+$ complex of vitexin, this complex serves as an excellent model to illustrate the general fragmentation genealogy of the metal complexes. Scheme 1 shows the m/z values of the product ions and neutral losses based on extensive MS^n experiments, and Scheme 2 illustrates proposed structures that reasonably account for the major fragment ions. Schemes 1 and 2 refer specifically to the ions seen in Figure 3-6b for the vitexin complex, but many of the pathways are general ones seen for the other isomers.

Table 3-3. MS^n spectra of Group I $[Co(II)\ (L-H)\ bpy]^+$ complexes.

		MS/MS[1]			MS/MS/MS[1]		
	m/z	**m/z**	**Loss**	**%**	**m/z**	**Loss**	**%**
apigenin-7-glucoside	646	484	162	100	364	120	100
					346	138	23
		376	270	4			
vitexin	646	556	90	100	497	59	100
					538	18	60
					510	46	42
					526	30	19
					484	72	9
		526	120	46	497	29	100
					469	57	15
		484	162	46	364	120	100
					346	138	20
					377	107	5
					456	28	5
					254	230	3
		628	18	38	610	18	100
					568	60	20
					497	131	16
					525	103	12
					550	78	10
					592	36	9
					508	120	7
					580	48	6
		538	108				
		496	150				
		536	110				
		610	36				
isovitexin	646	556	90	100	497	59	100
					538	18	86
					536	20	80
					498	58	61
					510	46	64
					496	60	25
					484	72	16
		526	120	90	508	18	100
					497	29	81
					498	28	81
					496	30	50
					232	294	31
					216	310	13
					469	57	11

rhoifolin	792	484	308	100	364	120	100
					346	138	28
		646	146	24	484	162	100
					376	270	4
		376	416	10			
isorhoifolin	792	484	308	100	364	120	100
					346	138	22
		646	146	45	484	162	100

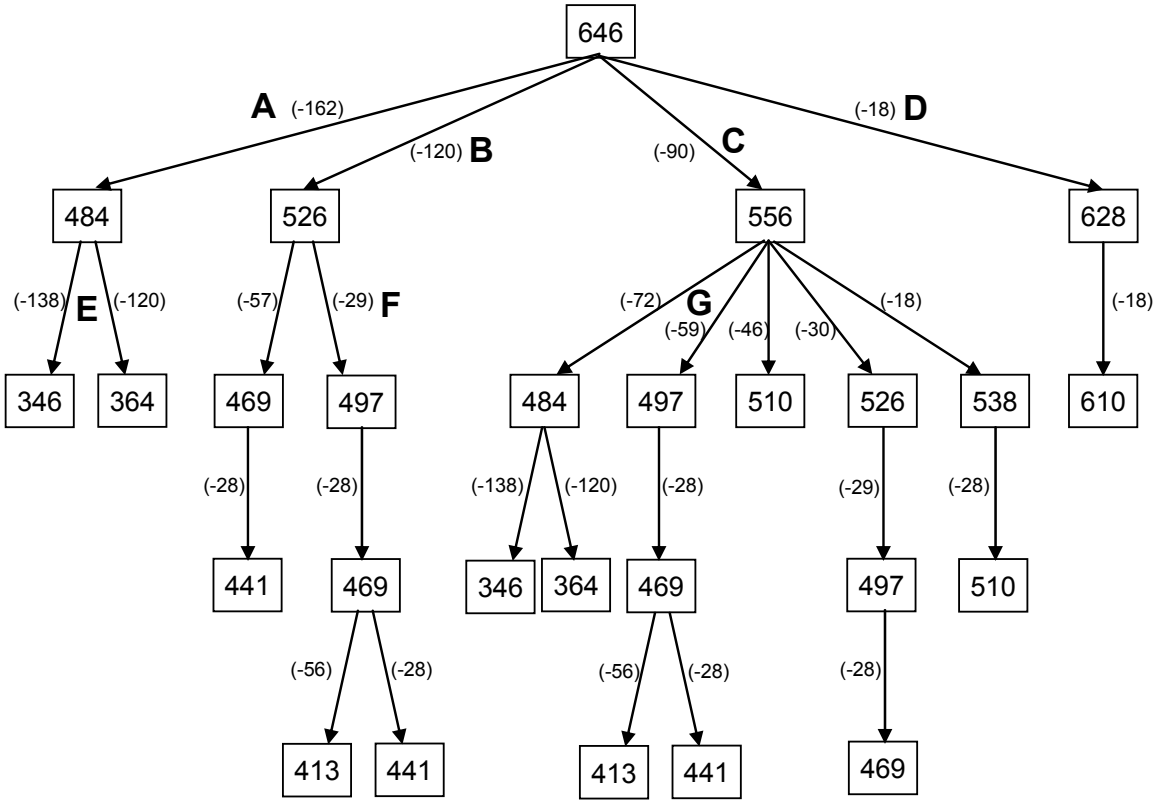

Scheme 3-1. CAD fragmentation pathways for [Co(II) (vitexin-H) bpy]$^{+}$ using m/z values of the fragment ions.

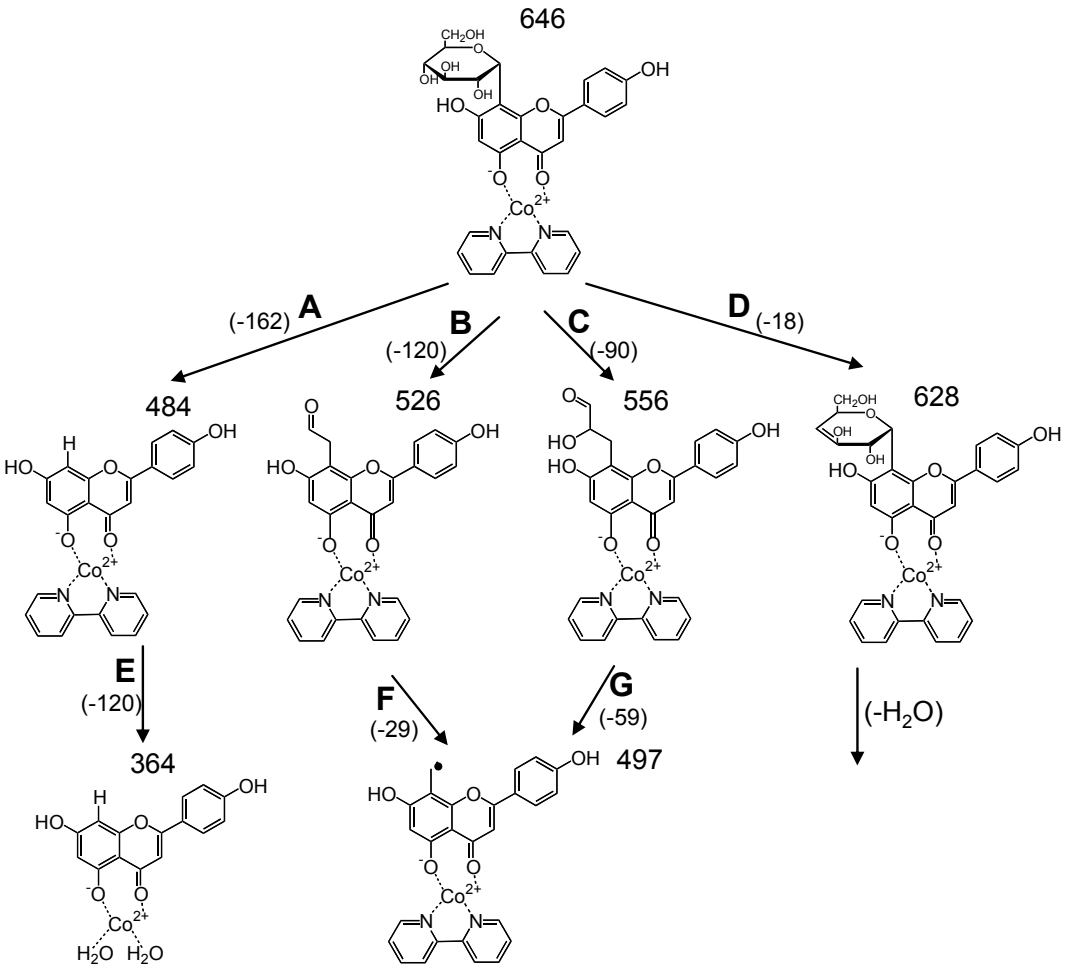

Scheme 3-2. CAD fragmentation pathways for [Co(II) (vitexin-H) bpy]$^{+}$ using proposed structures of the fragment ions.

Path A represents the loss of the terminal sugar, which is most prevalent with the O-glucosides. This fragmentation route is followed by path E, the loss of 2,2'-bipyridine and addition of two water molecules, resulting in the ion at m/z 364. Sometimes this pathway occurs with the addition of only one molecule of water (formation of m/z 346). Solvation of metal complexes in an ion trap has been noted previously[72-76] and is attributed to the coordinative unsaturation of the metal center which is resolved by the

adduction of water molecules, present at low levels in the trap. The pathway proposed as involving loss of 2,2'-bipyridine and attachment of water molecules (path E) was confirmed by CAD of a [Co(II) (L – H) phen]$^+$ complex containing cobalt with 1,10-phenanthroline (phen) instead of 2,2'-bipyridine. The appearance of the same product ions at m/z 346 and 364 confirmed that the auxiliary ligand was lost from the metal complexes upon activation, otherwise these fragment ions would be shifted upwards in m/z value by the difference between the nominal mass of 2,2'-bipyridine and 1,10-phenanthroline. Thus, path E for the [Co(II) (L – H) bpy]$^+$ complex is actually the loss of 2,2'-bipyridine (156 Da) followed by the rapid adduction of one or two water molecules.

Path B depicts the cross-ring cleavage resulting in a loss of 120 Da. The resulting ion further dissociates predominantly by path F, resulting in an interesting radical species of m/z 497 via the loss of CHO$^\cdot$ radical. There is also a less intense secondary fragment ion at m/z 469, assigned as the loss of CO from m/z 497. Path C depicts another cross-ring cleavage resulting in a loss of 90 Da, resulting in formation of the ion of m/z 556. This product ion further dissociates mainly by path G, resulting in the same radical species at m/z 497 as proposed for path B. Other comparatively minor pathways observed upon CAD of m/z 556 include the loss of water, which may occur in conjunction with the loss of CO (leading to the ion at m/z 510), the loss of formaldehyde, and the loss of 72 Da. The loss of formaldehyde from m/z 556 is followed by the loss of HCO$^\cdot$ radical, also resulting in the radical product ion at m/z 497. Paths B and C are the most prevalent fragmentation pathways for the C-bonded flavonoids studied. Path D represents a simple loss of water, mostly likely from the sugar. This dehydration reaction is followed by yet another loss of water or even loss of two water molecules. The identities of the hydroxyl groups that are lost as water molecule can't be

determined with certainty, so the dehydrated structure shown in Scheme 2 is just one possibility.

3.4.3.2 Group Ib Differentiation: Rhoifolin and Isorhoifolin (MW 578)

Both the $[Co(II) (L - H) bpy]^+$ complexes of rhoifolin and isorhoifolin (Figure 3-7a and 3-7b) undergo the same major loss of the disaccharide (loss of 308 Da) as was observed upon CAD of the deprotonated species (Figure 3-3a and b). However, the loss of Rha (-146 Da) is also observed for both isomers, and this fragmentation pathway was not observed for the deprotonated species.

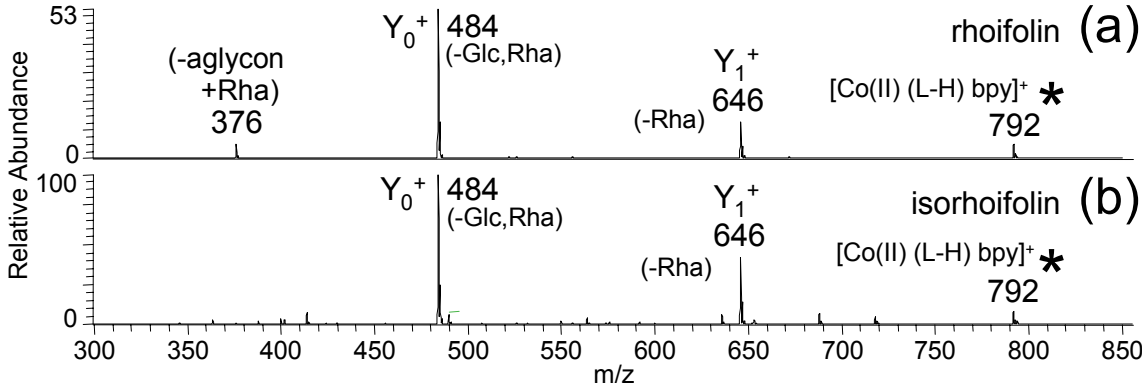

Figure 3-7. CAD spectra of parent $[Co(II) (L-H) bpy]^+$ complexes of Group Ib flavonoids. The parent ions are labeled with asterisks.

In addition to these two pathways, rhoifolin also undergoes the elimination of aglycon in conjunction with the loss of Glc (relative intensity 11%), leading to the unique fragment ion at m/z 376. Apparently the 1→ 6 linkage of the rutinoside on isorhoifolin disrupts this fragmentation pathway. Note that both rhoifolin and apigenin-7-glucoside, both with sugars at the 7 position like isorhoifolin, undergo this loss of the aglycon. This suggests that the loss of aglycon is indicative of a sugar at the 7-position or a 1→ 2 disaccharide. The appearance of the unique ion at m/z 376 is a promising diagnostic ion

for differentiation of isorhoifolin and rhoifolin, but an increase in the relative intensity of this key ion, which would be desirable, could not be obtained for the [Co(II) (L-H) bpy]$^+$ complexes.

3.4.3.3 Group II Differentiation (MW 448)

The CAD spectra for the Group II [Co(II) (L – H) bpy]$^+$ complexes are shown in Figure 3-8, and the MS^3 data is tabulated in Table 4. The CAD spectrum of the [Co(II) (L – H) bpy]$^+$ complex of orientin was the most interesting of the five Group II isomers, with cross-ring cleavages corresponding to both paths B and C (leading to the ions at m/z 542 and 572), in addition to loss of the entire sugar (path A, formation of m/z 500). This isomer is clearly differentiated based on these cross-ring cleavages (Figure 3-8a).

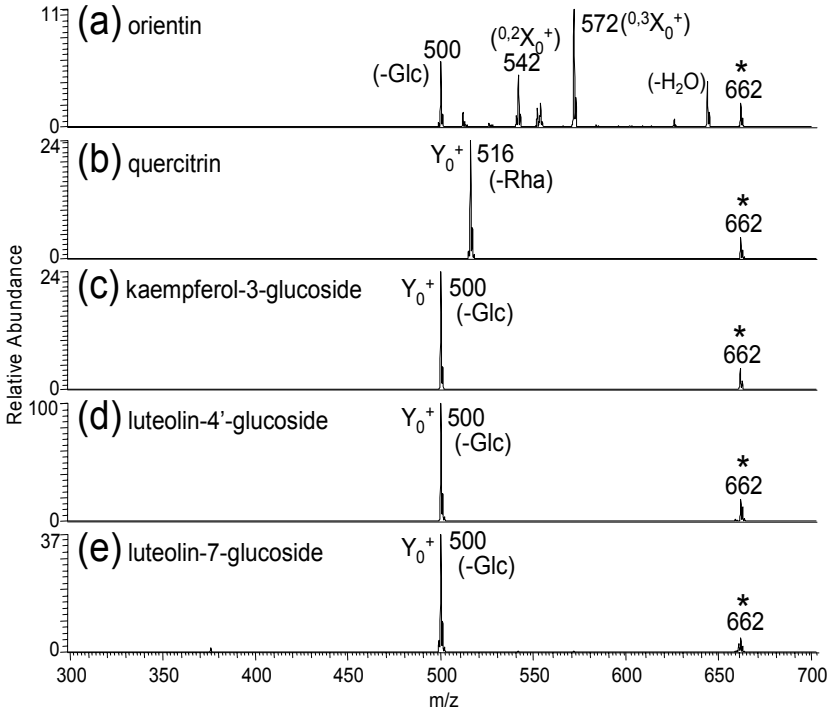

Figure 3-8. CAD spectra of [Co(II) (L-H) bpy]$^+$ complexes of Group II flavonoids. The parent ions are labeled with asterisks.

Table 3-4. MS^n spectra of Group II [Co(II) (L-H) bpy]$^+$ complexes.

		MS/MS[1]			MS/MS/MS[1]		
	m/z	**m/z**	**Loss**	**%**	**m/z**	**Loss**	**%**
orientin	662	572	90	100			
		500	162	60			
		542	120	45			
		644	18	40			
		541	121	10			
		528	134	15			
quercitrin	662	516	146	100			
kaempferol-3-glucoside	662	500	162	100	380	120	100
					233	267	13
					247	253	11
					472	28	8
					362	138	8
					308	192	7
					442	58	5
luteolin-4'-glucoside	662	500	162	100	380	120	100
					362	138	12
					472	28	5
					394	106	5
luteolin-7-glucoside	662	500	162	100	380	120	100
					233	267	34
					247	253	23
					362	138	11
					472	28	5
					394	106	5
					443	57	3

[1]MS/MS and MS/MS/MS data correspond to their parent ions (labeled m/z) on the left. The standard deviations of the fragment ion intensities are typically +/- 5%.

In addition, the [Co(II) (L – H) bpy]$^+$ complex of quercitrin is easily differentiated from the others because of its loss of Rha, resulting in the Y_0^+ complex at m/z 516 (Figure 3-8b), similar to what was observed for the deprotonated flavonoid. The

remaining three isomers, the O-glucosides, each dissociate by loss of their terminal sugars, resulting in Y_0^+ complexes at m/z 500 (Figure 3-8c, d and e), again like what was observed for the deprotonated isomers. These isomers are not differentiated via their MS^3 spectra either (Table 4). For example, isolation and CAD of the major primary fragment ion at m/z 500 for each isomer results in a dominant apparent loss of 120 Da which is the elimination of 2,2'-bipyridine and addition of two molecules of water (Scheme 1, path E), and the apparent loss of 138 Da which is the elimination of 2,2'-bipyridine and addition of one molecule of water. In addition, there are ions at m/z 233 and 247 which are non-specific complexes of 2,2'-bipyridine and cobalt with water or methanol, respectively. The inability to differentiate the two luteolin-glucoside isomers remained a persistent problem, and prompted us to consider the examination of other metal complexes.

3.4.4 Complexation with Cobalt and 4,7-Diphenyl -1,10-phenanthroline

Based on the improvements in isomer differentiation obtained for the [Co(II) (L – H) bpy]$^+$ complexes, the use of alternative auxiliary ligands in the metal complexes was explored with the goal of increasing the "tunability" of the CAD patterns and generating more distinctive fragmentation patterns for each set of isomers, particularly for rhoifolin and isorhoifolin in Group Ib and the three undifferentiated isomers in Group II (kaempferol-3-glucoside, luteolin-4'-glucoside, and luteolin-7-glucoside). The various auxiliary ligands were assessed based on the overall signal intensity of the metal complexes and the number and intensity of the diagnostic fragment ions observed in the CAD mass spectra. The following ligands were evaluated in comparison to the results obtained for the 2,2'-bipyridine complexes: 2,2':6',2"-terpyridine, 1,10-phenanthroline, 4,4'-dimethyl-2,2'-bipyridine and 4,7-diphenyl-1,10-phenanthroline. These ligands were selected because they retain the chelating ability attributed to the 2,2'-bipyridine

skeleton, but their metal affinities are altered by the electron-releasing alkyl groups appended remote from the nitrogen atoms.[77] An example of the series of CAD mass spectra obtained by varying the auxiliary ligand is shown in Figure 3-9 for rhoifolin with cobalt.

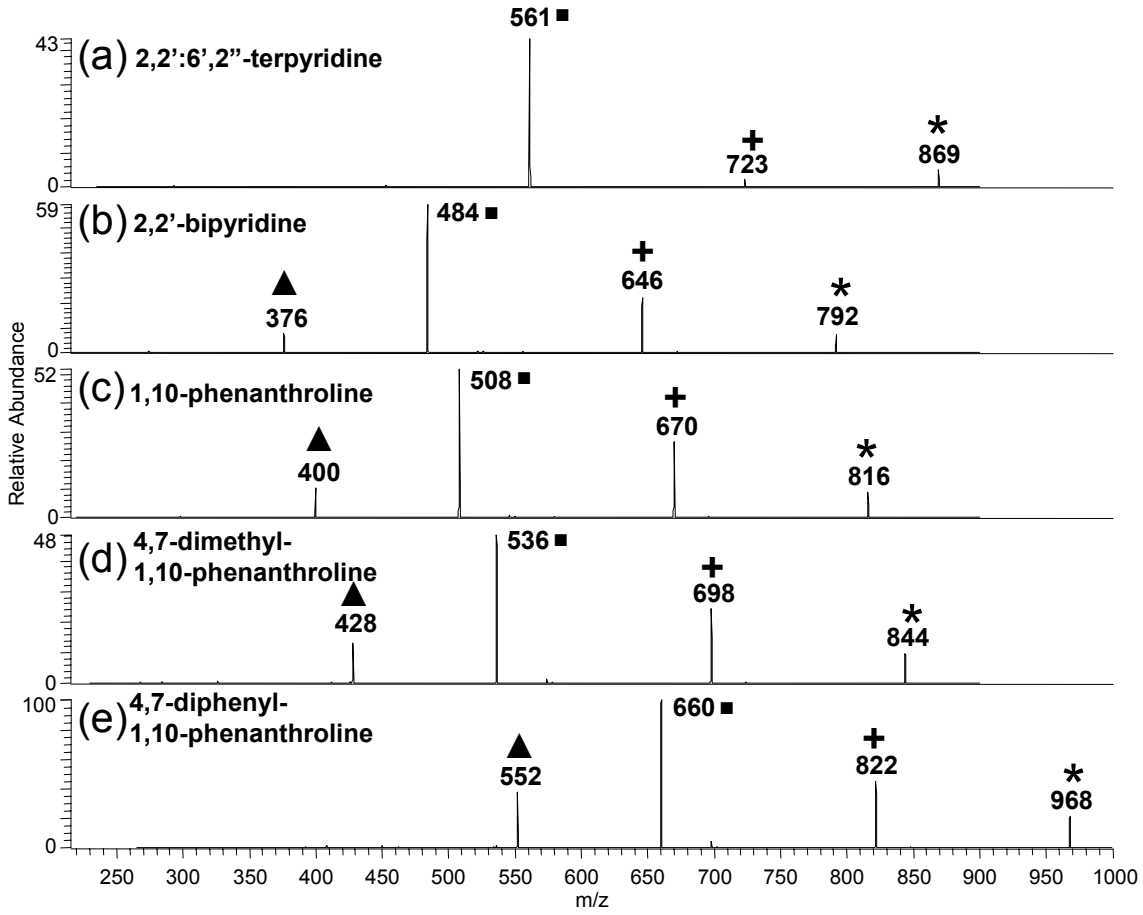

Figure 3-9. CAD mass spectra of [Co(II) (rhoifolin-H) pyridyl ligand]$^+$ complexes, showing relative intensities of the losses of aglycon and Rha with the variation of auxiliary ligand. The parent ion is designated with an asterisk, the loss of Rha is designated by a plus sign, the loss of disaccharide is designated by a solid box, and the loss of the aglycon and Rha is designated by a solid triangle.

For the spectra shown in Figure 3-9, the CAD energy was adjusted to give approximately the same level of parent ion survival, thus allowing a clear comparison of the competition among the three dominant dissociation channels for the complexes containing different auxiliary ligands. The intensity of the ion due to the consecutive losses of aglycon and Glc increased ongoing from the complexes containing 2,2':6,2"-terpyridine to 4,7-diphenyl-1,10-phenanthroline, corresponding with the increasing binding energy of the pyridyl ligand to cobalt in the gas phase as determined previously by energy-variable CAD.[77] Based on a comparative assessment, 4,7-diphenyl-1,10-phenanthroline (dpphen) resulted in metal complexes that gave the most distinctive CAD patterns, so it was used for the remainder of the study. In general, the types of fragment ions observed upon dissociation of the $[Co(II) (L - H) dpphen]^+$ complexes are the same as those already observed and rationalized for the $[Co(II) (L - H) bpy]^+$ complexes. However, the intensities of some of the key diagnostic ions which allow differentiation of isomers are increased for the $[Co(II) (L - H) dpphen]^+$ complexes, and a few new diagnostic ions are also observed upon CAD.

3.4.4.1 Group Ia Differentiation:Vitexin, Isovitexin and Apigenin-7-Glucoside (MW 432)

The CAD mass spectra of the Group Ia complexes $[Co(II) (L - H) dpphen]^+$ are shown in Figure 3-10, and the MS^n results are summarized in Table 5. As noted for the $[Co(II) (L - H) bpy]^+$ complex, the CAD spectrum for the $[Co(II) (L - H) dpphen]^+$ complex of apigenin-7-glucoside complex contains only one major ion (Y_0^+ complex) due to the loss of the Glc (Figure 3-10a), but the ion due to the subsequent loss of the aglycon (m/z 552) is more intense for this complex (12% for the dpphen complex versus 4% for the bpy complex, Figure 3-6a versus 3-10a).

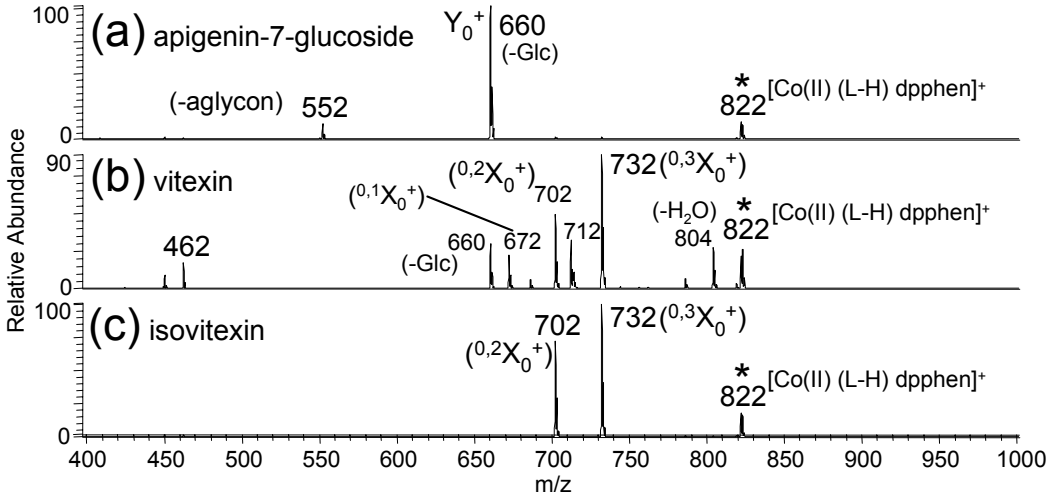

Figure 3-10. CAD spectra of parent [Co(II) (L-H) dpphen]$^+$ complexes of Group Ia flavonoids. The parent ions are labeled with asterisks.

Table 3-5. MS^n spectra of Group I [Co(II) (L-H) dpphen]$^+$ complexes.

		MS/MS[1]			MS/MS/MS[1]		
	m/z	m/z	Loss	%	m/z	Loss	%
apigenin-7-glucoside	822	660	162	100	404	256	100
					430	230	76
					632	28	41
					408	252	18
					484	176	12
					364	296	11
		552	270	12			
vitexin	822	732	90	100	673	59	100
					714	18	34
					686	46	26
					702	30	16
					660	72	8
		702	120	56	673	29	100
					645	57	22
		712	110	36			
		660	162	35			
		804	18	30	786	18	100

					673	131	31
					744	60	21
					701	103	15
		672	150	24			
		462	360	21			
		450	372	12			
isovitexin	822	732	90	100	673	59	100
					712	20	76
					714	18	64
					450	282	42
					686	46	38
					392	340	38
					408	324	19
					462	270	17
					424	308	13
		702	120	74	684	18	100
					673	29	94
					408	294	76
					672	30	62
					392	310	41
					645	57	22
rhoifolin	968	660	308	100	404	256	100
					430	230	75
					632	28	40
		822	146	32	660	162	
					552	270	
		552	416	30	450	102	100
					392	160	92
					408	144	40
					462	90	28
					424	128	26
isorhoifolin	968	660	308	100	404	256	100
					430	230	82
					632	28	45
		822	146	26	660	162	100
					552	270	12

[1]MS/MS and MS/MS/MS data correspond to their parent ions (labeled m/z) on the left. The standard deviations of the fragment ion intensities are typically +/- 5%.

The CAD pattern of the [Co(II) (L – H) dpphen]$^+$ complex of isovitexin is virtually the same as the one observed above for the analogous [Co(II) (L – H) bpy]$^+$ complex. The CAD spectrum of the [Co(II) (vitexin – H) dpphen] complex also contains two additional non-specific product ions (m/z 450 and 462, Figure 3-10b), which are dpphen-containing ions and not diagnostic for vitexin.

3.4.4.2 Group Ib Differentiation: Rhoifolin and Isorhoifolin (MW 578)

The major fragmentation pathways seen in the CAD mass spectra of the [Co(II) (L – H) dpphen]$^+$ complexes of rhoifolin and isorhoifolin (Figure 3-11a and 3-11b) are the same as those observed above for the analogous [Co(II) (L – H) bpy]$^+$ complexes (Figure 3-7a and 3-7b).

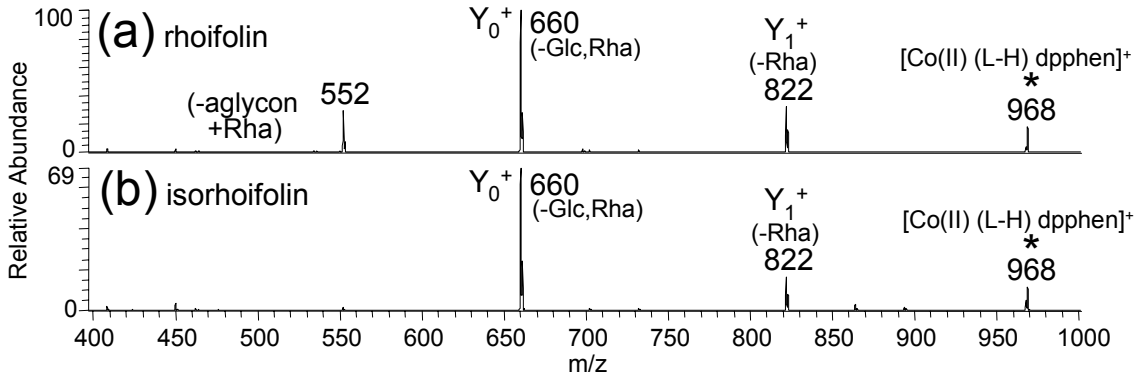

Figure 3-11. CAD spectra of parent [Co(II) (L-H) dpphen]$^+$ complexes of Group Ib flavonoids. The parent ions are labeled with asterisks.

A difference is that the key diagnostic ion for identifying rhoifolin (i.e. the pathway due to loss of the aglycon and Glc moieties, m/z 552) is significantly more pronounced for the [Co(II) (L – H) dpphen]$^+$ complex (30% relative intensity for the dpphen complexes versus 10% relative intensity for the corresponding bpy complex, m/z 376). This subtle but important change in the CAD mass spectrum is a good

demonstration of the ability to tune the fragmentation patterns and enhance the differentiation of isomers by modifying the metal affinity of the auxiliary ligand. A relatively small difference in the metal affinity of the auxiliary ligand alters the energetics for dissociation of the complex, thus changing both the accessibility of and competition among different fragmentation channels.

3.4.4.3 Group II Differentiation (MW 448)

Shown in Figure 3-12 are the CAD mass spectra of the $[Co(II) (L - H) dpphen]^+$ complexes of the Group II isomers. The CAD mass spectra of the $[Co(II) (L - H) dpphen]^+$ complexes of the Group II flavonoids are generally similar to those observed and rationalized above for the $[Co(II) (L - H) bpy]^+$ complexes (Figure 3-8), with a few exceptions. For example, the fragmentation pattern of the orientin complex (Figure 3-12a) has one extra diagnostic ion (loss of 110 amu, m/z 728). Also, the luteolin-7-glucoside isomer is now differentiated from luteolin-4'-glucoside by a new fragment ion stemming from the loss of the aglycon with the loss of the terminal sugar, resulting in the fragment ion at m/z 552 with 10% relative intensity (Figure 3-12e).

While kaempferol-3-glucoside and luteolin-4'-glucoside were better differentiated in the negative ion mode (Figure 3-4), luteolin-7-glucoside was only differentiated by using metal complexation. To differentiate kaempferol-3-glucoside and luteolin-4'-glucoside, the pair of isomers that remained the most resistant to mass spectral differentiation using metal complexation, MS^3 experiments were performed. In the MS/MS/MS spectra obtained for the [Co(II) (L – H) dpphen]+ complexes based on isolation and activation of the primary fragment ion (m/z 676, loss of the sugar, 162 Da), there are now numerous secondary fragment ions which uniquely differentiate kaempferol-3-glucoside from luteolin-4'-glucoside. These three isomers are a good example of how metal complexation may be used in conjunction with the negative ion

mode for complete isomer differentiation. The MS^n data for the complexes of the Group II isomers with Co/dpphen is tabulated in Table 3-6.

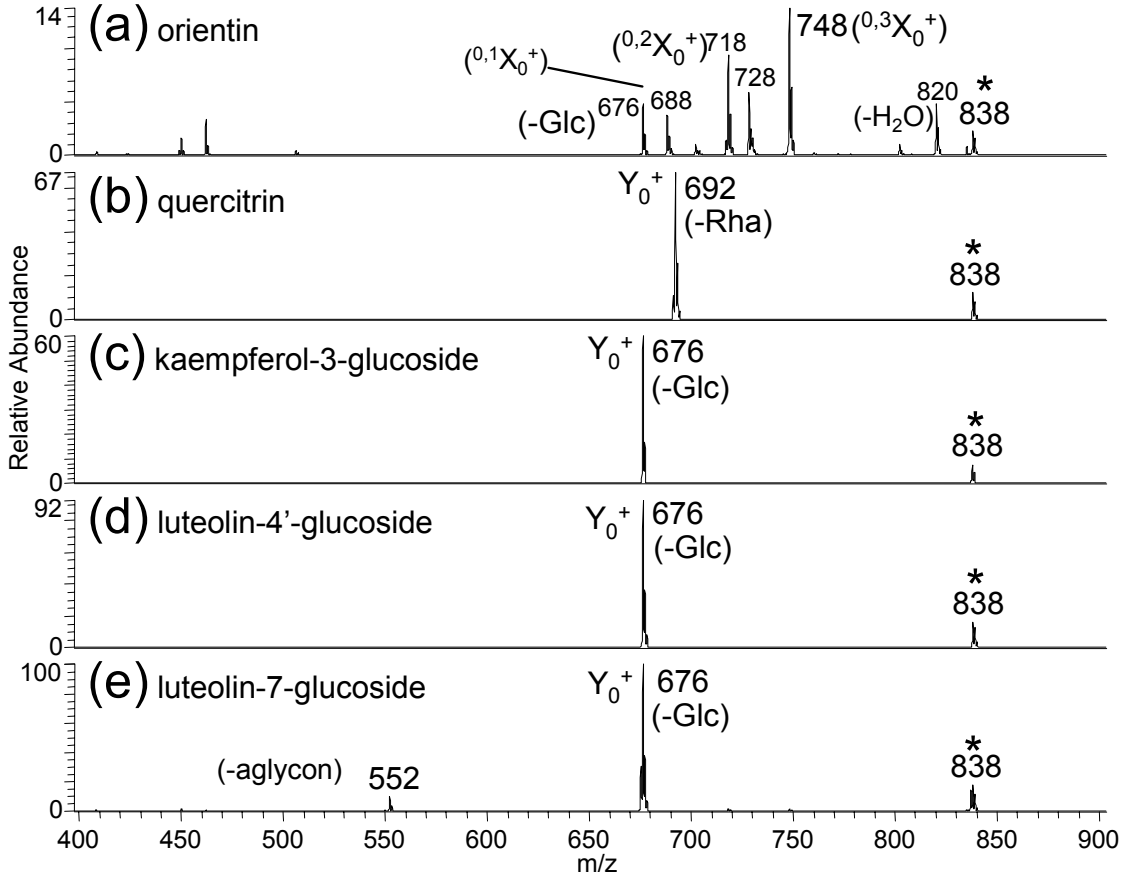

Figure 3-12. CAD spectra of parent $[Co(II)\ (L\text{-}H)\ dpphen]^+$ complexes of Group II flavonoids. The parent ions are labeled with asterisks.

3.4.4.4 Position of Glycosylation

Since complexation with cobalt and dpphen resulted in the most interesting fragmentation patterns in this chapter, it is worthwhile to compare the general types of diagnostic ions observed as a function of the positions of glycosylation for the various flavonoids. For example, it is interesting to note that for C-bonded isomers (vitexin, isovitexin, orientin), the $^{0,1}X_0^+$ is only observed for those flavonoids glycosylated at the

8-position as with vitexin and orientin (Figures 3-10b and 3-12a, respectively), but not for glycosylation at the 6-position as in the isovitexin isomer (Figure 3-10c).

Table 3-6. MS^n spectra of Group II $[Co(II)\ (L\text{-}H)\ dpphen]^+$ complexes.

		MS/MS[1]			MS/MS/MS[1]		
	m/z	**m/z**	**Loss**	**%**	**m/z**	**Loss**	**%**
orientin	838	748	90	100			
		718	120	71			
		728	110	46			
		820	18	36			
		676	162	32			
		688	150	29			
		462	376	25			
		450	388	11			
quercitrin	838	692	146	100			
kaempferol-3-glucoside	838	676	162	100	408	268	100
					423	253	48
					484	192	28
					648	28	19
					404	272	18
					496	180	13
					632	44	9
					392	284	9
					333	343	5
luteolin-4'-glucoside	838	676	162	100	404	272	100
					430	246	67
					648	28	53
					408	268	30
					658	18	30
					647	27	27
					630	46	20
					620	56	13
					392	284	12
					442	234	12
					500	176	10
					524	152	7
luteolin-7-glucoside	838	676	162	100	408	268	100
					423	253	51
					404	272	14
					619	57	10
					430	246	10
		675	163	30			
		552	286	11			

[1]MS/MS and MS/MS/MS data correspond to their parent ions (labeled m/z) on the left. The standard deviations of the fragment ion intensities are typically +/- 5%.

For the 7-O-bonded glucosides (apigenin-7-glucoside, rhoifolin, isorhoifolin, luteolin-7-glucoside), the loss of the aglycon or the aglycon and terminal sugar is always observed (Figures 3-10a, 3-11a and 3-12e) except for the rutinosides. The lack of this pathway for 7-O-bonded rutinoside isorhoifolin (Figure 3-11b) is likely related to the site of metal complexation and/or conformation of the disaccharide when coordinated to the metal ion. These general trends in the diagnostic ions observed with the position of glycosylation are an extremely useful feature of metal complexation for structural determination of flavonoids.

3.5 CONCLUSIONS

Metal complexation with an auxiliary ligand has been used to differentiate flavonoid glycoside isomers by ESI-tandem mass spectrometry. In the presence of a metal and an appropriate auxiliary ligand, complexes of the type [Co(II) (flavonoid-H) ligand]$^+$ are formed which are generally one to two orders of magnitude greater in intensity than the intensities of the molecular ions observed in positive or negative ionization modes, thereby improving limits of detection. CAD of the metal complexes results in fragmentation patterns which are often different that those of the protonated or deprotonated species and may be used separately or in conjunction with these modes for isomer differentiation. This general metal complexation technique has been improved with the use of 4,7-diphenyl-1,10-phenanthroline as a new auxiliary chelating ligand. In particular, the differentiation of disaccharide isomers with 1$\rightarrow$ 2 and 1$\rightarrow$ 6 linkages and the two luteolin-glucoside isomers is now possible based on formation and detection of unique fragment ions for each isomer.

3.6 REFERENCES

1. Pietta, P., Flavonoids in Medicinal Plants. In *Flavonoids in Health and Disease,* Rice-Evans, C.A.; Packer, L., Eds.; Marcel Dekker: New York, 1998; p. 62.

2. Berhow, M.A.; Vaughn, S.F., In *Principles and Practices in Plant Ecology, Allochemical Interactions;* CRC Press: Boca Raton, FL, 1999; pp. 423-437.

3. Lin, Y.Y.; Ng, K.J.; Yang, S. *J. Chromatogr.* **1993**, *629,* 389-393.

4. Morand, C.; Crespy, V.; Manach, C.; Besson, C.; Demigne, C.; Remesy, C. *Am. J. Physiol.* **1998**, *275*, R212-R219.

5. Rice-Evans, C.A.; Miller, N.J. *Biochem. Soc. Trans.* **1996**, *24*, 790-795.

6. Pratt, D.E. *ACS Symp. Ser.* **1992***, No. 507*, 54-71.

7. Dixon, R.A.; Steele, C.L. *Trends Plant Sci.* **1999**, *4*, 394-400.

8. Hertog, M.G.L.; Kromhout, D.; Aravanis, C.; Blackburn, H.; Buzina, R.; Fidanza, F.; Giampaoli, S.; Jansen, A.; Menotti, A.; Nedeljkovic, S.; Pekkarinen, M.; Simic, B.S.; Toshima, H.; Feskens, E.J.M.; Hollman, P.C.H.; Katan, M.B. *Arch. Intern. Med.* **1995***, 155,* 381-386.

9. Hertog, M.G.; Feskens, E.J.M.; Hollman, P.C.H.; Katan, M.B.; Kromhout, D. *Lancet* **1993***, 342,* 1007-1011.

10. Knekt, P.; Jarvinen, R.; Reunanen, A.; Maatela, J. *Br. Med. J.* **1996***, 312,* 478-481.

11. Bors, W.; Heller, W.; Michel, C., The Chemistry of Flavonoids. In *Flavonoids in Health and Disease,* Rice-Evans, C.A.; Packer, L., Eds.; Marcel Dekker: New York, 1998; p. 111-136.

12. Stobiecki, M. *Phytochemistry* **2000***, 54,* 237-256.

13. Mabry, T.J; Markham, K.R., Mass Spectrometry of Flavonoids. In *The Flavonoids*, Harborne, J.B.; Mabry, T.J.; Mabry, H., Eds.; Academic Press: New York, 1975, p. 79-126.

14. Besson, E.; Besset, A.; Bouillant, M.-L.; Chopin, J.; van Brederode, J.; van Nigtevecht, G. *Phytochemistry* **1979***, 18,* 657-658.

15. Bouillant, M.-L.; Ferreres de Arce, F.; Favre-Bonvin, J.; Chopin, J.; Zoll, A.; Mathieu, G. *Phytochemistry* **1984***, 23,* 2653-2657.

16. Sakushima, A.; Nishibe, S. *Phytochemistry* **1988***, 27,* 948-950.

17. Schels, H.; Zinsmeister, H.D.; Pfleger, K. *Phytochemistry* **1978***, 17, 523-526.*

18. Becchi, M.; Fraisse, D. *Biomed. Environm. Mass Spectrom.* **1989***, 18,* 122-130.

19. Bridle, P.; Loeffler, R.S.T.; Timberlake, C.F.; Self, R. *Phytochemistry* **1984***, 23,* 2968-2969.

20. Claeys, M.; Li, Q.; Van den Heuvel, H.; Dillen, L., Mass Spectrometric Studies on Flavonoid Glycosides. In *Applications of Modern Mass Spectrometry in Plant Sciences*, Newton, R.P.; Walton, T.J. Eds.; Clarendon Press: Oxford, 1996, pp. 182-194.

21. Crow, F.C.; Tomer, K.B.; Looker, J.H.; Gross, M.L. *Anal. Biochem.* **1986***, 155,* 286-297.

22. Domon, B.; Hostettmann, K. *Phytochemistry* **1985***, 24,* 575-580.

23. Li, Q.M.; van den Heuvel, H.; Dillen, L.; Claeys, M. *Biol. Mass Spectrom.* **1992***, 21,* 213-221.

24. Li, Q.M.; Claeys, M. *Biol. Mass Spectrom.* **1994***, 23,* 406-416.

25. Saito, N.; Abe, K.; Honda, R.; Timberlake, C.F.; Bridle, P. *Phytochemistry* **1985***, 24,* 1583-1586.

26. Sakushima, A.; Nishibe, S.; Takeda, T.; Ogihara, Y. *Mass Spectroscopy* **1988***, 36,* 71-80.

27. Sakushima, A.; Nishibe, S. *Phytochemistry* **1988***, 27,* 915-919.

28. Stobiecki, M.; Olechnowicz-Stepien, W.; Rzadkowska-Bodalska, H.; Cisowski, W.; Budko, E. *Biomed. Environm. Mass Spectrom.* **1988***, 15,* 589-594.

29. Sumner, L.W.; Paiva, N.L.; Dixon, R.A.; Geno, P.W. *J. Mass Spectrom.* **1996***, 31,* 472-485.

30. Wolfender, J.-L.; Maillard, M.; Marston, A.; Hostettmann, K. *Phytochem. Anal.* **1992***, 3,* 193-214.

31. Ma, Y.L.; Li, Q.M.; Van den Heuvel, H.; Claeys, M. *Rapid Commun. Mass Spectrom.* **1997***, 11,* 1357-1364.

32. Cuyckens, F.; Shahat, A.A.; Pieters, L.; Claeys, M. *J. Mass Spectrom.* **2002***, 37,* 1272-1279.

33. Ma, Y.-L.; Cuyckens, F.; Van den Heuvel, H.; Claeys, M. *Phytochem. Anal.* **2001***, 12,* 159-165.

34. Ma, Y.L.; Van den Heuvel, H.; Claeys, M. *Rapid Comm. Mass Spectrom.* **1999***, 13,* 1932-1942.

35. Ma, Y.-L.; Vedernikova, I.; Van den Heuvel, H.; Claeys, M. *J. Am. Soc. Mass Spectrom.* **2000***, 11,* 136-144.

36. Hughes, R.J.; Croley, T.R.; Metcalfe, C.D.; March, R.E. *Int. J. Mass Spectrom.* **2001***, 210/211,* 371-385.

37. Brolis, M.; Gabetta, B.; Fuzzati, N.; Pace, R.; Panzeri, F.; Peterlongo, F. *J. Chromatogr. A* **1998***, 825,* 9-16.

38. Pietta, P.; Facino, R.M.; Carini, M.; Mauri, P. *J. Chromatogr. A* **1994***, 661,* 121-126.

39. Iida, J.; Murata, R. *Analytical Sciences* **1991***, 7,* 963-966.

40. Grayer, R.J.; Kite, G.C.; Abou-Zaid, M.; Archer, L.J. *Phytochem. Anal.* **2000***, 11,* 257-267.

41. Jensen, A.G.; Ndjoko, K.; Wolfender, J.-L.; Hostettmann, K.; Camponovo, F.; Soldati, F. *Phytochem. Anal.* **2002***, 13,* 31-38.

42. Krishnan, H.B. *Crop Sci.* **1998***, 38,* 1052-1056.

43. Barnes, K.A.; Smith, R.A.; Williams, K.; Damant, A.P.; Shepherd, M.J. *Rapid Commun. Mass Spectrom.* **1998***, 12,* 130-138.

44. Poon, G.K. *J. Chromatogr., A* **1998***, 794,* 63-74.

45. Fabre, N., Rustan, I., de Hoffmann, E., Quetin-Leclercq, J. *J. Am. Soc. Mass Spectrom*., **2001**, *12,* 707-715.

46. Raffaelli, A.; Moneti, G.; Mercati, V.; Toja, E. *J. Chromatogr., A* **1997***, 777,* 223-231.

47. Stevens, J.F.; Taylor, A.W.; Deinzer, M.L. *J. Chromatogr., A* **1999***, 832,* 97-107.

48. Hakkinen, S.H.; Karenlamp, S.O.; Herinonen, I.M.; Mykkanen, H.M.; Torronen, A.R. *J. Agric. Food Chem.* **1999***, 47,* 2274-2279.

49. Satterfield, M.; Black, D.M.; Brodbelt, J.S. *J. Chromatogr. B* **2001,** *759,* 33-41.

50. Cuyckens, F.; Rozenburg, R.; Hoffmann, E.; Claeys, M. *J. Mass Spectrom.* **2001**, *36*, 1203-1210.

51. Waridel, P.; Wolfender, J.-L.; Ndjoko, K.; Hobby, K.R.; Major, H.J.; Hostettmann, K. *J. Chromatogr. A* **2001***, 926,* 29-41.

52. Hvattum, E.; Ekeberg, D. *J. Mass Spectrom.* **2003***, 38,* 43-49.

53. Alvarez E.; Vartanian, V.; Brodbelt, J.S. *Anal. Chem.* **1997***, 69,* 1147-1155.

54. Alvarez, E.; Brodbelt, J.S. *J. Am. Soc. Mass Spectrom.* **1998***, 9,* 463 - 472. *Rapid Comm. Mass Spectrom.* **1999***, 13,* 1381-1389.

56. Satterfield, M.; Brodbelt, J.S. *Anal. Chem.* **2000***, 72,* 5898-5906.

57. Satterfield, M.; Brodbelt, J.S. *J. Am. Soc. Mass Spectrom*., **2001***, 12,* 537-549.

58. Zhang, J.; Brodbelt, J.S. *J. Mass Spectrom.* **2003**, *38*, 555-572.

59. Mateos, R.; Espartero, J.L.; Trujillo, M.; Rios, J.J.; Leon-Camacho, M.; *J. Agric. Food Chem.* **2001**, *49,* 2185-2192.

60. Gil-Izquierdo, A.; Gil, M.I.; Ferreres, F.; Tomas-Barberan, F.A. *J. Agric. Food Chem.* **2001**, *49*, 1035-1041.

61. Trichopoulou, A.; Vasilopoulou, E.; Hollman, P.; Chamalides, Ch.; Foufa, E.; Kaloudis, Tr.; Kromhout, D.; Miskaki, Ph.; Petrochilou, I.; Poulima, E.; Stafilakis, K.; Theophilou, D. *Food Chem.* **2000**, *70*, 319-323.

62. Miean, K.; Mohamed, S. *J. Agric. Food Chem.* **2001**, *49,* 3106-3112.

63. Bilyk, A.; Sapers, G.M. *J. Agric. Food Chem.* **1985**, *33,* 226-228.

64. Price, K.R.; Colquhoun, I.J.; Barnes, K.A.; Rhodes, M.J.C. *J. Agric. Food Chem.* **1998**, *46,* 4898-4903.

65. Karadeniz, F.; Durst, R.; Wrolstad, R. *J. Agric. Food Chem.* **2000**, *48,* 5343-5350.

66. Hertog, M.; Hollman, P.; Venema, D. *J. Agric. Food Chem.* **1992**, *40,* 1591-1598.

67. Domon, B.; Costello, C.E. *Glycoconjugate J.* **1988***, 5,* 397-409.

68. Quemener, B.; Desire, C.; Debrauwer, L.; Rathahao, E. *J. Chrom. A*., **2003**, *984,* 185-194.

69. Pfenninger, A.; Karas, M.; Finke, B.; Stahl, B. *J. Am. Soc. Mass Spectrom.*, **2002**, *13,* 1331-1340.

70. Sheeley, D.M.; Reinhod., V.N. *Anal. Chem*., **1998**, *70,* 3053-3059.

71. Salpin, J.-Y.; Tortajada, J. *J. Mass Spectrom*., **2002**, *37,* 379-388.

72. Reid, G.E.; O'Hair, A.J.; Styles, M.L.; McFadyen, W.D.; Simpson, R.J. *Rapid Commun. Mass Spectrom*., **1998**, *12,* 1701-1708.

73. Vachet, R.W.; Hartman, J.A.R.; Callahan, J.H. *J. Mass Spectrom*. **1998**, *33,* 1209-1225.

74. Vachet, R.W.; Hartman, J.A.R.; Gerner, J.W.; Callahan, J.H. *Int. J. Mass Spectrom.* **2001**, *204,* 101-112.

75. Perera, B.A.; Gallardo, A.L.; Barr, J.M.; Tekarli, S.M.; Anbalagan, V.; Talaty, E.R.; Van Stipdonk, M.J. *J. Mass Spectrom.* **2002***, 37,* 401-413.

76. Perera, B.A.; Ince, M.P.; Talaty, E.R.; Van Stipdonk, M.J. *Rapid Commun. Mass Spectrom.* **2001***, 15,* 615-622.

77. Satterfield, M.; Brodbelt, J.S. *Inorg. Chem.* **2001***, 40,* 5393-5400.

Chapter 4: Tunable Transition Metal-Ligand Complexation for Enhanced Elucidation of Flavonoid Diglycosides by Electrospray Ionization Mass Spectrometry

4.1 OVERVIEW

A tunable ESI-MS/MS strategy for differentiation of flavone and flavanone diglycoside isomers based on metal complexation with auxiliary ligands is described in this chapter. The addition of a metal salt and an auxiliary ligand to a flavonoid solution results in the formation of [M(II) (flavonoid-H) auxiliary ligand]$^+$ complexes, where M(II) is a transition metal. A series of auxiliary ligands with electron-withdrawing substituents were synthesized in order to tailor the relative metal binding affinities of the ligands and thus directly influence the stabilities, and consequently the dissociation pathways, of the complexes. Upon collisionally activated dissociation, the complexes yield fragmentation patterns in which the abundances of key diagnostic ions are enhanced, thus facilitating isomer differentiation.

4.2 INTRODUCTION

Differentiation of isomers remains a challenging analytical problem, and confirming structures of isomers is difficult even when they can be adequately separated from mixtures. Tandem mass spectrometry has been used extensively for structural elucidation of isomers [1-12] and there continues to be interest in applying existing tandem mass spectrometric methods, such as MS^n,[9, 13, 14] and developing new ones, such as STEP, [15, 16] a statistical-based method that relies on comparison of abundances of fragment ions obtained for different collision activation conditions, to differentiate isomers. The work presented in this dissertation focuses on the development of metal complexation strategies [17-23] to enhance the differentiation of isomers because metal complexation often

alters the dissociation pathways of ions, thus giving additional diagnostic fragment ions. Several metal complexation strategies that have been useful for distinguishing flavonoid isomers have been reported, and in this chapter we expand this approach by developing a "tunable" CAD method based on the use of rationally selected auxiliary ligands to form metal complexes. The concept of this tunable CAD strategy is applied for the differentiation of flavonoid isomers.

Flavonoids are phytochemicals found in almost all plants, including fruits and vegetables. Several studies have indicated their antioxidant, chemopreventive, anti-viral, anti-bacterial and radical-scavenging properties.[17-21] In addition, they have been implicated in cardiovascular protection.[22-29] While all flavonoids are structurally similar, many exist as glycosides and there are subtle differences in their structure that lead to important changes in their biological activity. These differences include hydroxylation position of the aglycon, glycosylation site, sequence of glycosylation and interglycosidic linkages of the glycan portion. It is because of these subtle differences that there is a need for sensitive analytical techniques to elucidate these similar compounds.

Mass spectrometry has become an ideal tool for the analysis of flavonoids, and two recent reviews provide an excellent background of the techniques used and the analyses performed.[30, 31] ESI-MS/MS has been used extensively to differentiate several sets of flavonoid isomers over the past decade. For example, for a series of flavonoid diglycosides, CAD has been used to pinpoint the intersaccharide linkages (rutinosides: $1\rightarrow$ 6 disaccharides versus neohesperidosides: $1 \rightarrow 2$ disaccharides) in flavonoid-O-glycosides based on relative abundances of the fragment ions obtained from protonated flavonoids.[7] However, in general it has been noted that flavonoids don't protonate particularly well because they are acidic, phenolic compounds. Although flavonoids deprotonate efficiently, the resulting fragmentation patterns often do not give diagnostic

ions adequate for differentiation of isomers. Metal complexation is an alternative ionization strategy that has been explored in our group for improved analysis of flavonoids,[32-38] and we have explored metal complexation both with and without the use of an auxiliary ligand to produce stable complexes. For example, using an auxiliary ligand, typically a pyridyl-type chelating agent, complexes of the type [M(II) (flavonoid – H) auxiliary ligand]$^+$ are formed. Metal complexation not only provides greater ion abundances but also enhances the structural differentiation of isomeric flavonoids.

In the study presented in the previous chapter, the impact of the auxiliary ligand on the abundances of metal complexes and the resulting fragmentation pathways of the complexes of flavonoid diglycosides was evaluated.[36] It was demonstrated that the nature of the auxiliary ligand affected the types of fragment ions and their abundances in the CAD mass spectra. Specifically, it was found that as the alkyl substituents of the ligands changed (i.e. 1,10-phenanthroline versus 4,7-diphenyl-1,10-phenanthroline), the abundances of several diagnostic fragment ions observed for flavone rutinoside and neohesperidoside isomeric pairs varied systematically. This result revealed that it was possible to tune the CAD spectra by careful selection of the auxiliary ligand. However, the only suitable commercially available auxiliary ligands were ones with electron-releasing alkyl substituents, thus limiting the scope of the study. Electron-releasing substituents increase the metal binding energies of pyridyl ligands and therefore in some cases destabilize the desired [M(II) (flavonoid – H) pyridyl ligand]$^+$ complexes. Pyridyl ligands have intrinsically high metal binding energies, both in solution [39-43] and in the gas phase,[44, 45] due to their ability to chelate metal ions via their nitrogen atoms. Addition of electron-withdrawing substituents should temper the metal binding energies and thus expand the options for creating tunable auxiliary ligands for the differentiation of isomers, such as flavonoids, via metal complexation strategies.

In this chapter, we explore the effect of incorporating electron-withdrawing substituents into the pyridyl ligands for metal complexation, evaluated in terms of the success of differentiating flavonoid isomers. The halogens are interesting substituents because of their inductive electron-withdrawing effects. For assessment of the method, twelve isomers of 7-O-flavonoid diglycosides are evaluated, including three isomeric pairs from the flavone class (both $1 \rightarrow 2$ vs. $1 \rightarrow 6$ disaccharide linkages) and three pairs from the flavanone class ($1 \rightarrow 2$ vs. $1 \rightarrow 6$), (Figure 4-1).

4.3 EXPERIMENTAL

4.3.1 Chemical Reagents

The flavonoids rhoifolin, isorhoifolin, neodiosmin, diosmin and narirutin were purchased from Indofine (Somerville, NJ, USA). Fortunellin, linarin, poncirin and didymin were purchased from Extrasynthese (Genay, France). Naringin, neohesperidin, hesperidin, $CoBr_2$, $CuBr_2$, 2,2'-bipyridine, 6,6'-dibromo-2,2'-bipyridine, 4,4'-dimethyl-2,2'-bipyridine, 1,10-phenanthroline and 5-nitro-1,10-phenanthroline were purchased from Sigma (St. Louis, MO, USA).

4.3.2 Ligand Syntheses

4,4'-dibromo-2,2'-bipyridine was synthesized from 2,2'-bipyridine according to a literature procedure[46, 47] and was purified using silica gel flash chromatography. ^{1}H NMR (CD_3Cl_3) δ = 7.509 (2H, dd, J = 5.2 Hz, 1.6 Hz), 8.486 (2H, d, J = 5.2 Hz), 8.608 (2H, d, J = 1.6 Hz).

4,4'-bis(bromomethyl)-2,2'-bipyridine was synthesized from 4,4'-dimethyl-2,2'-bipyridine according to a literature procedure [48] and was purified using silica gel flash chromatography. ^{1}H NMR (CD_3Cl_3) δ = 7.507 (2H, d, J = 8 Hz), 7.671 (2H, t, J = 7.6 Hz, 8Hz), 8.378 (2H, d, J = 7.6 Hz).

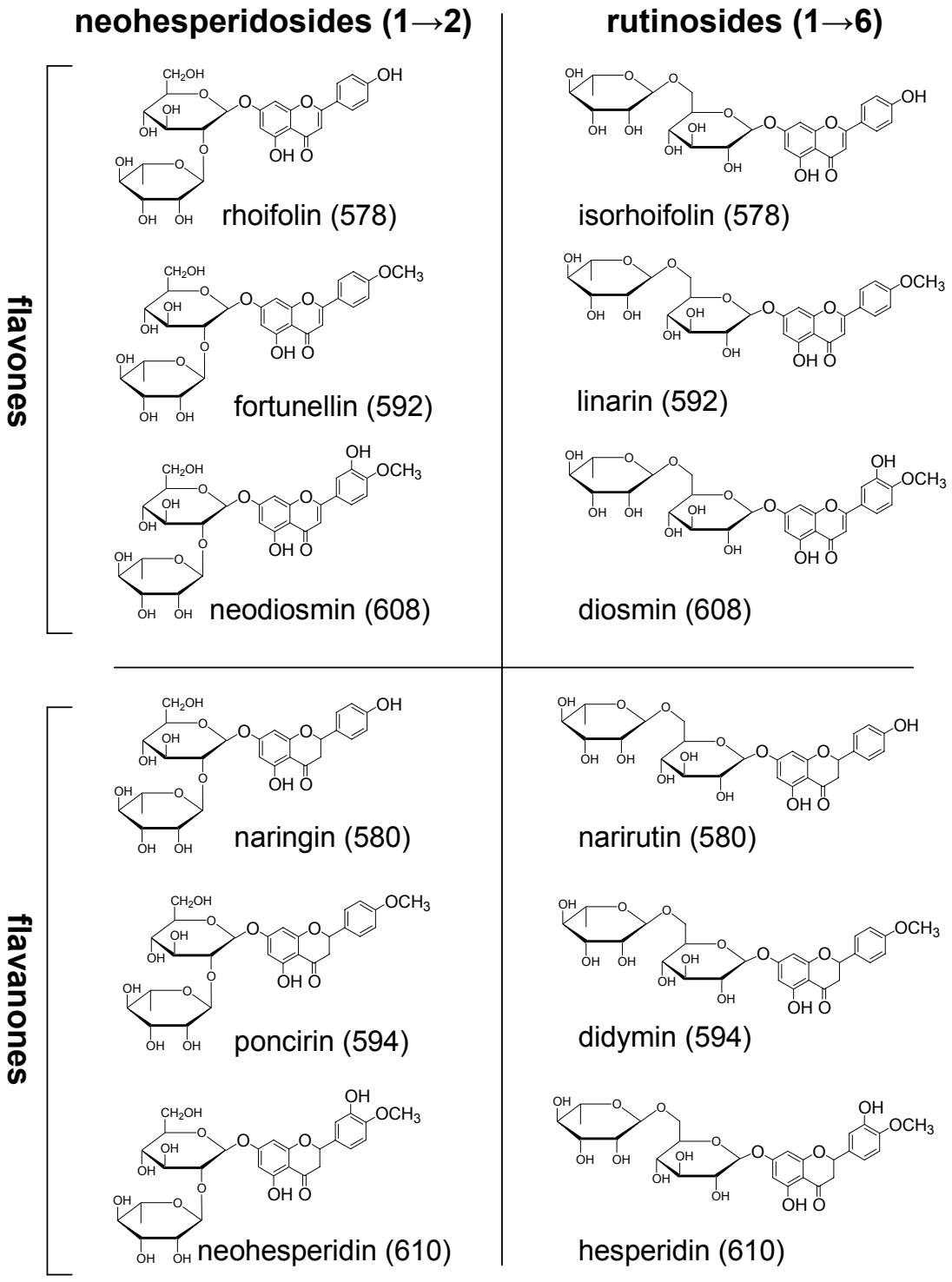

Figure 4-1. 7-O-Flavonoid diglycosides used in this chapter. Molecular weight is indicated in parentheses.

5,6-dibromo-1,10-phenanthroline, 3,5,6-tribromo-1,10-phenanthroline and 3,5,6,8-tetrabromo-1,10-phenanthroline were synthesized from 1,10-phenanthroline according to a literature procedure.[49] The phenanthrolines were purified using successive recrystallizations. 5,6-dibromo-1,10-phenanthroline ^{1}H NMR (CD_3Cl_3) δ = 7.740 (2H, dd, J = 8.4 Hz, 8.0 Hz), 8.782 (2H, dd, J = 8.8 Hz, 1.2Hz), 9.226 (2H, dd, J = 4.4 Hz, 1.2 Hz). 3,5,6-tribromo-1,10-phenanthroline ^{1}H NMR (CD_3Cl_3) δ = 7.748 (1H, dd, J = 8.8 Hz, 4.2 Hz), 8.765 (1H, dd, J = 8.8 Hz, 1.6Hz), 8.928 (1H, d, J = 2 Hz), 9.201 (2H, m). 3,5,6,8-tetrabromo-1,10-phenanthroline ^{1}H NMR (CD_3Cl_3) δ = 8.920 (2H, d, J = 2.2 Hz), 9.190 (2H, d, J = 2 Hz).

A Varian 400 MHz instrument was used for all NMR spectroscopy.

4.3.3 Metal Complexation/Mass Spectrometry

Stock solutions of $4x10^{-4}$ M metal salts and auxiliary ligands were prepared in methanol. Solutions containing the flavonoid, metal salt and auxiliary ligands were prepared in ~1:1:1 ratios at $1x10^{-5}$ M.

The experiments were performed using a Thermo Finnigan (San Jose, CA, USA) LCQ Duo quadrupole ion trap (QIT) mass spectrometer equipped with an electrospray ionization (ESI) source. The flow rate of the solutions was 5 μl min^{-1}. The heated capillary temperature was 200 °C and the ESI voltage was set at +4.5 kV. The ionization times were set to 5-25 ms and each spectrum was an average of 20 scans. The lens and octapole voltages, sheath gas flow rate and capillary voltage were optimized for maximum intensity of the ion corresponding to $[M(II)\ (flavonoid - H)\ L]^+$, where M is the metal and L is the auxiliary ligand. During MS/MS experiments, these parent ions were isolated and the CAD voltage was adjusted so that the parent ion intensity decreased to ~10% of the base peak. An isolation window sufficient to exclude all but the carbon-12 isotope was used for most experiments, and an isolation window sufficient to include all

bromine isotopes was used for confirmation of the presence of the brominated ligands in selected fragment ions.

4.3.4 Molecular Modeling

Preoptimization and generation of coordinates was performed with CAChe Worksystem Pro using MM3/AM1. Final optimization was performed with the Gaussian '03 software package at the B3LYP/6-31G* level.

4.4 RESULTS AND DISCUSSION

A series of six brominated pyridyl ligands were used in this chapter (Figure 4-2), three based on the 2,2'-bipyridine skeleton (4,4'-dibromo-2,2'-bipyridine, 6,6'-dibromo-2,2'-bipyridine, and 4,4'-bis(bromomethyl)-2,2'-bipyridine) and three based on the 1,10-phenanthroline skeleton (5,6-dibromo-1,10-phenanthroline; 3,5,6-tribromo-1,10-phenanthroline; and 3,5,6,8-tetrabromo-1,10-phenanthroline), with the overreaching goal of using them as "tunable" auxiliary ligands for complexation and structural characterization of isomers, as demonstrated specifically for flavonoids. Complexation with 4,4'- and 6,6'-dibromo-2,2'-bipyridine was compared to allow evaluation of the influence of the position of the electron-withdrawing groups. 4,4'-bis(bromomethyl)-2,2'-bipyridine was synthesized to investigate the effect of moving the bromine groups further from the aromatic ring. Three different brominated 1,10-phenanthroline compounds were synthesized to allow evaluation of the impact of the number of bromine groups on formation and dissociation of complexes. 5-nitro-1,10-phenanthroline was used to evaluate the effect of an alternative electron-withdrawing substituent. For the experiments described in the following sections, ESI-MS/MS was used to analyze solutions containing either 2,2'-bipyridine or a brominated ligand in a solution containing one of twelve different flavonoids and either a copper or cobalt salt.

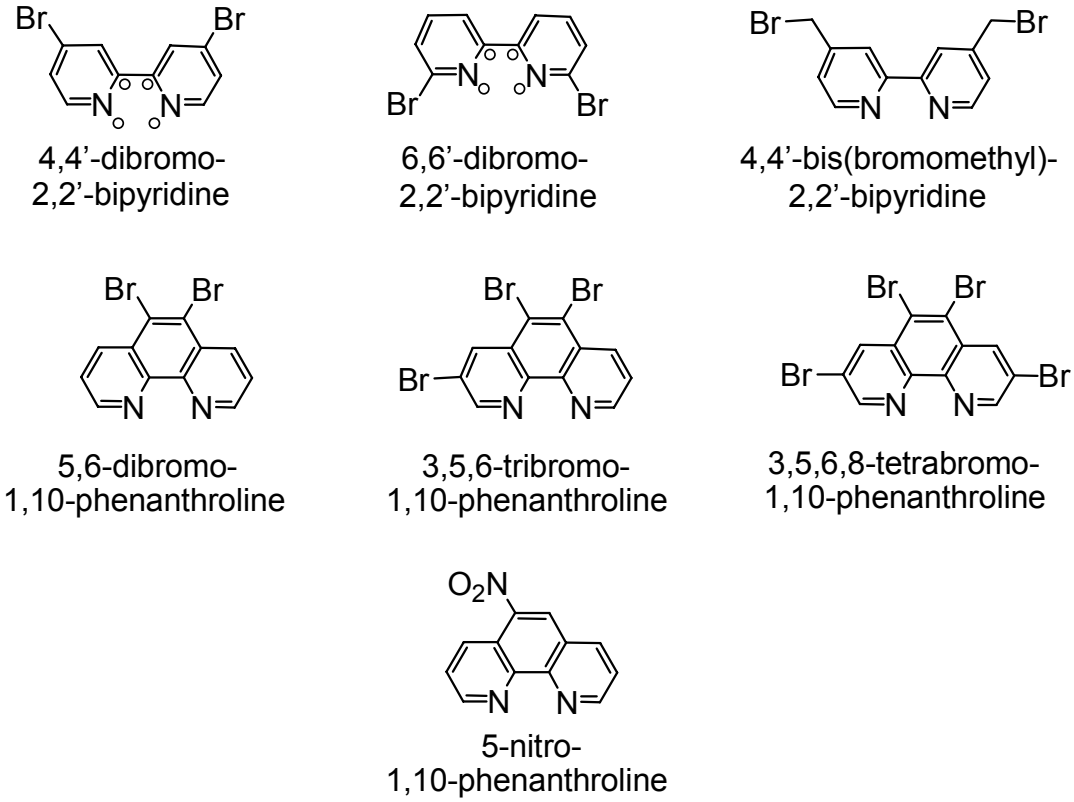

Figure 4-2. Ligands used in this chapter. The '○' symbols represent atoms discussed in the molecular modeling part of the chapter.

4.4.1 Complexation with Bromobipyridines

In the ESI mass spectra of each solution containing one flavonoid with 4,4'-dibromo-2,2'-bipyridine and either $CuBr_2$ or $CoBr_2$, the abundances of the resulting complexes are comparable. The spectra are dominated by the [M(II) (flavonoid - H) 4,4'-dibromo-2,2'-bipyridine]$^+$ complexes, without interference from the formation of numerous other metal-ligand species (Figure 4-3). Division of the total ion current among several different metal-containing products has been one shortcoming noted in some previous metal complexation studies, thus having a negative impact on ultimate detection limits.

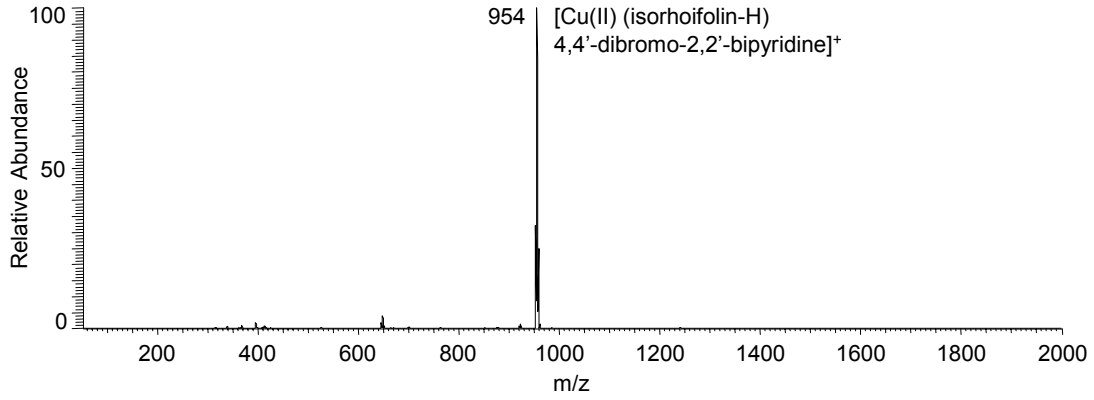

Figure 4-3. Full scan spectrum of a solution of rhoifolin/Cu(II)/4,4'-dibromo-2,2'-bipyridine showing the flavonoid/metal/ligand complex as the dominant species.

Since both copper and cobalt resulted in the formation of equally abundant flavonoid complexes, the CAD spectra were acquired for all the complexes of the flavonoids used in this chapter. Figure 4-4 shows this comparison for one representative flavonoid from each of the four classes summarized in Figure 4-1 (i.e. one flavone neohesperidoside, one flavone rutinoside, one flavanone neohesperidoside, one flavanone rutinoside). All of the copper complexes dissociate predominantly by the loss of the disaccharide moiety, corresponding to the neutral loss of 308 Da (top panel of Figure 4-4). The copper complex of isorhoifolin exhibits two additional fragment ions due to cross-ring cleavages of the disaccharide (cross-ring cleavages are designated by X in the figures) in conjunction with loss of the 4,4'-dibromo-2,2'-bipyridine ligand, yielding the fragment ions at m/z 523 and 495. The cobalt complexes exhibit more intricate fragmentation pathways with unique ions for each flavonoid (bottom panel of Figure 4-4). The most common ones include the loss of the terminal rhamnose group (-146 Da), loss of the disaccharide moiety (-308 Da), loss of the auxiliary 4,4'-dibromo-2,2'-

bipyridine ligand (-314 Da), loss of the aglycon group (-A), and other combined losses thereof.

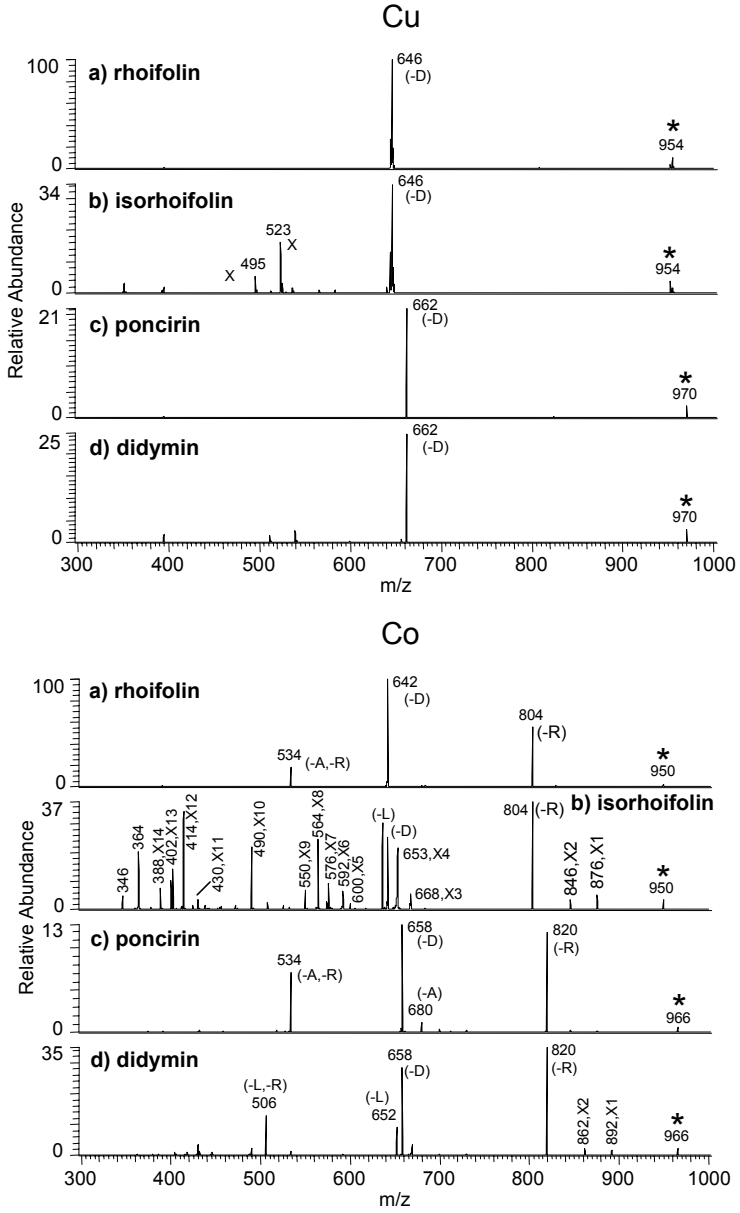

Figure 4-4. Representative spectra for CAD of flavonoid/metal/4,4'-dibromo-2,2'-bipyridine with a flavone rutinoside/neohesperidoside and a flavanone rutinoside/neohesperidoside, comparing the Cu and Co complexes. (-D) indicates the loss of disaccharide moiety, (-R) indicates the loss of rhamnose moiety, (-L) indicates the loss of ligand, and X indicates a cross-ring cleavage of the sugar moiety.

There is at least one diagnostic fragment ion for each of the isomers, and in most cases there are at least two. In addition, there are two diagnostic cross-ring cleavages involving the disaccharide group for each of the flavone and flavanone rutinosides (i.e. isorhoifolin and didymin in Figure 4-4). The resulting ions are observed at m/z 876 (-74, X1) and m/z 846 (-104, X2) for the isorhoifolin complex and m/z 892 (-74, X1) and m/z 862 (-104, X2) for they didymin complex. Proposed cleavages that are consistent with the observed fragment ions are shown in Scheme 1 for these cross-ring cleavages. There is another notable series of cross-ring cleavages for the flavone rutinoside isomers (fragment ions labeled XN in the bottom panel of Figure 4-3B for the isorhoifolin complex, also seen for the analogous complexes of diosmin and linarin). Some of these cross-ring cleavages occur in conjunction with loss of the 4,4'-dibromo-2,2'-bipyridine ligand.

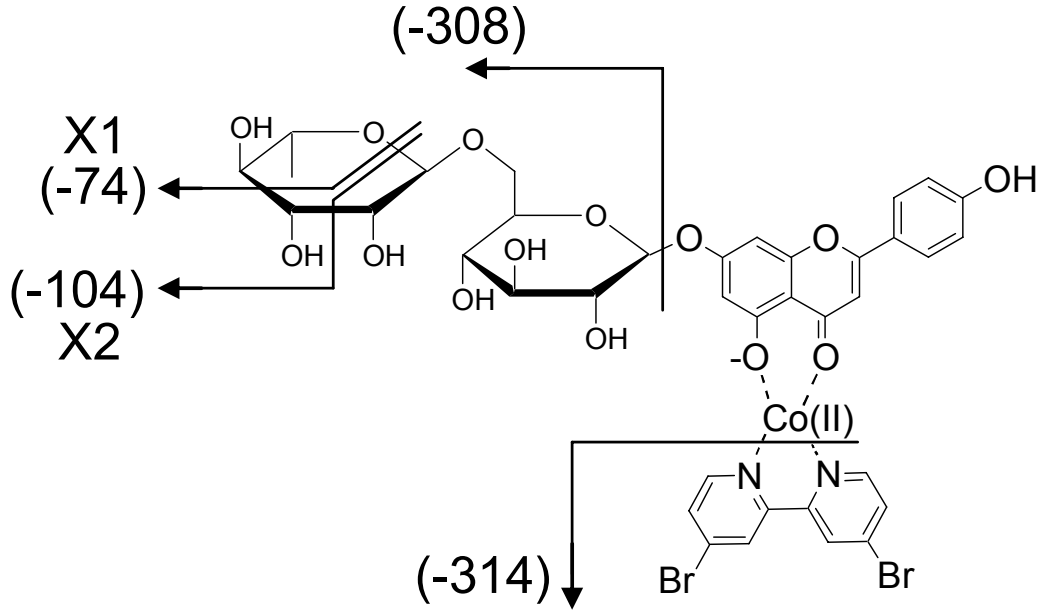

Scheme 4-1. Proposed cleavages for a flavonoid/Co/4,4'-dibromo-2,2'-bipyridine cobalt complex using isorhoifolin as an example.

It is interesting that these extensive cross-ring fragmentations are observed for the flavone rutinoside complexes but not the flavanone rutinoside complexes. We speculate that this striking difference in the degree of cross-ring cleavages is related to the ability of the rutinose moiety to interact with the metal center in the complexes, which may influence the migration of the metal or auxiliary ligand chelate upon activation, as well as the strength of the glycosidic bond. Previous computational modeling of [Co(II) (flavonoid-H) (2,2'-bipyridine)]$^+$ complexes by Zhang and Brodbelt[50] revealed that the most favorable metal coordination sites involved the carbonyl oxygen atom and adjacent deprotonated oxygen atom of the aglycon. Moreover, it was shown that for the rutinosides, the disaccharide folds toward the metal center, thus increasing the interaction of the disaccharide with the metal.[50] This factor presumably could enhance the possibility of migration of the metal/auxiliary ligand chelate in the complexes containing the 4,4'-dibromo-2,2'-bipyridine ligands and/or modify the electron density in the glycoside bonds, thus promoting cross-ring cleavages instead of glycosidic bond cleavage. It was also found that the glycosidic bond energies and point charges for the aglycon-disaccharide bonds were greater for the flavonoid rutinosides than for the flavonoid neohesperidosides.[50] This effect may be further exaggerated for the complexes containing the 4,4'-dibromo-2,2'-bipyridine ligand since the electron-withdrawing bromine atoms should temper the metal binding energy of the auxiliary ligand which could translate into alternate fragmentation pathways to glycosidic bond cleavage, such as cross-ring cleavages.

The analytical utility of two other brominated bipyridine ligands, 6,6'-dibromo-2,2'-bipyridine and 4,4'-bis(bromomethyl)-2,2'-bipyridine, was also evaluated. The only complexes observed by ESI-MS for solutions containing a flavonoid, a metal salt, and 6,6'-dibromo-2,2'-bipyridine were ligand/metal complexes of the type [M(I) 6,6'-

dibromo-2,2'-bipyridine + $H_2O]^+$. Molecular modeling was used to evaluate the 4,4'-dibromo-2,2'-bipyridine/Co(II) and 6,6'-dibromo-2,2'-bipyridine/Co(II) complexes in order to assess the potential hindrance to flavonoid binding. The dihedral angles of the N-C-C-N bonds on the ligand (labeled with a '○' in Figure 4-2) were found to have a minimum energy at 0° for both complexes, and this is consistent with previous modeling studies of other flavonoid metal complexes containing pyridyl ligands.[50] The C-Br bond distances were 1.9248 Å for the 6,6'-dibromo-2,2'-bipyridine complex. These distances, coupled with the dihedral angle that shows that the bromine atoms are in the same plane with Co, indicates that the proximity of the bromine atoms to the cobalt ion causes substantial steric hindrance which prevents simultaneous coordination of 6,6'-dibromo-2,2'-bipyridine and a flavonoid to the metal ion, thus making 6,6'-dibromo-2,2'-bipyridine a poor auxiliary ligand.

In contrast to the ESI-MS results for the 6,6'-dibromo-2,2-bipridine/flavonoid/metal solutions, abundant flavonoid complexes were observed for solutions containing 4,4'-bis(bromomethyl)-2,2'-bipyridine and a transition metal. However, the CAD spectra were dominated by the loss of the rhamnose moiety and the loss of the disaccharide group. These CAD spectra did not allow differentiation of the various isomers, and thus 4,4'-bis(bromomethyl)-2,2'-bipyridine proved to be an unsatisfactory auxiliary ligand.

4.4.2 Complexation with Phenanthroline Ligands

The complexation of each of the bromophenanthrolines (structures shown in Figure 4-2) was studied with each of the twelve flavonoids. Figure 4-5 illustrates the CAD mass spectra of the complexes containing the 3,5,6,8-tetrabromo-1,10-phenanthroline ligand, four representative flavonoids, and cobalt. The dominant dissociation route for all four flavonoid complexes in Figure 4-5 is the loss of the

rhamnose moiety, as well as elimination of the disaccharide group, two pathways that are commonly observed for other types of flavonoid/metal complexes. The presence of other unique fragment ions in each CAD spectrum allow each pair of isomers to be readily distinguished.

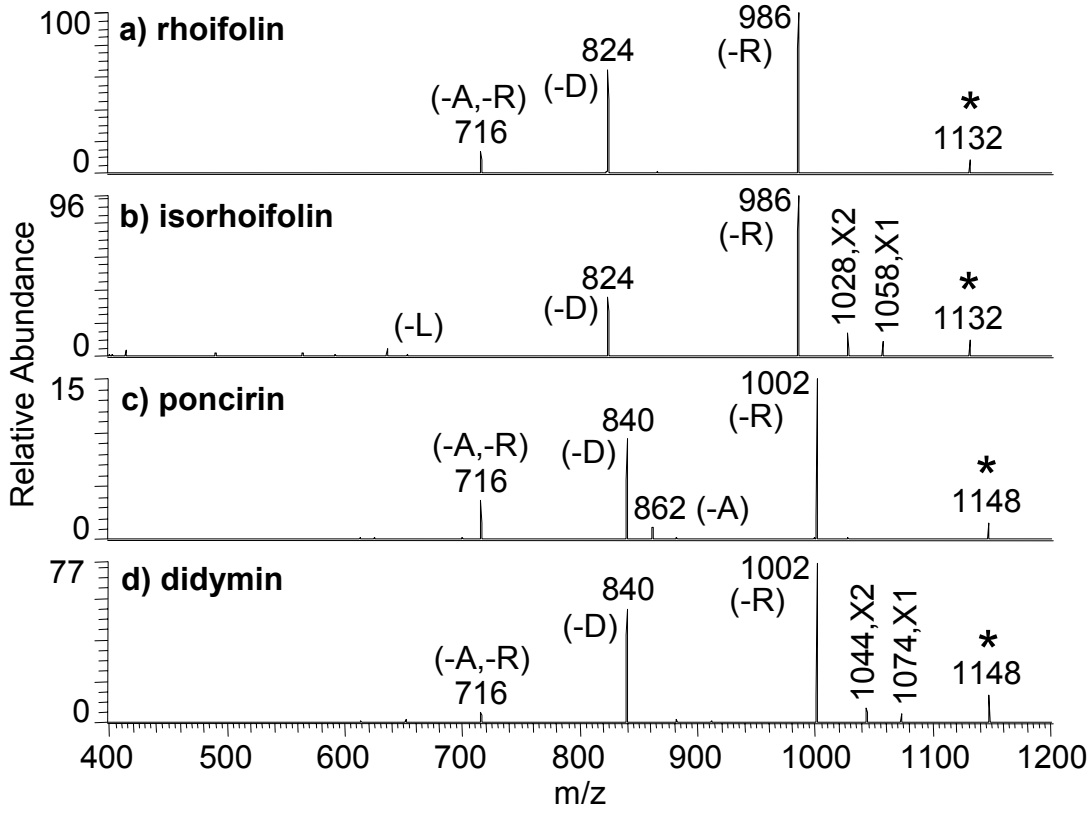

Figure 4-5. Representative CAD mass spectra of the [3,5,6,8-tetrabromo-1,10-phenanthroline (flavonoid – H) Co(II)]$^+$ complexes containing the following flavonoids: a) rhoifolin, b) isorhoifolin, c) poncirin, and d) didymin. (-D) indicates the loss of disaccharide moiety, (-R) indicates the loss of rhamnose moiety, and (-A) indicates the loss of aglycon.

The types of fragment ions observed for all of the cobalt complexes containing each of the bromophenanthroline ligands as compared to unmodified 1,10-phenanthroline and each of the flavonoids are summarized in Table 4-1. In general, the types of

fragmentation pathways are similar to those noted earlier for the complexes containing the 4,4'-dibromo-2,2'-bipyridine ligand, including the loss of the rhamnose group, the elimination of the disaccharide moiety, and the loss of the aglycon and rhamnose groups. The most notable difference between the fragmentation patterns of the flavonoid rutinosides and the neohesperidosides are two cross-ring cleavages (-74 Da, -104 Da) that were also observed for the analogous flavonoid rutinoside complexes containing the 4,4'-dibromo-2,2'-bipyridine ligand. In addition, the flavanone neohesperidosides are differentiated from the flavones by the characteristic loss of the aglycon moiety.

The summary in Table 4-1 reveals that the number of different fragment ions increases as the number of electron-withdrawing bromine atoms on the 1,10-phenanthroline auxiliary ligand increases. The number of fragmentation pathways correlates with the relative stabilities of the metal complexes. Complexes in which one of the two coordinated molecules (i.e. flavonoid vs. auxiliary ligand) has a significantly greater metal binding energy than the other tend to dissociate by just a few routes, thus typically being less useful for confident differentiation of isomers. Among the three brominated phenanthroline ligands, the 3,5,6,8-tetrabromo-1,10-phenanthroline ligand is expected to have the lowest metal binding energy due to the influence of the four electron-withdrawing bromine atoms on the metal-coordinating nitrogen atoms. This makes the metal binding energy of the 3,5,6,8-tetrabromo-1,10-phenanthroline ligand closer to the metal binding energy of a typical flavonoid, thus increasing the stability of the 3,5,6,8-tetrabromo-1,10-phenanthroline/flavonoid complexes and resulting in a greater array of competitive dissociation routes. In fact, of the three bromophenanthroline ligands, the tetrabromo ligand (3,5,6,8-tetrabromophenanthroline) is the only one that allows successful differentiation of all of the flavonoid isomers, in terms of providing at least one unique diagnostic fragment ion for each isomer.

Table 4-1. Summary of fragment ion distributions observed in the CAD spectra for selected Co/flavonoid/ligand complexes grouped by flavonoid diglycoside class.

4,4'-dibromo-2,2'-bipyridine/Co	(-R)	(-D)	(-A)	(-A,-R)	(-L)	X1	X2
flavone neohesperidoside (rhoifolin)	54	100		19			
flavone rutinoside (isorhoifolin)	100	68			80	10	14
flavanone neohesperidoside (poncirin)	95	100	8	58			
flavanone rutinoside (didymin)	100	83			29	5	7
1,10-phenanthroline/Co	(-R)	(-D)	(-A)	(-A,-R)	(-L)	X1	X2
flavone neohesperidoside (rhoifolin)	15	100		6			
flavone rutinoside (isorhoifolin)	14	100					4
flavanone neohesperidoside (poncirin)	38	100		32			
flavanone rutinoside (didymin)	16	100		8			
5,6-dibromo-1,10-phenanthroline/Co	(-R)	(-D)	(-A)	(-A,-R)	(-L)	X1	X2
flavone neohesperidoside (rhoifolin)	73	100		23			
flavone rutinoside (isorhoifolin)	94	100				15	21
flavanone neohesperidoside (poncirin)		100					
flavanone rutinoside (didymin)		100					
3,5,6-tribromo-1,10-phenanthroline/Co	(-R)	(-D)	(-A)	(-A,-R)	(-L)	X1	X2
flavone neohesperidoside (rhoifolin)	100	89		15			
flavone rutinoside (isorhoifolin)	100	61		4		12	18
flavanone neohesperidoside (poncirin)	79	100	5	26			
flavanone rutinoside (didymin)	94	100		8		4	11
3,5,6,8-tetrabromo-1,10-phenanthroline/Co	(-R)	(-D)	(-A)	(-A,-R)	(-L)	X1	X2
flavone neohesperidoside (rhoifolin)	100	68		14			
flavone rutinoside (isorhoifolin)	100	36			5	8	14
flavanone neohesperidoside (poncirin)	100	56	8	20			
flavanone rutinoside (didymin)	100	72		6		11	6
5-nitro-1,10-phenanthroline/Co	(-R)	(-D)	(-A)	(-A,-R)	(-L)	X1	X2
flavone neohesperidoside (rhoifolin)	38	100		14			
flavone rutinoside (isorhoifolin)	31	100			8	6	12
flavanone neohesperidoside (poncirin)	100	100		66			
flavanone rutinoside (didymin)	48	100			10	6	14

(-D) indicates loss of disaccharide moiety, (-R) indicates loss of rhamnose moiety, (-L) indicates loss of ligand, (-A) indicates loss of aglycon, and X1 and X2 represent the cross-ring cleavages of (-74) and (-104), respectively; (+/- 2%).

To further assess the impact of electron-withdrawing groups on the tunability of the auxiliary ligands, 5-nitro-1,10-phenanthroline was evaluated because the nitro group is known to be one of the most electron-withdrawing groups available. Abundant complexes of the type [M(II) (flavonoid-H) 5-nitro-1,10-phenanthroline]$^+$ were formed with the flavonoids, and the resulting CAD spectra also displayed the enhanced diagnostic cross-ring cleavages observed with the brominated ligands (Table 4-1). This result further underscores the strategy of adding electron-withdrawing groups to alter the dissociation pathways of the targeted complexes.

4.4.3 Comparison of All Ligands

Figure 4-6 shows the CAD mass spectra for a series of cobalt/isorhoifolin complexes, each containing one of six different auxiliary ligands. Figure 4-6 illustrates comprehensively how the bromination of the auxiliary ligands affects the tunability of the CAD patterns. The CAD mass spectra for the complexes containing either 2,2'-bipyridine or 1,10-phenanthroline are also shown for comparison. A quick inspection of the CAD mass spectra reveals notable differences in the relative abundances of specific fragment ions, in addition to the emergence of new diagnostic fragment ions as the identity of the auxiliary ligand changes.

For all of the complexes, the elimination of the rhamnose moiety (-R) and the loss of the disaccharide group (-D) is consistently observed, and the relative abundances of the two resulting fragment ions vary significantly for the series of CAD spectra. As the degree of bromination increases for the phenanthroline ligands, the ratio of (-R)/(-D) increases (Figure 4-6c – 4-6e). Another notable difference is the increase in the abundance of the two cross-ring cleavages X1 (-74, labeled with a square) and X2 (-104, labeled with a circle) upon bromination of the auxiliary ligands. Also noteworthy is the increase in the abundance of the fragment ion of 414 Da (Figure 4-6f, labeled with a

diamond) for the complex containing 4,4'-dibromo-2,2'-bipyridine, which results from the loss of the ligand in conjunction with a cross-ring cleavage of the sugar. While the CAD spectra of complexes containing 2,2'-bipyridine or 1,10-phenanthroline yielded some of the same diagnostic fragments, there was an enhancement in the abundance of these fragment ions using the brominated ligands.

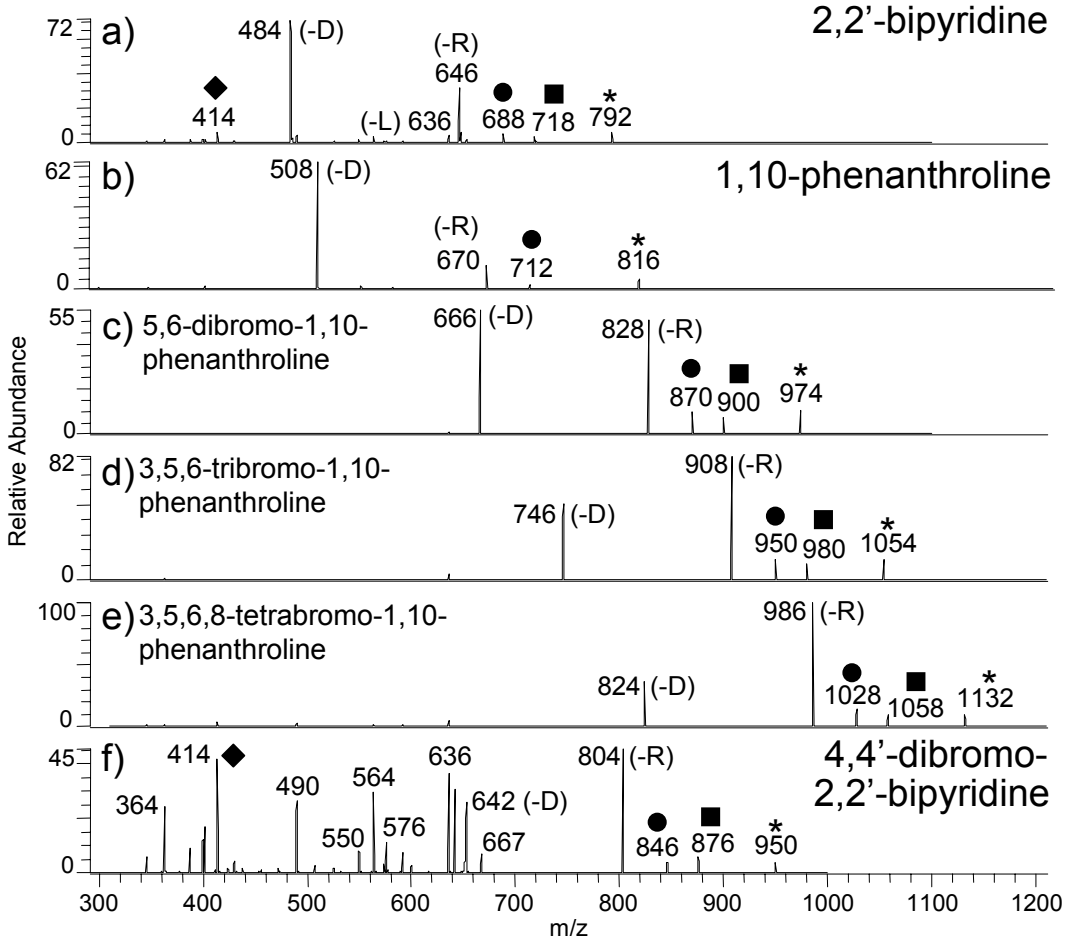

Figure 4-6. Comparison of the CAD mass spectra of [Co(II) (isorhoifolin-H) L]$^+$ complexes containing each brominated ligand, where L is the brominated ligand. A square and a circle are used to represent the cross-ring cleavages resulting in losses of 74 and 104 Da, respectively. A diamond is used to represent loss of the ligand in conjunction with a cross-ring cleavage of the sugar. (-D) indicates the loss of disaccharide moiety, (-R) indicates the loss of rhamnose moiety, (-L) indicates the loss of ligand, and X indicates a cross-ring cleavage of the sugar moiety.

Overall, Figure 4-6 and Table 4-1 clearly demonstrate the tunability of the CAD patterns promoted by the use of different auxiliary ligands. This tunability is related to the relative metal binding energies of the auxiliary ligand and flavonoids. Based on the significant differences in fragmentation pathways of pairs of isomeric complexes observed earlier in Figure 4-4 and compared to the performance of the other auxiliary ligands, 4,4'-dibromo-2,2'-bipyridine was judged to be the best overall auxiliary ligand for the differentiation of the series of flavonoids in this chapter.

4.4.4 Electron-Withdrawing Group Effect

The results presented in this chapter shows that the tunability of dissociation of flavonoid complexes is accomplished by adding electron-withdrawing substituents to the auxiliary ligands used to coordinate the transition metal and stabilize the flavonoid complexes. To understand the impact of the electron-withdrawing substituents on the stabilities and dissociation pathways of the flavonoid complexes in the gas phase, it is instructive to consider the influence of electron-withdrawing substituents on the binding energies of pyridyl ligands in solution. Although extensive solution data is not available, numerous binding constants have been measured for pyridyl ligands with Co(II) and Fe(II), two representative transition metals, in aqueous solution. Fe(II) was not a metal used in the present ESI-MS study, but the binding constants for Fe(II) complexes were compiled because this is the only metal for which brominated ligands have been studied.

The binding constants for cobalt/pyridyl ligand complexes in solution decrease in the order: 5,6-dimethyl-1,10-phenanthroline (log K 7.47) > 5-methyl-1,10-phenanthroline (log K 7.14) > 1,10-phenanthroline (log K 7.08) > 5-nitrophenanthroline (log K 6.3) [43], thus showing the impact of the addition of electron-releasing versus electron-withdrawing substituents on 1,10-phenanthroline. The binding constants for Fe(II)/pyridyl complexes decrease in the order: 5,6-dimethyl-1,10-phenanthroline (log

K 6.37) > 5-methyl-1,10-phenanthroline (log K 6.00) > 1,10-phenanthroline (log K 5.85) > 5-bromo-1,10-phenanthroline (log K 5.65) > 5-nitrophenanthroline (log K 5.06).[43] This trend indicates that the metal/ligand binding energies decrease as the substituents on the ligand become more electron-withdrawing. A similar inductive effect would be expected for the metal/ligand binding energies in the gas phase. The variations in the metal/ligand binding energies may influence the energetics of dissociation pathways and also affect the preferred coordination sites of the flavonoid complexes. The ligand also has an impact on the way the disaccharide moiety of the flavonoid interacts with the metal. As mentioned previously, modeling studies have indicated that for the rutinoside isomers, the disaccharide folds toward the metal center.[47] The addition of bromo substituents changes the steric environment of the auxiliary ligands, which may influence the conformations of the complexes and thus the degree of interaction of the disaccharide group with the metal center.[50]

4.5 CONCLUSIONS

The fragmentation pathways of flavonoids can be tuned by using a metal complexation strategy that incorporates auxiliary ligands containing electron withdrawing substituents. Upon collisional activation, the resulting [Co(II) (flavonoid-H) auxiliary ligand]$^+$complexes dissociate by pathways that are characteristic of flavone and flavanone 7-O-diglycosides (i.e. loss of rhamnose and disaccharide groups), in addition to ones that allow differentiation of isomers that differ only in the type of intersaccharide linkage. In this chapter, the pathways that distinguish flavone and flavanone disaccharides with 1→2 and 1→6 linkages have been enhanced by adding electron-withdrawing substituents to the auxiliary ligands. The addition of electron-withdrawing groups to the auxiliary ligands reduces their metal-ligand binding affinities and consequently alters the stabilities

and conformations of the [M(II) (flavonoid – H) L]$^+$ complexes, thus resulting in the enhancement of diagnostic fragmentation pathways.

4.6 REFERENCES

1. Reddy, P. N.; Ramesh, V.; Srinivas, R.; Sharma, G. V. M.; Nagendar, P.; Subash, V. *Int. J. Mass Spectrom.* **2006**, *248*, 115-123.

2. Song, F. R.; Liu, Z. Q.; Liu, S. Y.; Cai, Z. W. *Anal. Chim. Acta* **2005**, *531*, 69-77.

3. Wu, L. M.; Cooks, G. *Eur. J. Mass Spectrom.* **2005**, *11*, 231-242.

4. Song, F. R.; Cui, M.; Liu, Z. Q.; Yu, B.; Liu, S. Y. *Rapid Commun. Mass Spectrom.* **2004**, *18*, 2241-2248.

5. Matamoros, F. L., E.; Obel, N.; Scheller, H.C.; Roepstorff, P. *Carbohydr. Res.* **2004**, *339*, 655-664.

6. Zhang, J. H.; Lindsay, L. L.; Hedrick, J. L.; Lebrilla, C. B. *Anal. Chem.* **2004**, *76*, 5990-6001.

7. Cuyckens, F.; Rozenberg, R.; de Hoffmann, E.; Claeys, M. *J. Mass Spectrom.* **2001**, *36*, 1203-1210.

8. Desaire, H.; Leary, J. A. *Anal. Chem.* **1999**, *71*, 4142-4147.

9. Waridel, P.; Wolfender, J. L.; Ndjoko, K.; Hobby, K. R.; Major, H. J.; Hostettmann, K. *J. Chromatogr., A* **2001**, *926*, 29-41.

10. Gaucher, S. P.; Leary, J. A. *Int. J. Mass Spectrom.* **2000**, *197*, 139-148.

11. Desaire, H.; Leary, J. A. *Anal. Chem.* **1999**, *71*, 1997-2002.

12. Leavell, M. D.; Kruppa, G. H.; Leary, J. A. *Int. J. Mass Spectrom.* **2003**, *222*, 135-153.

13. Hashii, N.; Kawasaki, N.; Itoh, S.; Harazono, A.; Matsuishi, Y.; Hayakawa, T.; Kawanishi, T. *Rapid Commun. Mass Spectrom.* **2005**, *19*, 3315-3321.

14. Li, R.; Wu, Z. J.; Zhang, F.; Ding, L. S. *Rapid Commun. Mass Spectrom.* **2006**, *20*, 157-170.

15. Bandu, M. L.; Desaire, H. *Analyst* **2006**, *131*, 268-274.

16. Bandu, M. L.; Wilson, J.; Vachet, R. W.; Dalpathado, D. S.; Desaire, H. *Anal. Chem.* **2005**, *77*, 5886-5893.

17. vanAcker, S. A. B. E.; vandenBerg, D. J.; Tromp, M. N. J. L.; Griffioen, D. H.; VanBennekom, W. P.; VanderVijgh, W. J. F.; Bast, A. *Free Radic. Biol. Med.* **1996**, *20*, 331-342.

18. Pietta, P. *Flavonoids in Medicinal Plants*; Marcel Dekker: New York, 1998.

19. Paganga, G.; Miller, N.; Rice-Evans, C. A. *Free Radical Res.* **1999**, *30*, 153-162.

20. Jovanovic, S. V.; Steenken, S.; Tosic, M.; Marjanovic, B.; Simic, M. G. *J. Am. Chem. Soc.* **1994**, *116*, 4846-4851.

21. RiceEvans, C. A.; Miller, N. J. *Biochem. Soc. Trans.* **1996**, *24*, 790-795.

22. Hertog, M. G. L. *Arch. Intern. Med.* **1995**, *155*, 1184-1184.

23. Knekt, P.; Jarvinen, R.; Reunanen, A.; Maatela, J. *Br. Med. J.* **1996**, *312*, 478-481.

24. Hollman, P. C. H.; Feskens, E. J. M.; Katan, M. B. *Proc. Soc. Exp. Biol. Med.* **1999**, *220*, 198-202.

25. Mojzisova, G.; Kuchta, M. *Physiol. Res.* **2001**, *50*, 529-535.

26. Amic, D.; Davidovic-Amic, D.; Beslo, D.; Trinajstic, N. *Croat. Chem. Acta* **2003**, *76*, 55-61.

27. Cao, G. H.; Sofic, E.; Prior, R. L. *Free Radic. Biol. Med.* **1997**, *22*, 749-760.

28. Bors, W. H. M., C. In *Flavonoids in Health and Disease*; Rice-Evans, C. A., Ed.; Marcel Dekker: New York, 1998, pp 111-136.

29. RiceEvans, C. A.; Miller, N. J.; Paganga, G. *Free Radic. Biol. Med.* **1996**, *21*, 417-417.

30. Stobiecki, M. *Phytochemistry* **2000**, *54*, 237-256.

31. Cuyckens, H.; Claeys, M. *J. Mass Spectrom.* **2004**, *39*, 461-461.

32. Satterfield, M.; Brodbelt, J. S. *Anal. Chem.* **2000**, *72*, 5898-5906.

33. Satterfield, M.; Brodbelt, J. S. *J. Am. Soc. Mass Spectrom.* **2001**, *12*, 537-549.

34. Zhang, J. M.; Brodbelt, J. S. *Anal. Chem.* **2005**, *77*, 1761-1770.

35. Zhang, J. M.; Wang, J. M.; Brodbelt, J. S. *J. Mass Spectrom.* **2005**, *40*, 350-363.

36. Pikulski, M.; Brodbelt, J. S. *J. Am. Soc. Mass Spectrom.* **2003**, *14*, 1437-1453.

37. Davis, B. D.; Brodbelt, J. S. *J. Am. Soc. Mass Spectrom.* **2004**, *15*, 1287-1299.

38. Davis, B. D.; Brodbelt, J. S. *Anal. Chem.* **2005**, *77*, 1883-1890.

39. Nord, G. *Comments Inorg. Chem.* **1985**, *4*, 193-212.

40. Constable, E. C. *Polyhedron* **1983**, *2*, 551-572.

41. Brandt, W. D., F.P.; Gyarfas, E.C. *Chemical Reviews* **1954**, *1954*, 959-1017.

42. McWhinnie, W. R. M., J.D. *Adv. Inorg. Radiochem.* **1969**, *12*, 135-173.

43. Martell, A. E. H., R.D. *Metal Complexes in Aqueous Solutions*, 1 ed.; Plenum Press: New York, 1996.

44. Satterfield, M.; Brodbelt, J. S. *Inorg. Chem.* **2001**, *40*, 5393-5400.

45. Wu, H. F.; Brodbelt, J. S. *Inorg. Chem.* **1995**, *34*, 615-621.

46. Maerker, G. C. *J. Am. Chem. Soc.* **1958**, *80*, 2745-2748.

47. Carlson, B.; Phelan, G. D.; Kim, J. H.; Jen, A. K. Y.; Dalton, L. R. *Abstr. Pap. Am. Chem. Soc.* **2004**, *227*, U1314-U1314.

48. Ward, R. S.; Branciard, D.; Dignan, R. A.; Pritchard, M. C. *Heterocycles* **2002**, *56*, 157-170.

49. Denes, V.; Chira, R. *Journal Fur Praktische Chemie* **1978**, *320*, 172-175.

50. Zhang, J. M.; Brodbelt, J. S. *J. Am. Soc. Mass Spectrom.* **2005**, *16*, 139-151.

Chapter 5: Amplification of Infrared Multiphoton Dissociation Efficiency in a Quadruple Ion Trap by Using IR-Active Ligands

5.1 OVERVIEW

A strategy for increasing the efficiency of infrared multiphoton dissociation (IRMPD) in a quadrupole ion trap (QIT) is described in this chapter. IR-active ligands (IRALs) are incorporated into non-covalent complexes of the type $[M^{2+}$ (analyte) IRAL$]^{+}$, where M is a transition metal such as copper or cobalt and IRAL is an auxiliary ligand with an IR-active phosphonate functional group. The complexes are formed via self-assembly in solution directly prior to ESI-MS analysis. We demonstrate this new IRMPD approach for the structural characterization of flavonoids. The fragment ions obtained by IRMPD are similar to those obtained by CAD and allow facile isomer differentiation of flavonoids. Fourier transform infrared absorption attenuated total reflectance (FTIR-ATR) and energy-variable CAD experiments indicate that the high IRMPD efficiencies stem from the very large IR absorptivities of the IR-active ligands.

5.2 INTRODUCTION

One of the most powerful techniques for the structural determination of analytes is tandem mass spectrometry (MS/MS).[1, 2] Trapping instruments such as Fourier transform ion cyclotron resonance (FTICR) mass spectrometers and quadrupole ion trap (QIT) mass spectrometers are in many ways ideal for multiple stages of ion isolation, activation and mass analysis (MS^n) because they allow efficient manipulation of ion populations temporally. The QIT has been the most popular of the trapping instruments over the past decade due to its cost, ruggedness and ease of use. Collisionally activated dissociation (CAD) is the most common dissociation technique used with the QIT. However, there are shortcomings to conventional CAD that include ion losses due to

scattering from collisions and the loss of ions below a low mass cutoff (typically one-third the parent mass) due to the resonant nature of the excitation in the QIT.[3] New methods of ion activation for QITs have emerged, including electron transfer dissociation,[4, 5] thermally assisted CAD,[6] pulsed Q dissociation[7] and photodissociation,[8-29] that alleviate some of the problems of conventional CAD, and these methods have further fueled the popularity of ion trap instruments.

Infrared multiphoton dissociation (IRMPD) has several advantages as an activation method for quadrupole ion traps.[8-29] For example, ion losses due to scattering, a collision-based phenomenon, are alleviated with photoactivation. Reduction of ion losses is a critical feature when analyzing small ion populations while maintaining adequate detection sensitivity. Because photodissociation does not require the use of a collision gas, it has also been popular for FTICR applications.[30-35] Another phenomenon of IRMPD in a QIT stems from the non-resonant nature of IR photoactivation compared to conventional resonant CAD, meaning that energy absorption by primary fragment ions during the photodissociation period can result in secondary fragmentation. While these additional fragments occasionally complicate spectra, they often provide important additional structural information. Thus IR photoactivation may produce a greater range of diagnostic ions than CAD. Moreover, IR photoactivation is independent of the rf voltage used to trap ions, a significant factor in collisional activation in QITs that results in a low mass cut-off below which fragment ions can not be trapped and detected. Thus, conventional CAD often leads to loss of information in the low m/z range. This latter shortcoming has largely been overcome by the recently developed pulsed Q dissociation method.[7] However, one well-recognized drawback to IRMPD methods is that as ions are irradiated by the laser, collisional cooling with the He bath gas competes with the increase in internal energy due to photoabsorption which ultimately may result in

inefficient dissociation. This drawback has been somewhat compensated for by heating the bath gas,[6, 18] using CAD-assisted IRMPD,[23] using a pulsed gas introduction method,[20] or optimization of the bath gas pressure between the accumulation and dissociation timeframes.[24] Although improving energy deposition, these methods have often resulted in lower sensitivity, mass accuracy and resolution of the QIT.

To circumvent the problem of low energy deposition due to competition from collisional cooling, a new method to enhance IRMPD efficiencies by increasing the IR absorptivities of ions via non-covalent addition of strong IR-active ligands (IRAL) via metal complexation strategies is presented in this chapter. In particular, phosphate and phosphonate functional groups have outstanding IR absorptivities at 10.6 μm. In fact, it has been shown by our group and others that the IRMPD efficiencies of compounds containing phosphate functional groups, such as phosphopeptides and nucleic acids, are superior to that of non-phosphorylated compounds.[9, 11, 35, 36] This improvement is surmised to be due to the efficient absorption of the phosphate groups at the 10.6 μm wavelength of the IR laser.[35, 36] In this chapter, we improve the efficiency of ion dissociation by addition of IR-active phosphonate groups to analytes by using a metal complexation strategy, thus avoiding covalent modification of the analytes. The phosphonate functional group was chosen over the phosphate because the latter can result in a facile loss of the IR-active group upon activation, thus resulting in few diagnostic fragmentation routes.[9, 36] The phosphonate groups are actually incorporated into chelating ligands that are then non-covalently bound to the analyte of interest via metal coordination through a simple self-assembly process in solution prior to ESI-MS analysis. The resulting complexes, $[M^{2+}$ (analyte - H) (phosphonated chelating ligand)$]^{+}$ have high IR absorptivities and thus undergo significant energy deposition and dissociation faster than they undergo collisional cooling. The phosphonated ligands synthesized for the

study presented in this chapter are shown in Figure 5-1. We demonstrate this versatile method for the analysis of flavonoids, a class of phytochemicals.

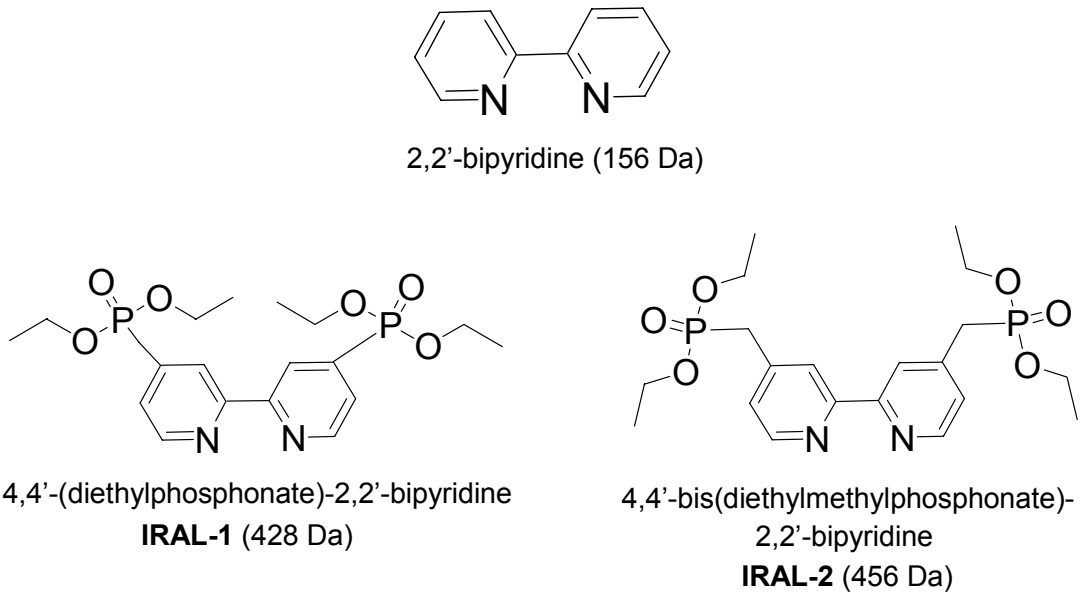

Figure 5-1. IR-active ligands based on the 2,2'-bipyridine skeleton synthesized and used in this chapter. Molecular weight is shown in parentheses.

Flavonoids, phenolic compounds which are known for their antioxidant properties and chemopreventive health benefits, have been extensively studied by our group.[37-43] We have considerable experience with the structural characterization and isomer differentiation of flavonoids, so they proved to be a convenient group of compounds to exploit our IRMPD enhancement approach afforded by the phosphonated chelating ligands. Figure 5-2 shows the structures of the twelve flavonoid diglycosides that were used in this chapter.

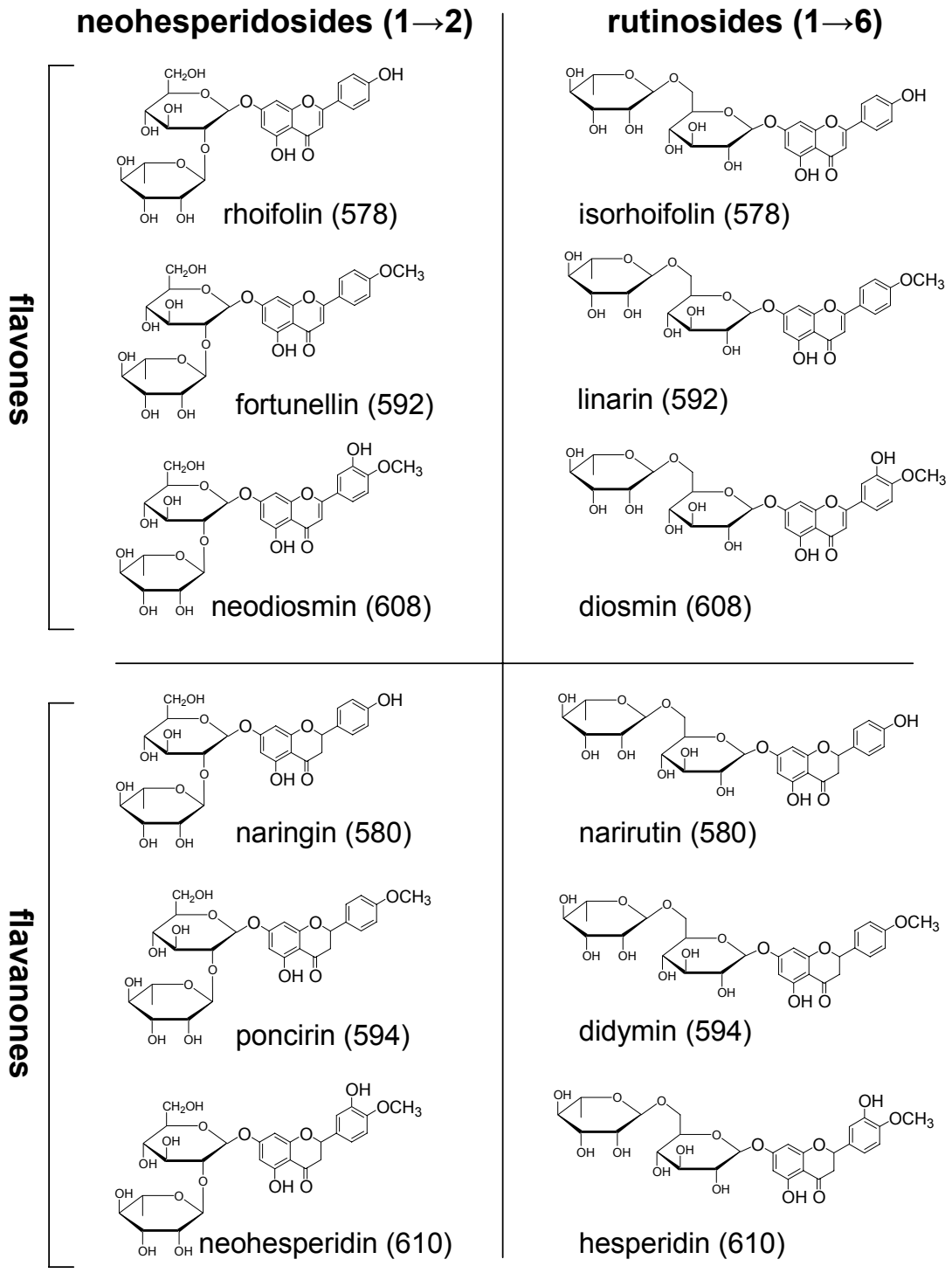

Figure 5-2. Structures of the flavonoid diglycosides used in this chapter. Molecular weight is shown in parentheses.

5.3 EXPERIMENTAL

5.3.1 Chemical Reagents

The flavonoids rhoifolin, isorhoifolin, neodiosmin, diosmin and narirutin were purchased from Indofine (Somerville, NJ, USA). Fortunellin, linarin, poncirin and didymin were purchased from Extrasynthese (Genay, France). Naringin, neohesperidin, hesperidin, $CoBr_2$, $CuBr_2$, 2,2'-bipyridine and 4,4'-dimethyl-2,2'-bipyridine were purchased from Sigma (St. Louis, MO, USA).

5.3.2 Metal Complexation/Mass Spectrometry

A Finnigan LCQ Deca XP mass spectrometer with an electrospray ionization source and interfaced with a Synrad CO_2 50 W laser (10.6 μm) was used for the work presented in this chapter. The details of the system were previously described.[8] The analytes, metal salts and auxiliary ligands were each 10^{-5} M in methanol, and the resulting solutions were analyzed in the positive ion mode. Typical IRMPD parameters included an irradiation time of 10-25 msec at a power of 50 W. The helium pressure for both IRMPD experiments and comparative CAD experiments was nominally 2.4 x 10^{-5} Torr (corresponding to approximately 1 mtorr in the QIT) as measured by an ionization gauge. The non-covalent complexes are formed in solution by simple addition of the analyte, a transition metal salt, and an auxiliary pyridyl ligand just prior to ESI-MS analysis.

5.3.3 Ligand Syntheses

Ligands were synthesized from 2,2'-bipyridine and 4,4'-dimethyl-2,2'-bipyridine in two major steps involving bromination[44-47] followed by phosphonation.[46-49] The ligand structures were confirmed by proton NMR using a 400 MHz Varian instrument. FTIR

analysis of the ligands was performed using a Thermo Mattson Infinity Gold FTIR equipped with a Spectra-Tech Thermal ARK module, an ATR accessory.

5.4 RESULTS AND DISCUSSION

We have employed the use of auxiliary chelating ligands and metal complexation strategies in the past to increase ionization efficiencies and improve the diagnostic CAD patterns of analytes, such as flavonoids.[37-43] For example, by the addition of a suitable metal and an auxiliary ligand to a flavonoid solution, complexes of the type $[M^{2+}$ (flavonoid - H) $L]^+$ are formed, where M is a transition metal such as copper(II) or cobalt(II) and L is an auxiliary ligand such as 2,2'bipyridine. The ease of forming these robust non-covalent complexes made them a natural choice for use in IRMPD applications by incorporation of phosphonate groups into the auxiliary ligand. The two ligands shown in Figure 5-1 incorporate the phosphonate groups remote from the chelating nitrogen atoms to prevent impairment of metal coordination. The phosphonate groups in IRAL-2 are separated from the 2,2'-bipyridine skeleton by methylene units in order to allow evaluation of whether the connectivity of the IR-active groups has an impact on absorption. ESI of the solutions containing a flavonoid, a copper or cobalt salt, and an IRAL result in dominant formation of $[M^{2+}$ + (flavonoid – H) + IRAL$]^+$ complexes with ion abundances that exceed those of protonated flavonoids by two orders of magnitude and deprotonated flavonoids by up to one order of magnitude. In this chapter, we have exploited this system to increase the IRMPD efficiency in a QIT at normal operating pressures.

5.4.1 Comparison of CAD Spectra

CAD mass spectra of the metal/flavonoid complexes incorporating 2,2'-bipyridine, a standard chelating ligand, and the two new IRALs were acquired as

benchmarks. Both copper and cobalt were employed as metals. The CAD mass spectra for neodiosmin are shown in Figure 5-3 as representative data.

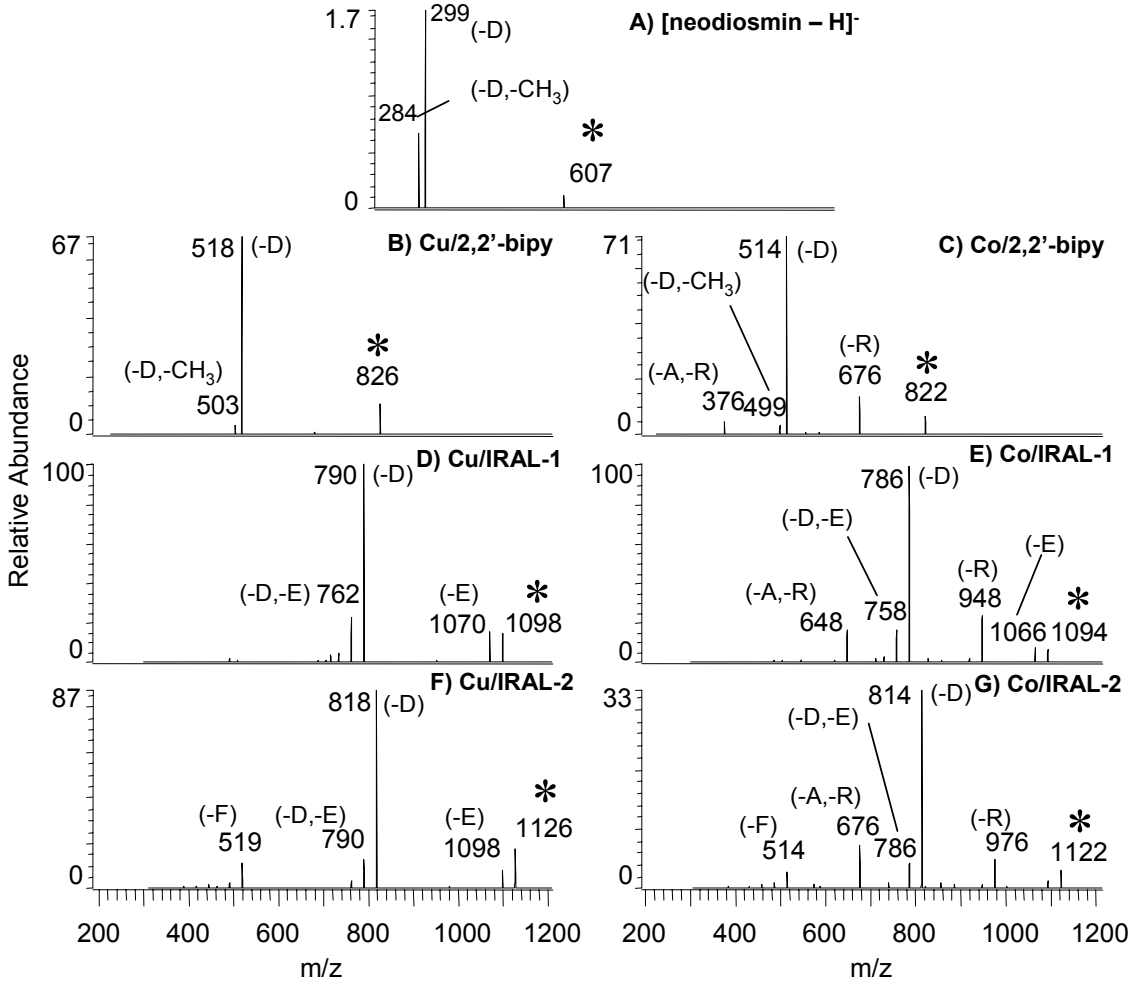

Figure 5-3. CAD spectra of deprotonated neodiosmin and the metal complexes as benchmark data: A) (neodiosmin – H)$^-$, B) [Cu^{2+} (neodiosmin – H) 2,2'-bipyridine]$^+$, C) [Co^{2+} (neodiosmin – H) 2,2'-bipyridine]$^+$, D) [Cu^{2+} (neodiosmin – H) IRAL-1]$^+$, E) [Co^{2+} (neodiosmin – H) IRAL-1]$^+$, F) [Cu^{2+} (neodiosmin – H) IRAL-2]$^+$, and G) [Co^{2+} (neodiosmin – H) IRAL-2]$^+$. The loss of ethylene is indicated by (-E), the loss of rhamnose moiety is indicated by (-R), the loss of disaccharide moiety is indicated by (-D), the loss of aglycon moiety is indicated by (-A) and the loss of flavonoid moiety is indicated by (-F).

In the negative ion mode (Figure 5-3a) and with Cu/2,2'-bipyridine complexation (Figure 5-3b), the only fragmentation routes include loss of the disaccharide moiety (-D), which may occur in conjunction with a loss of methyl radical (-D, -CH_3). The [Co^{2+} (neodiosmin-H) 2,2'-bipyridine]$^+$ complex undergoes the additional diagnostic loss of the terminal rhamnose group (-R) which may occur in conjunction with the loss of the aglycon group (-A,-R), (Figure 5-3c). In the previous two chapters,[37, 41] it was shown that the cobalt complexes typically afford more diagnostic fragment ions than the corresponding copper complexes.

Similar types of fragment ions were observed upon CAD of the neodiosmin complexes containing the IR-active ligands. The spectrum for the Cu/IRAL-1 complex (Figure 5-3d) reveals the same fragment ions as obtained for the analogous Cu/2,2'-bipyridine complex (Figure 5-3b), along with of losses of ethylene from the ligand. CAD of the Co/IRAL-1 complex (Figure 5-3e) likewise results in similar fragment ions as the corresponding Co/2,2'-bipyridine complex described above. Interestingly, for the Co/IRAL-1 complex, there are no losses of ethylene in conjunction with the loss of the rhamnose moiety or the aglycon/rhamnose moieties. Figures 5-3f and 5-3g show the data for the Cu/IRAL-2 and Co/IRAL-2 complexes. The only notable difference between these CAD spectra and those of the corresponding IRAL-1 complexes is the new loss of flavonoid moiety (-F) observed for the former. The emergence of this new fragmentation pathway suggests that the metal/ligand binding interactions in the IRAL-2 complexes are somewhat stronger than those in the IRAL-1 or 2,2'-bipyridine complexes. The CAD data confirms that the flavonoid/metal/IRAL complexes give structurally diagnostic information for identifying the flavonoids and the fragmentation pathways are not significantly different between the ligand complexes.

5.4.2 Comparison of IRMPD Spectra of the Copper Complexes

Next IRMPD was used to evaluate the fragmentation patterns of the same flavonoid complexes. Figure 5-4 shows a striking comparison of the dissociation efficiencies of the neodiosmin complexes containing the standard chelating ligand, 2,2'-bipyridine, (Figure 5-4a and 5-4b) versus those containing the new ligands, IRAL-1 or IRAL-2, (Figure 5-4c and 5-4d) upon IR irradiation. For the spectra shown in Figures 5-4a, 5-4c and 5-4d, the isolated complexes were irradiated for 25 ms at 50 W power. Only the complexes containing the two IRALs underwent extensive dissociation, while the analogous complex containing 2,2-bipyridine did not dissociate at all. In fact, even when the latter complex was irradiated for 2.5 s, there was still no evidence of any dissociation (Figure 5-4b). The lack of dissociation for the complexes containing 2,2'-bipyridine is attributed to rapid collisional cooling that occurs at 1 mtorr in the ion trap, in addition to the potential for efficient radiative relaxation that may occur for the flavonoids. The addition of the phosphonate groups to the ligands apparently increases their IR absorptivities by a tremendous amount, thus allowing efficient cumulative energy deposition above and beyond the collisional cooling and radiative relaxation that occurs.

Comparison of the IRMPD mass spectra in Figures 5-4c and 5-4d reveals greater abundances of ions in the mid m/z range (i.e. m/z 600 to 800) for the complexes containing IRAL-1 and greater abundances of ions in the lower m/z range (i.e. m/z 300 to 520) for the complexes containing IRAL-2. Since the types of fragmentation pathways are the same for both of these IRAL complexes, the shift in the fragment ion distributions suggests that there is more extensive secondary dissociation for the IRAL-2 complexes (i.e. the mid m/z fragment ions undergo IR absorption and subsequently dissociate to form the lower m/z fragment ions), a process which implies a greater IR absorption efficiency for IRAL-2.

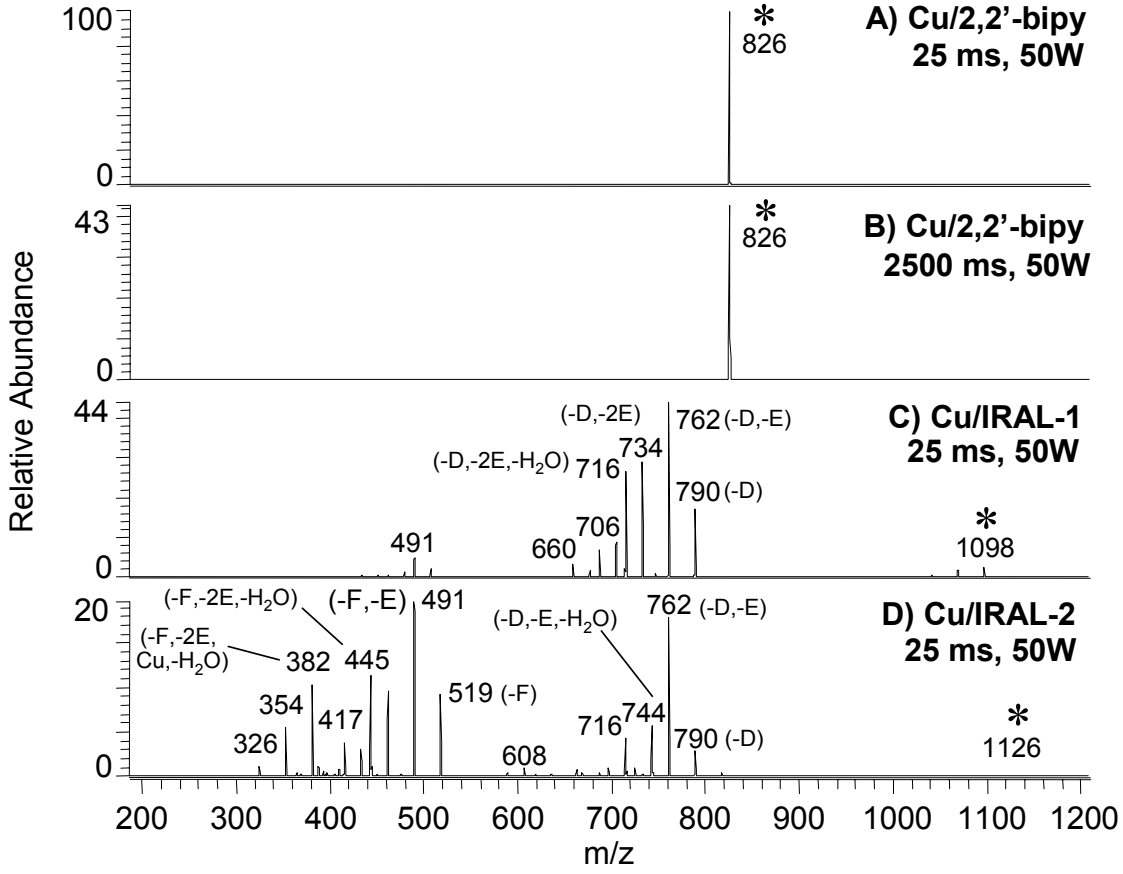

Figure 5-4. Irradiation of the $[Cu^{2+}$ (neodiosmin-H) auxiliary ligand$]^+$ complexes containing different ligands. A) $[Cu^{2+}$ (neodiosmin – H) 2,2-bipy$]^+$, 50 W for 25 ms, B) $[Cu^{2+}$ (neodiosmin – H) 2,2-bipy$]^+$, 50 W for 2500 ms, C) $[Cu^{2+}$ (neodiosmin – H) IRAL-1$]^+$, 50 W for 25 ms, and D) $[Cu^{2+}$ (neodiosmin – H) IRAL-2$]^+$, 50 W for 25 ms.

For both of the complexes containing the two IRALs, the dominant IRMPD pathway is the loss of the disaccharide moiety, which may occur in conjunction with ethylene losses. This behavior is analogous to the general fragmentation patterns of the complexes obtained upon CAD (Figures 5-3d and 5-3f) and suggests that the IR activation process is similar to that of collisional activation.

The relative dissociation energies and efficiencies of these complexes were further evaluated by using energy-variable CAD. Energy-variable CAD entails monitoring the extent of dissociation of selected ions as a function of internal energy deposition, a factor largely controlled by the magnitude of the resonant CAD voltage applied to the QIT. For these experiments, the normalized CAD voltage (% of 5 V_{o-p}) was increased in 1% increments, and the relative abundances of the parent and product ions were recorded for the Cu/2,2'-bipyridine and Cu/IRAL-1 complexes to compare the dissociation behaviors in terms of the magnitude of CAD voltage needed to initiate dissociation or attain some arbitrary extent of dissociation (such as 50%). Since IRAL-1 has a greater number of atoms (and thus more vibrational modes) as compared to 2,2'-bipyridine, a correction for the degrees of freedom was incorporated into the measurements. Because compounds that have a greater number of atoms have more degrees of freedom (DOF) for energy distribution, more energy is consequently required to break a bond in a larger molecule than an equivalent bond in a smaller molecule.[50] This correction was made using the following formula:

$$E_{CAD,\ corrected} = E_{CAD} * N_{ref}/N_{complex}$$

where N = 3n – 6 and n is the number of atoms in the complex.

This equation is based on the assumption that there is a linear relationship between the collision energy and DOF. While the exact correlation between the excitation voltage and the internal energy of ions is not well described, it has been shown that they are correlated.[51, 52]

Figure 5-5 shows a plot of the percentage fragmentation of the complexes observed as a function of the corrected CAD voltages for the $[Cu^{2+}$ + (neodisomin – H) 2,2-bpy$]^+$ and $[Cu^{2+}$ + (neodisomin – H) IRAL-1$]^+$ complexes. Since the curves nearly overlay each other, it indicates that the complexes have very similar CAD dissociation

energies and efficiencies. At 50% dissociation, the difference between the corrected CAD voltages for the 2,2'-bipyridine and IRAL-1 complexes are <0.05 V (1.08 V for 2,2'-bipyridine complex and 1.04 V for the IRAL-1 complex). Therefore it is surmised that the increase in fragmentation efficiencies of the IRAL-1 (and IRAL-2) complexes upon IRMPD is directly related to their greater IR absorptivities, not due to lower intrinsic dissociation energies.

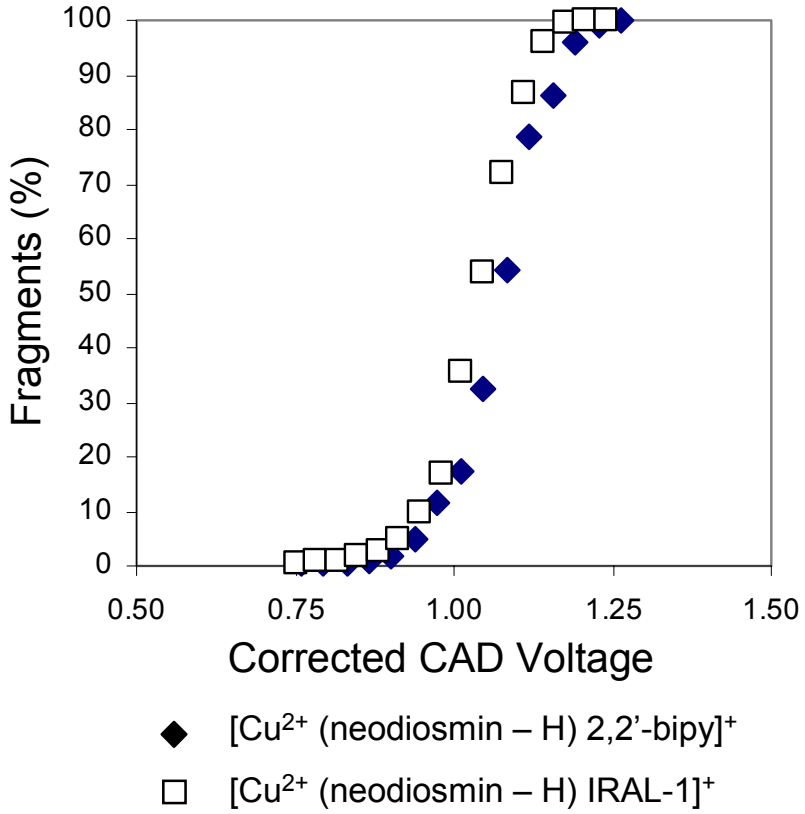

Figure 5-5. Energy-variable CAD of the $[Cu^{2+}$ (neodiosmin-H) auxiliary ligand$]^{+}$ complexes containing 2,2'-bipyridine or IRAL-1.

The absorption of IR radiation by the three auxiliary ligands was further investigated by using attenuated total reflectance (ATR) Fourier transform infrared (FTIR) spectroscopy. The resulting spectra are shown in Figure 5-6. The absorption in

the wavelength range of the IR laser centered at 10.6 μm increases in the order IRAL-2 > IRAL-1 >>> 2,2'-bipyridine, consistent with the IRMPD efficiencies noted in Figure 5-4. This result for the IR-active ligands is consistent with the FTIR data obtained by Flora and Muddiman for phosphopeptides[36] which showed an increase in the IR absorption at 10.6 μm with an increase in the degree of phosphorylation of the peptides. In addition, since both IRAL-1 and IRAL-2 have the same overall degree of phosphonation, the FTIR spectra confirm that the IR absorptivity increases when the phosphonate group is not directly attached to the aromatic ring. The FTIR results support the reason for the excellent IRMPD characteristics of the flavonoid complexes containing the IRALs.

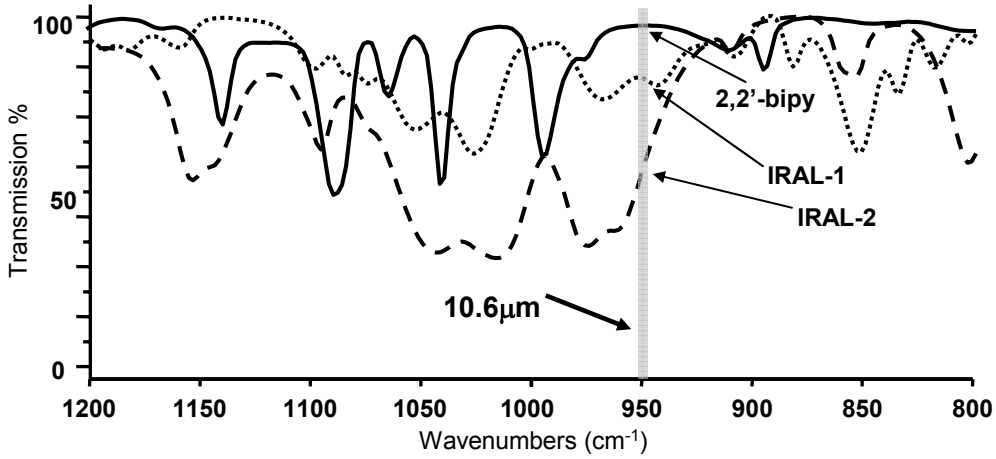

Figure 5-6. FTIR ATR spectra of the ligands used in this chapter, showing the enhanced absorption of the IR-active ligands, IRAL-1 and IRAL-2, at 10.6 μm as compared to 2,2'-bipyridine.

5.4.3 Comparison of IRMPD Spectra of the Cobalt Complexes

The IRMPD spectra of the cobalt/IRAL complexes with the flavonoids in Figure 5-2 were also acquired for neodiosmin and the other flavonoids. The major fragmentation routes include loss of the disaccharide group, the loss of the rhamnose moiety, and loss of ethylene units, consistent with losses observed in previous CAD

spectra. For the IRAL-2 complexes, some new fragment ions that emerge in the m/z range of 350 – 520 are ones in which the flavonoid has been lost. A comparison of the IR irradiation time needed to cause 90-95% dissociation of the parent complexes was undertaken for each metal/neodiosmin/IRAL complex in order to obtain a relative comparison of the dissociation efficiencies as a function of the metal ion (Cu or Co) and auxiliary ligand (IRAL-1 or IRAL-2). For the IRAL-2 complexes containing either Cu or Co, the irradiation times needed to promote 90-95% dissociation of the complexes were 15 ms. For the corresponding IRAL-1 complexes, the irradiation times were 25 to 50 ms, thus again reflecting the higher IR absorption efficiencies of the IRAL-2 complexes. The IRMPD spectra for eight other flavonoids (shown in Figure 5-2) were also obtained. The same types of fragment ions summarized above (loss of disaccharide group, loss of rhamnose moiety, loss of aglycon group) were also observed for these complexes containing the IRALs.

To further evaluate the ability of the complexes containing the IRALs to undergo sequential dissociation upon IR irradiation, the fragmentation patterns of the neodiosmin complexes ($[Co^+$ (neodisomin – H) IRAL-1$]^+$) were obtained as the IR irradiation period was increased (Figure 5-7). As the irradiation time was increased, the mid m/z ions (m/z 750 - 950 decreased in abundance while the lower m/z ions (m/z 350 - 750) increased in abundance. This result supports a sequential fragmentation process due to efficient IR absorption by the mid m/z fragment ions, thus resulting in secondary dissociation to form the lower m/z fragment ions. The ability to vary the irradiation time provides an easy way to tune the fragmentation patterns and obtain MS^n information at longer irradiation times.

Figure 5-8 shows a comparison of the IRMPD spectra acquired for complexes containing two flavanone isomers (naringin versus narirutin) with cobalt and the two

different IR-active ligands. The irradiation time was adjusted to promote 90-95% dissociation of the selected complexes. The dominant fragmentation pathways are ones that are diagnostic for the structures of flavanones, including loss of the rhamnose group, loss of the disaccharide moiety, and the loss of both the rhamnose and aglycon groups.

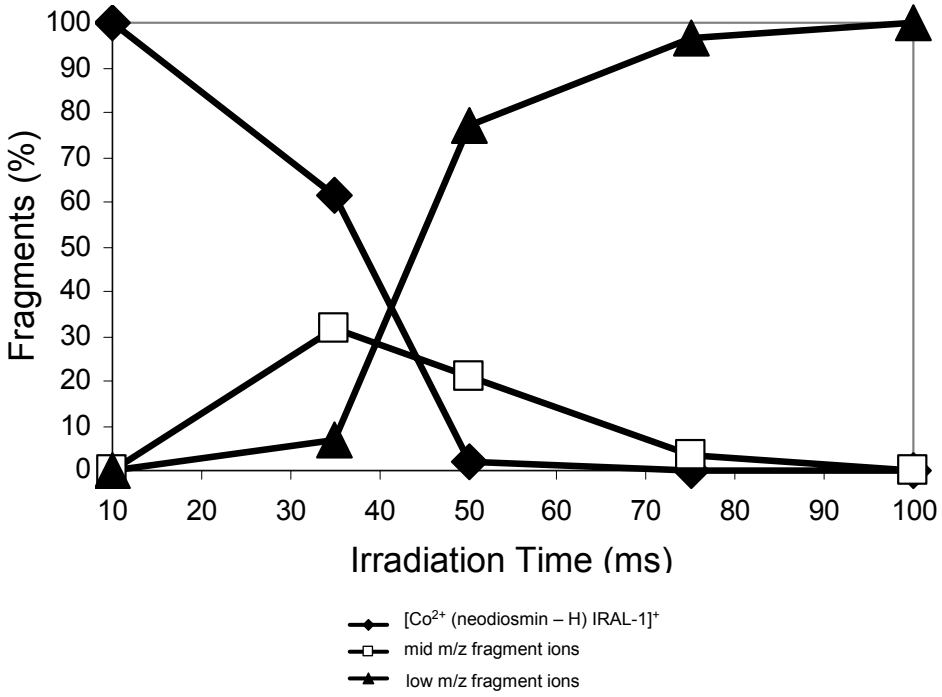

Figure 5-7. Time-resolved plot of the irradiation of the $[Co^{2+}$ (neodiosmin-H) IRAL-1$]^{+}$ complexes as a function of irradiation time.

The irradiation times needed to obtain the IRMPD spectra for these two flavanone complexes (narirutin and naringen) are lower than those needed for the flavone (neodiosmin and diosmin) IRAL-1 complexes, and the irradiation time needed for efficient dissociation of the naringin complexes is substantially lower than that needed for the narirutin complexes. These variations in irradiation time may be in part related to the IR radiative relaxation rates of the various complexes, in addition to changes in the dissociation energetics as a function of the flavonoid.

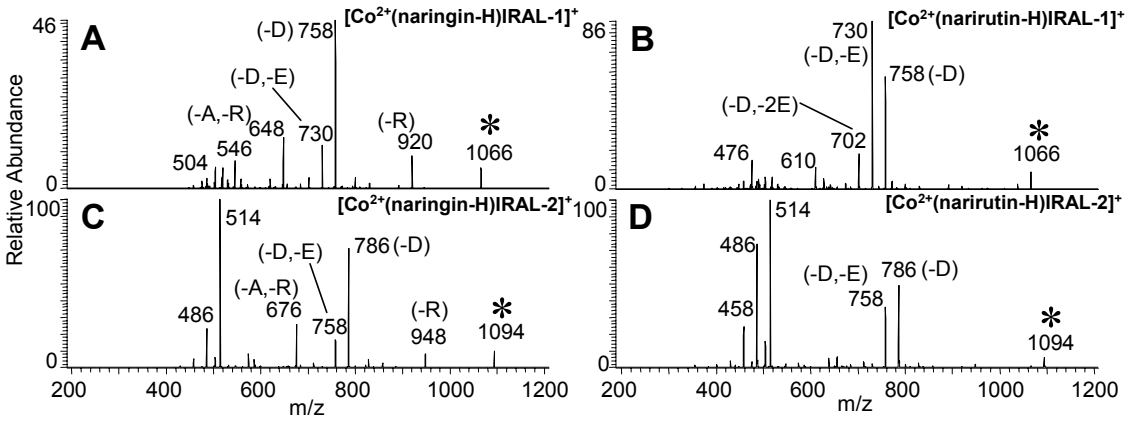

Figure 5-8. IRMPD spectra of the cobalt/flavanone complexes containing either IRAL-1 or IRAL-2. A) $[Co^{2+}$ (naringin – H) IRAL-1$]^+$, 50 W for 12 ms, B) $[Co^{2+}$ (narirutin – H) IRAL-1$]^+$, 50 W for 25 ms, C) $[Co^{2+}$ (naringin – H) IRAL-2$]^+$, 50 W for 10 ms, and D) $[Co^{2+}$ (narirutin – H) IRAL-2$]^+$, 50 W for 25 ms.

In general, IRMPD of the cobalt complexes is more successful for differentiation of isomers, such as those shown in Figure 5-2, than the copper complexes. A diagnostic ion due to the loss of the aglycon and rhamnose moieties can be used for differentiation of the neohesperidosides versus rutinosides, as demonstrated in Figure 5-8 for complexes containing either IRAL-1 or IRAL-2 ligand.

5.5 CONCLUSIONS

The IRMPD efficiency in a QIT has been substantially improved by use of a metal complexation strategy that incorporates an IR-active ligand, in this case containing two phosphonate groups. Complexes of the type $[M^{2+}$ (flavonoid-H) IRAL$]^+$ were formed, where M was a transition metal such as copper or cobalt and IRAL is a phosphonated bipyridine ligand. The flavonoids undergo substantial and informative dissociation indicating that the IR energy is efficiently transferred throughout the entire non-covalent complex. The complexes containing the IR-active ligands dissociated with

high efficiencies upon irradiation times of ~15 msec, whereas complexes without IR-active ligands did not dissociate even when irradiated for 2.5 sec. This strategy, which does not involve covalent modification of the analyte but only entails self-assembly of the complexes in solution directly prior to ESI-MS analysis, should be generally applicable to many other classes of compounds, thus greatly increasing the versatility of IRMPD methods in quadrupole ion traps.

5.6 REFERENCES

1. Sleno, L.; Volmer, D. A. *J. Mass Spectrom.* **2004**, *39*, 1091-1112.
2. de Hoffmann, E. *J. Mass Spectrom.* **1996**, *31*, 129-137.
3. March, R. E. *J. Mass Spectrom.* **1997**, *32*, 351-369.
4. Syka, J. E. P.; Coon, J. J.; Schroeder, M. J.; Shabanowitz, J.; Hunt, D. F. *Proc. Natl. Acad. Sci. U. S. A.* **2004**, *101*, 9528-9533.
5. Gunawardena, H. P.; Emory, J. F.; McLuckey, S. A. *Anal. Chem.* **2006**, *78*, 3788-3793.
6. Racine, A. H.; Payne, A. H.; Remes, P. M.; Glish, G. L. *Anal. Chem.* **2006**, *78*, 4609-4614.
7. Schwartz, J. C.; Thermo Finnigan LLC: United States, 2005.
8. Wilson, J. J. B., J.S. *Anal. Chem.* **2006**, *78*, 6855-6862.
9. Crowe, M. C.; Brodbelt, J. S. *J. Am. Soc. Mass Spectrom.* **2004**, *15*, 1581-1592.
10. Crowe, M. C.; Brodbelt, J. S. *Anal. Chem.* **2005**, *77*, 5726-5734.
11. Crowe, M. C.; Brodbelt, J. S.; Goolsby, B. J.; Hergenrother, P. *J. Am. Soc. Mass Spectrom.* **2002**, *13*, 630-649.
12. Keller, K. M.; Brodbelt, J. S. *Anal. Biochem.* **2004**, *326*, 200-210.
13. Goolsby, B. J.; Brodbelt, J. S. *J. Mass Spectrom.* **1998**, *33*, 705-712.
14. Goolsby, B. J.; Brodbelt, J. S. *J. Mass Spectrom.* **2000**, *35*, 1011-1024.

15. Goolsby, B. J.; Brodbelt, J. S. *Anal. Chem.* **2001**, *73*, 1270-1276.

16. Vartanian, V. H.; Goolsby, B.; Brodbelt, J. S. *J. Am. Soc. Mass Spectrom.* **1998**, *9*, 1089-1098.

17. Shen, J.; Brodbelt, J. S. *Analyst* **2000**, *125*, 641-650.

18. Payne, A. H.; Glish, G. L. *Anal. Chem.* **2001**, *73*, 3542-3548.

19. Black, D. M. P., A.H.; Glish, G.L. *J. Am. Soc. Mass Spectrom.* **2006**, *17*, 932-938.

20. Boue, S. M.; Stephenson, J. L.; Yost, R. A. *Rapid Commun. Mass Spectrom.* **2000**, *14*, 1391-1397.

21. Stephenson, J. L.; Booth, M. M.; Shalosky, J. A.; Eyler, J. R.; Yost, R. A. *J. Am. Soc. Mass Spectrom.* **1994**, *5*, 886-893.

22. Stephenson, J. L. Y., R.A. In *Practical Aspects of Ion Trap Mass Spectrometry*, 1995.

23. Hashimoto, Y.; Hasegawa, H.; Yoshinari, K.; Waki, I. *Anal. Chem.* **2003**, *75*, 420-425.

24. Hashimoto, Y.; Hasegawa, H.; Waki, L. *Rapid Commun. Mass Spectrom.* **2004**, *18*, 2255-2259.

25. Drader, J. J.; Hannis, J. C.; Hofstadler, S. A. *Anal. Chem.* **2003**, *75*, 3669-3674.

26. Colorado, A.; Shen, J. X. X.; Vartanian, V. H.; Brodbelt, J. *Anal. Chem.* **1996**, *68*, 4033-4043.

27. Kim, T. Y.; Thompson, M. S.; Reilly, J. P. *Rapid Commun. Mass Spectrom.* **2005**, *19*, 1657-1665.

28. Devakumar, A.; Thompson, M. S.; Reilly, J. P. *Rapid Commun. Mass Spectrom.* **2005**, *19*, 2313-2320.

29. Stephenson, J. L.; Booth, M. M.; Boue, S. M.; Eyler, J. R.; Yost, R. A. *Biochemical and Biotechnological Applications of Electrospray Ionization Mass Spectrometry* **1996**, *619*, 512-564.

30. Goldberg, D.; Bern, M.; Li, B. S.; Lebrilla, C. B. *J. Proteome Res.* **2006**, *5*, 1429-1434.

31. Cooper, H. J.; Heath, J. K.; Jaffray, E.; Hay, R. T.; Lam, T. T.; Marshall, A. G. *Anal. Chem.* **2004**, *76*, 6982-6988.

32. Little, D. P.; Speir, J. P.; Senko, M. W.; Oconnor, P. B.; Mclafferty, F. W. *Anal. Chem.* **1994**, *66*, 2809-2815.

33. Meng, F. Y.; Cargile, B. J.; Patrie, S. M.; Johnson, J. R.; McLoughlin, S. M.; Kelleher, N. L. *Anal. Chem.* **2002**, *74*, 2923-2929.

34. Sannes-Lowery, K. A.; Hofstadler, S. A. *J. Am. Soc. Mass Spectrom.* **2003**, *14*, 825-833.

35. Flora, J. W.; Muddiman, D. C. *Anal. Chem.* **2001**, *73*, 3305-3311.

36. Flora, J. W.; Muddiman, D. C. *J. Am. Chem. Soc.* **2002**, *124*, 6546-6547.

37. Satterfield, M.; Brodbelt, J. S. *Anal. Chem.* **2000**, *72*, 5898-5906.

38. Satterfield, M.; Brodbelt, J. S. *J. Am. Soc. Mass Spectrom.* **2001**, *12*, 537-549.

39. Zhang, J. M.; Brodbelt, J. S. *Anal. Chem.* **2005**, *77*, 1761-1770.

40. Zhang, J. M.; Wang, J. M.; Brodbelt, J. S. *J. Mass Spectrom.* **2005**, *40*, 350-363.

41. Pikulski, M.; Brodbelt, J. S. *J. Am. Soc. Mass Spectrom.* **2003**, *14*, 1437-1453.

42. Davis, B. D.; Brodbelt, J. S. *J. Am. Soc. Mass Spectrom.* **2004**, *15*, 1287-1299.

43. Davis, B. D.; Brodbelt, J. S. *Anal. Chem.* **2005**, *77*, 1883-1890.

44. Maerker, G. C. *J. Am. Chem. Soc.* **1958**, *80*, 2745-2748.

45. Carlson, B.; Phelan, G. D.; Kim, J. H.; Jen, A. K. Y.; Dalton, L. R. *Proceeding of SPIE* **2003**, *4800*, 93-104.

46. Penicaud, V.; Odobel, F.; Bujoli, B. *Tetrahedron Lett.* **1998**, *39*, 3689-3692.

47. Peng, Z. H.; Gharavi, A. R.; Yu, L. P. *J. Am. Chem. Soc.* **1997**, *119*, 4622-4632.

48. Montalti, M.; Wadhwa, S.; Kim, W. Y.; Kipp, R. A.; Schmehl, R. H. *Inorg. Chem.* **2000**, *39*, 76-84.

49. Will, G.; Boschloo, G.; Rao, S. N.; Fitzmaurice, D. *J. Phys. Chem. B* **1999**, *103*, 8067-8079.

50. Jones, J. L.; Dongre, A. R.; Somogyi, A.; Wysocki, V. H. *J. Am. Chem. Soc.* **1994**, *116*, 8368-8369.

51. Dongre, A. R.; Jones, J. L.; Somogyi, A.; Wysocki, V. H. *J. Am. Chem. Soc.* **1996**, *118*, 8365-8374.

52. Jellen, E. E.; Chappell, A. M.; Ryzhov, V. *Rapid Commun. Mass Spectrom.* **2002**, *16*, 1799-1804.

Chapter 6: Sequencing and Characterization of Oligosaccharides Using Infrared Multiphoton Dissociation and Boronic Acid Derivatization in a Quadrupole Ion Trap

6.1 OVERVIEW

A simplified method for determining the sequence and branching of oligosaccharides using infrared multiphoton dissociation (IRMPD) in a quadrupole ion trap (QIT) is described in this chapter. An IR-active boronic acid (IRABA) reagent is used to derivatize the oligosaccharides prior to IRMPD analysis. The IRABA ligand is designed to both enhance the efficiency of the derivatization reaction and to facilitate the photon absorption process. The resulting IRMPD spectra display oligosaccharide fragments that are formed from primarily one type of diagnostic cleavage, thus making sequencing straightforward. The presence of sequential fragment ions, a phenomenon of IRMPD, permit the comprehensive sequencing of the oligosaccharides studied in a single stage of activation. We demonstrate this approach for two series of oligosaccharides, the lacto-N-fucopentaoses (LNFPs) and the lacto-N-difucohexaoses (LNDFHs).

6.2 INTRODUCTION

Oligosaccharides are in many ways more structurally complex than other biologically important molecules such as proteins and nucleic acids in that they are often highly branched and have several different linkage types between their fundamental monosaccharide units. Even excluding stereochemistry, a glycosidic bond between two hexoses can be formed at any of five positions. This results in a great number of structural possibilities that make characterization of oligosaccharides a challenging but vital task because they have important roles in numerous biological processes. Oligosaccharides are known to play roles in cell-cell signaling, cellular differentiation,

regulation of biochemical pathways, viral replication, parasitic infection, immune response and inflammation.[1-7] More than half of mammalian proteins are glycosylated,[1] and the functions attributed to the oligosaccharides are broadly grouped as structural/modulatory and specific recognition by receptors.[8] For example, some oligosaccharides are involved in cell wall formation and have protective and stabilizing roles while others are very specific receptors for bacteria and viruses. In addition, the alteration of oligosaccharide expression has been associated with disease progression, suggesting that oligosaccharides may be used as biomarkers.[9] For instance, malignancy has been correlated with changes in the glycosylation process, and some cell surface oligosaccharides are linked with prognosis in human cancers.[10, 11] To fully understand the roles of glycosylation in these biological processes, it is critical to develop sensitive methods of characterization.

Mass spectrometry (MS) has become an invaluable tool for the structural determination of oligosaccharides mainly due to the minimal sample consumption and specificity of the information obtained. Matrix assisted laser desorption ionization (MALDI) time-of-flight (TOF) MS has been used for the analysis of native, metal adducted and derivatized oligosaccharides.[12-15] Structural isomers have been differentiated successfully by comparing the intensities of post source decay (PSD) fragment ions. While MALDI-TOFMS has provided some detailed information about isomers, more detailed structural analysis is generally performed by using tandem mass spectrometry.

Trapping instruments such as the quadrupole ion trap (QIT) and Fourier transform ion cyclotron resonance (FTICR) mass spectrometers have also been used for the analysis of oligosaccharides because of the ability to undertake MS^n experiments which is often required to fully map the branching patterns and sequences of oligosaccharides.

Collisionally activated dissociation (CAD) of oligosaccharides primarily leads to fragment ions due to B-/Y- and C-/Z-type cleavages.[15-25] The number of cleavages in the first stage of activation is often limited, and thus frequently it requires several stages of activation to obtain partial sequence information, particularly for larger oligosaccharides. In addition, CAD often leads to cleavages from both the reducing and non-reducing ends of oligosaccharides in addition to internal losses, thus complicating spectral interpretation. To provide more extensive structural information and alleviate the need for elaborate MS^n strategies, other activation methods have also been applied to glycopeptides and oligosaccharides in trapping instruments. For example, Adamson *et al.* used electron capture dissociation (ECD) in an FTICR to promote cross-ring over glycosidic cleavages and increase the amount of linkage information obtained.[26] Wolff *et al.* used electron detachment dissociation (EDD) to promote cross-ring cleavages and identify sites of sulfation in glycosaminooligosaccharide tetrasaccharides.[27] Most recently, Devakumar et al. 157-nm UV light to photofragment glycans in an ion trap. Extensive high energy cross-ring cleavages were observed that provided branching information.[28]

Infrared multiphoton dissociation (IRMPD) is another alternative activation method that has generated substantial recent interest. Several studies have explored the use of IRMPD in an FTICR mass spectrometer for the analysis of oligosaccharides.[16, 29-33] For example, Lancaster *et al.* compared the IRMPD spectra of O-linked and N-linked type oligosaccharides and found that cross-ring cleavages were observed only for the N-type oligosaccharides that are not readily fragmented by using CAD.[16] Goldberg *et al.* used IRMPD in an FTICR instrument and developed a strategy using a computer algorithm to determine oligosaccharide sequence. While the spectra were informative, poor signal-to-noise ratios often made spectral interpretation difficult. Fukui *et al.* used

wavelength-tunable IRMPD in an FTICR mass spectrometer to determine the optimal dissociation wavelengths for sodium-cationized oligosaccharides. While this technique is powerful, these types of lasers are not readily available. Zhang *et al.* used IRMPD in an FTICR instrument on oligosaccharide alditols and discovered specific fragments corresponding to structural motifs that revealed sequence and linkage information.

IRMPD has also been implemented in quadrupole ion traps for the analysis of flavonoids, antibiotics, peptides, and oligonucleotides[34-44] and affords a promising alternative to CAD for the characterization of oligosaccharides as described in this chapter. The IRMPD process is independent of the rf trapping voltage, meaning that storage and detection of ions over a wide m/z range is possible, including very low m/z fragment ions at the same time as high m/z precursors. Since IRMPD is not a collision-based method, there are fewer ion losses due to scattering. This reduction of ion losses is a critical feature when ion populations are low, which is often the case for oligosaccharides. Another potential advantage of IRMPD involves the ease of controlling photon flux to enhance or limit sequential fragmentation processes. Since IRMPD is not a resonant process, energy absorption by primary fragment ions during the activation period may result in secondary fragmentation, and the extent can be varied by adjusting the activation time or laser power. The secondary fragments often provide important structural information without the need for more elaborate MS^n strategies. One drawback to IRMPD in a quadrupole ion trap stems from the relative slow rate of energy accumulation (only ~ 0.1 eV per photon) that allows competition from collisional cooling due to the helium bath gas. In addition to other recent methods designed to overcome this drawback, such as thermally assisted IRMPD and collision-activated IRMPD,[45-49] a method that incorporates chromophores that absorb IR radiation very efficiently into analytes of interest was developed. For example, the use of IR-active ligands (IRALs)

for the enhancement of IRMPD efficiency of flavonoids in a quadrupole ion trap was described in Chapter 5.[34] In this previous chapter, IR-active phosphonate groups were attached to chelating ligands that were then noncovalently bound to the analytes of interest via metal coordination through a self-assembly process. The resulting complexes underwent highly efficient IRMPD. Companion FTIR and energy-variable CAD results confirmed that the chromogenic ligands were effective because of the high IR absorptivities of the phosphonate groups, thus providing strong IR chromophores for rapid energy accumulation. The use of a phosphonate-based IR chromophore is also exploited in this chapter.

While it has become common practice to form chromophore-labeled carbohydrate derivatives for UV and fluorescence detection following chromatographic separation, various chemical derivatization strategies of oligosaccharides have also been used in conjunction with mass spectrometry to increase ionization sensitivity, as well as yield more informative fragmentation patterns that reveal linkage and anomeric configuration.[52-58] Some of the derivatization techniques used for ESI-MS analysis of carbohydrates include permethylation for linkage information,[50, 51] reductive amination for attachment of chromophores for HPLC detection,[52] p-aminobenzoic ethyl ester derivatization via formation of a glycosylamine for determination of linkage and branching information,[53] and modification of cis-diol groups of disaccharides with boronic acids for stereochemical determination.[54, 55] Most recently, phenylboronic acid was used as a reagent ion for the analysis of biologically active diol compounds by desorption electrospray ionization (DESI) MS.[56]

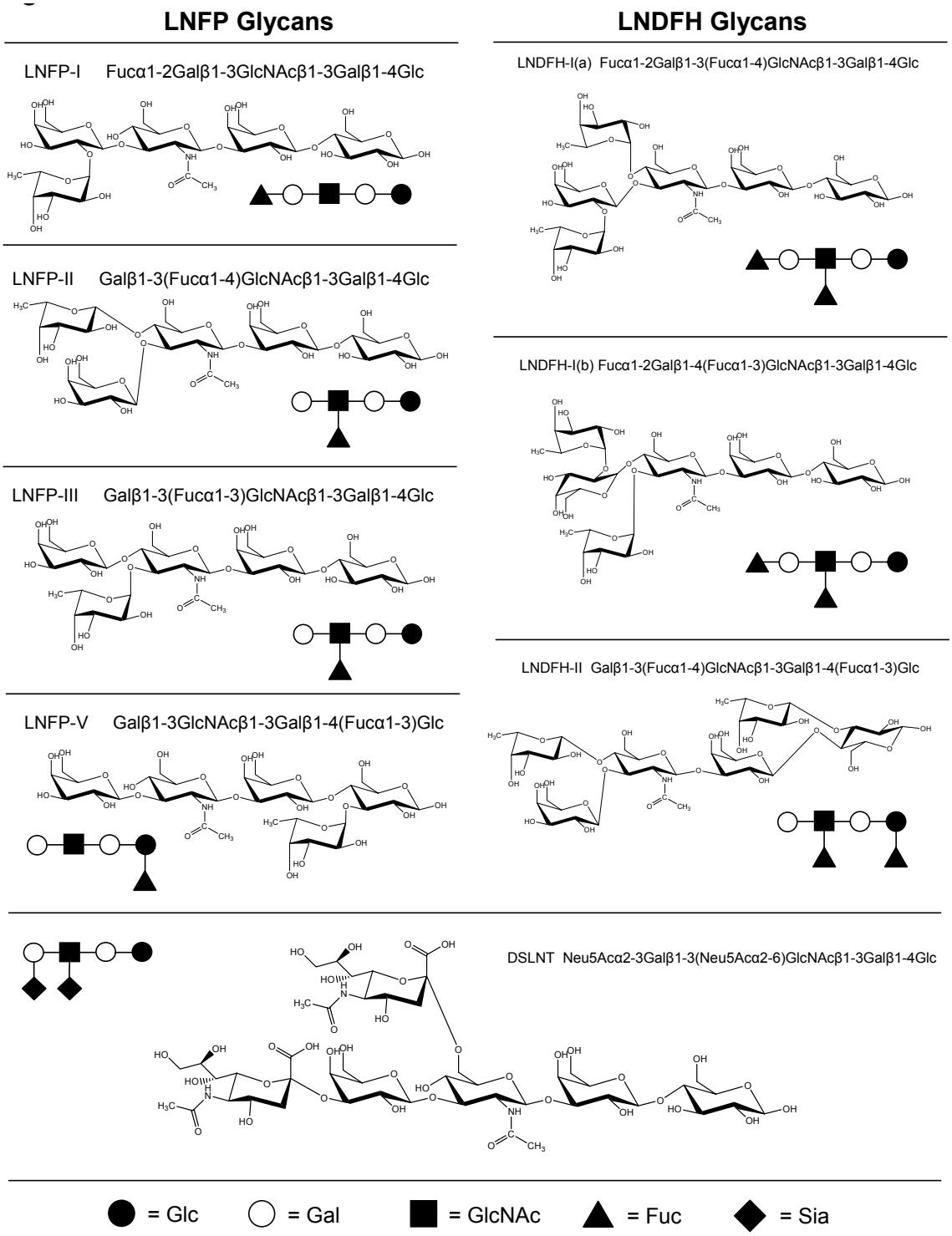

Figure 6-1. Chemical and cartoon structures of the oligosaccharides used in this chapter.

In the work presented in this chapter, we develop a method for the characterization of oligosaccharides in a quadrupole ion trap using IRMPD to attain complete sequencing and branching information. In contrast to other recent methods developed to promote cross-ring cleavages to enhance linkage information, the goal of the study in this chapter was to simplify and limit the spectra to glycosidic cleavages for comprehensive and straightforward sequencing. The sequence and branching positions of two series of isomeric oligosaccharides were determined (Figure 6-1).

The first series, the lacto-N-fucopentaoses (LNFPs), all have the same backbone sequence but differ either in the connectivity of fucose (Fuc) or the linkage of their terminal Gal and Fuc moieties. The second series, the lacto-N-difucohexaoses (LNDFHs), also have the same backbone structure but have two Fuc residues and differ either in the connectivity or linkage of one of the Fuc residues. These series were natural choices for method development since they have been characterized by different mass spectrometric techniques previously.[12, 19-21, 23, 33, 57] For example, MALDI-MS methods have been developed that differentiate some of the LNFP isomers based on ions due to internal losses and others that reveal the interglycosidic linkage.[12, 33, 57] While several of these fragment ions facilitate isomer differentiation, they often do not provide complete sequence information and may complicate spectral interpretation of unknown oligosaccharides since they are a product of cleavage from both the reducing and non-reducing ends coupled with internal and unidentified fragments. Several methods using ESI-MS for characterization of the LNFPs and LNDFHs have also been reported. For example, Konig and Leary used metal ion coordination to alter the fragmentation pathways of the LNFPs; however, the study was focused on specific linkage determination and not sequencing.[23] Chai and Lawson used ESI-MS in conjunction with a Q-TOF mass spectrometer and identified specific “D-type” fragments that differentiated

the LNFPs and LNDFHs.[21] These fragments and several other lower mass fragments are only observed upon several stages of CAD (MS^n) in the QIT.[19-21] Pfenninger and Karas developed an elaborate and comprehensive method for the isomer differentiation of oligosaccharides[19-21] that also provides linkage information, although the resulting spectra are complicated by several different types of fragment ions.

In this chapter, a simplified method for the sequencing of oligosaccharides in a single stage of activation by exploiting the supplementary information obtained from sequential fragmentation that is promoted by non-resonance IRMPD is described. Additionally, our method is further extended to an oligosaccharide with two acidic sialic acid moieties. To increase the IR absorption efficiency of the oligosaccharides, a phosphonate group was incorporated into a boronic acid that was used as a derivatizing reagent. The IR-active boronic acid (IRABA) was designed so that a nitrogen atom was adjacent to the boron atom to enhance the reactivity of the boronic acid functionality to the oligosaccharides.[58] When the IRABA is added to a solution containing an oligosaccharide of interest, the chemical reaction between the IRABA and diol functionalities of the oligosaccharide is responsible for the covalent addition of the IR-active phosphonate group. The modified analytes proved to be ideal for characterization and differentiation using IRMPD. The LNFP and LNDFH series provide a considerable challenge for differentiation and thus allow a convenient means of assessing the analytical merits of the new IRMPD method.

6.3 EXPERIMENTAL

6.3.1 Chemical Reagents

LNFP-I, II, III, V, LNDFH Ia and II and DSLNT were purchased from V-Labs (Covington, LA). LNDFH-Ib was purchased from Sigma (St. Louis, MO).

Diethyl(aminomethyl)phosphonate oxalate was purchased from Acros (Belgium). 2-formylphenylboronic acid, methanol and methylene chloride were purchased from Fisher (Somerville, NJ). All chemicals were used without further purification.

6.3.2 Derivatization

Stock solutions of the oligosaccharides (500 μM) and the IRABA (mM) were mixed to form a 1:10 molar ratio and a 5 μL aliquot of 0.5% TEA was added to achieve a pH ~9. The reaction is reversible and a lower pH would result in a competition of hydrolysis of the new bonds formed. The solutions were then sonicated for 1 min and diluted with 0.1% TEA to pH ~8 and spiked with ammonium acetate (to 0.01%) to eliminate the domination of derivatized sodium adducts. The final solution had an oligosaccharide concentration of 10 μM.

6.3.3 Mass Spectrometry

A Finnigan LCQ Deca XP mass spectrometer equipped with an electrospray ionization source and interfaced with a Synrad CO_2 50 W laser (10.6 μm) was used for the work presented in this chapter. The details of the system were previously described.[35] The solutions analyzed were 10 μM in oligosaccharide. Typical IRMPD parameters included an irradiation time of 5 - 25 msec at a power of 50 W. The helium pressure for IRMPD experiments of the derivatized oligosaccharides and comparative CAD experiments was nominally 2.8×10^{-5} Torr (corresponding to approximately 1 mtorr normally used in the quadrupole ion trap) as measured by an ionization gauge. For the underivatized oligosaccharides (i.e. without IR chromophores), the helium pressure was lowered to nominally 2.7×10^{-5} Torr to promote the IRMPD process.

Throughout this chapter, the laser power was 50W and the irradiation time was adjusted to tune sequential fragmentation such that the most complete structural

information was obtained. At prolonged irradiation times sequential fragmentation was extensive and higher mass fragments were not observed.

6.3.4 Synthesis OF IRABA

The procedure used was a modification of the synthesis described by Zhu and Anslyn.[59] 3.9 mmol 2-formylphenylboronic acid (mM) was dissolved in anhydrous CH_3OH under argon protection. 16 mmol (4X) Hunig's base was added followed by 3.9 mmol diethyl(aminomethyl)phosphonate oxalate and the solution was stirred for 16 hours before 2.9 mmol $NaBH_4$ was added slowly. The solution was stirred at rt for 1 hour, followed by addition of another batch of $NaBH_4$. One hr later, the solvent was removed under vacuum and the residue was diluted with CH_2Cl_2. The white ppt was removed with vacuum filtration, with the filtrate subsequently concentrated. The residue was purified by flash chromatography on neutral alumina (2-5% NH_3-saturated CH_3OH in CH_2Cl_2). 1H NMR (400 MHz, CD_3OD) δ 1.39 (t, J=7.04, 6H, CH3) δ 3.23 (d, J=11.6, 2H CH's) δ 4.17 (s, 2H CH's) δ 4.20-4.26 (m, 4H CH's) δ 7.15-7.43 (m, 4H CH's). 13C NMR(CD_3OD): = 16.8, 42.2, 43.4, 56.2, 64.4, 124.1, 127.9, 128.7, 131.4, 142.9. HRMS: calcd. $(M + Na)^+$ 324.1148, found 324.1135.

6.4 RESULTS AND DISCUSSION

The goal in this chapter was to develop a method for sequencing the backbone of the LNFPs and to pinpoint the sites of attachment of the fucose moieties. To allow the comprehensive evaluation of the new IRABA derivatization/IRMPD strategy for the characterization of oligosaccharides, companion CAD and IRMPD studies of the underivatized oligosaccharides were undertaken to provide benchmark comparisons. These studies are briefly described in the first section prior to presentation of the results for the IRABA-derivatized oligosaccharides.

6.4.1 LNFP Oligosaccharides

The LNFP oligosaccharides used in this chapter (Figure 6-1) differ only in the branching position of the fucose moiety (LNFP I vs. II and III vs. V) or have the same position but differ only in the linkage (LNFP II vs. III). The oligosaccharides are characterized using the residue masses for the monosaccharide units that are listed in Table 6-1 and are further described using the nomenclature of Domon and Costello [60]. Since the structures of the oligosaccharides used in this chapter are known, it was possible to also include specific hexose identification upon analysis. In the case of an unknown, less specific identifications (unknown identifications such as Hex instead of Gal) would be determined. The abbreviations, residue masses and unknown identifications used are provided in Table 6-1.

Table 6-1. Residue Masses and Identification Abbreviations Used

Monosaccharide	ID	Unknown ID	Residue Mass
Fucose	Fuc	Fuc	146
Galactose	Gal	Hex	162
Glucose	Glc	Hex	162
N-acetyl-glucosamine	GlcNAc	HexNAc	203
Hexose	Hex	Hex	162
N-acetyl-hexosamine	HexNAc	HexNAc	203
Sialic acid	Sia	Sia	219

6.4.1.1 CAD and IRMPD of Deprotonated Oligosaccharides

The CAD mass spectra of the four deprotonated oligosaccharides, ($[L - H]^-$), are shown in Figure 6-2, a-d, and the data is tabulated in Table 6-2. Losses of the residue masses are labeled with the corresponding residues (e.g., loss does not include the intersaccharide oxygen atom). Losses that include the intersaccharide oxygen atom are

labeled with the monosaccharide identity and an asterisk. The types of fragments observed in the CAD and IRMPD spectra (shown in Figure 6-2, e-h, and briefly described below) are consistent with those previously reported, although the IRMPD spectra exhibit several additional sequential fragment ions. The spectra include mainly Z- or C- and B- or Y-type cleavage. The detailed fragmentation pathways of the deprotonated LNFPs have been described previously [19-21]. The CAD spectra do not display as many fragment ions as were observed in the previous studies (Figure 6-2); however the IRMPD spectra (described below) display even more. In several cases there is limited information in the first stage of fragmentation and further analysis of these oligosaccharides using multiple sequential stages of tandem mass spectrometry is not generally viable since ion populations are too low.

The IRMPD mass spectra of the underivatized oligosaccharides were acquired to exploit the benefits of sequential fragmentation that often occur when using this non-resonant activation method. Sequential fragmentation was evident for the oligosaccharides because increases in the laser irradiation time resulted in an increase in the abundance of lower mass fragments coupled with a decrease in the abundance of higher mass fragments. For these experiments, a slightly reduced helium pressure was necessary to enhance energy accumulation at the expense of trapping efficiency (less effective collisional cooling of ions). The irradiation time was adjusted to optimize the number of informative fragment ions, and the resulting spectra are shown in Figure 6-2, e-h. The data is tabulated in Table 6-2.

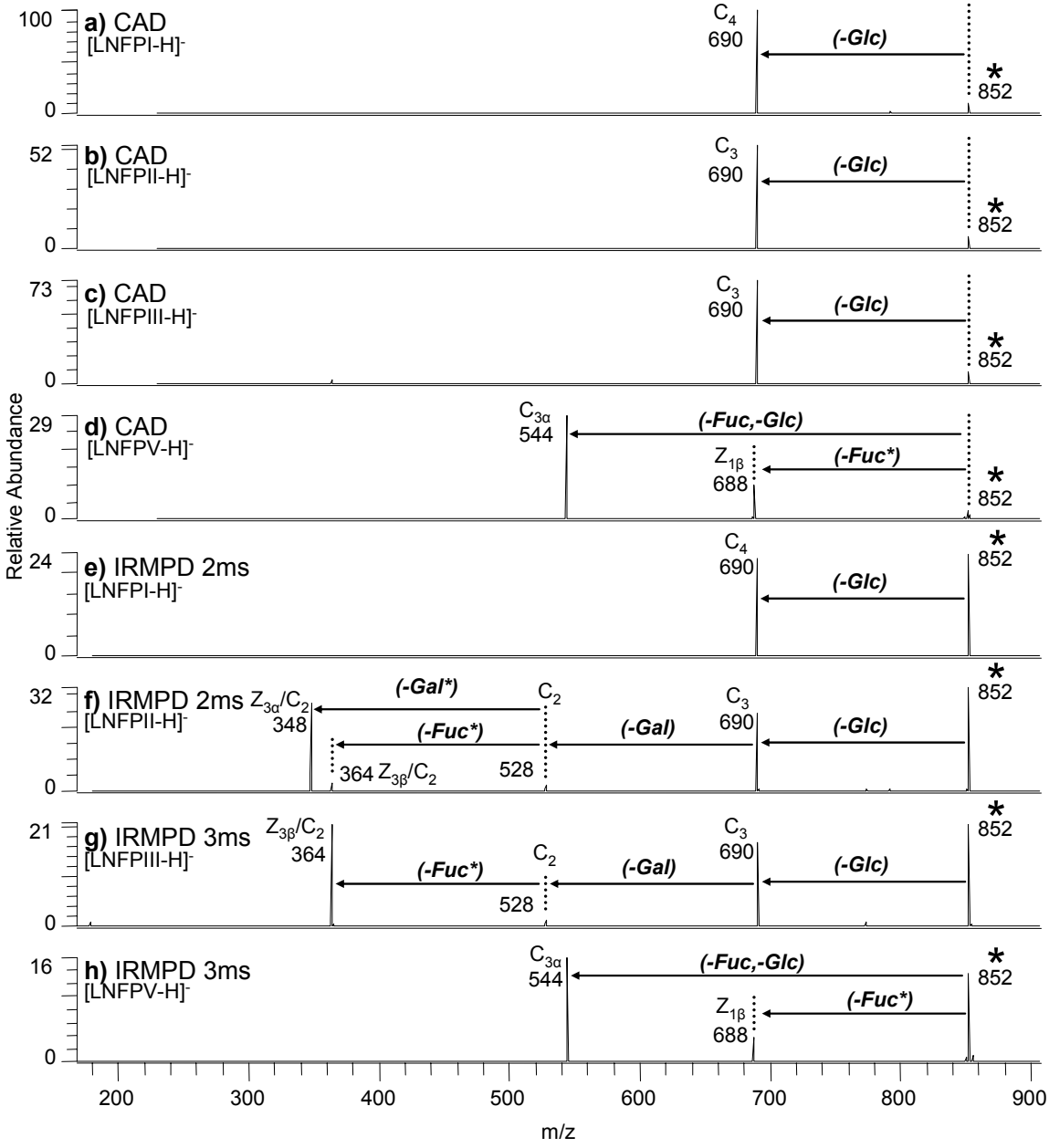

Figure 6-2. CAD and IRMPD spectra of the deprotonated oligosaccharides used in the chapter. CAD: a) $[LNFPI-H]^-$, b) $[LNFPII-H]^-$, c) $[LNFPIII-H]^-$, d) $[LNFPV-H]^-$; IRMPD: e) $[LNFPI-H]^-$, f) $[LNFPII-H]^-$, g) $[LNFPIII-H]^-$, h) $[LNFPV-H]^-$.

Table 6-2. Underivatized LNFP Oligosaccharide Fragment Ion Abundances

$(M - H)^-$ CAD	C_4[a], C_3[b,c]	$Z_{1\beta}$	$C_{3\alpha}$	C_2	$C_{3\beta}/C_2$	$Z_{3\alpha}$
LNFP-I	91	-	-	-	-	-
LNFP-II	89	-	-	-	-	-
LNFP-III	89	-	-	-	-	-
LNFP-V	-	24	71	-	-	-
$(M - H)^-$ IRMPD	C_4[a], C_3[b,c]	$Z_{1\beta}$	$C_{3\alpha}$	C_2	$C_{3\beta}/C_2$	$Z_{3\alpha}$
LNFP-I	48	-	-	-	-	-
LNFP-II	28	-	-	2	2	32
LNFP-III	29	-	-	2	35	-
LNFP-V	-	11	49	-	-	-
$(M + Na)^+$ CAD	Y_4[a] or Y_3[b,c]	B_4	Y_4/B_4[a], $Y_{3\beta}/B_3$[b,c], B_3[d]	Y_4/B_3, $Y_{3\beta}/B_2$, B_2	$X_2^{2,3}$	$X_3^{2,4}$
LNFP-I	83	6	3	-	-	-
LNFP-II	68	14	7	-	-	-
LNFP-III	68	14	5	-	-	-
LNFP-V	83		3	-	-	-
$(M + Na)^+$ IRMPD	Y_4[a] or Y_3[b,c]	B_4	Y_4/B_4[a], $Y_{3\beta}/B_3$[b,c], B_3[d]	Y_2/B_4	$X_2^{2,3}$	$X_3^{2,4}$
LNFP-I	35	-	2	-	13	11
LNFP-II	40	-	4	12	-	-
LNFP-III	34	-	4	20	-	-
LNFP-V	49	-	2	2	-	-

* as a percentage of total sequence and parent ion abundances, +/- 5%

[a]LNFP-I

[b]LNFP-II

[c]LNFP-III

[d]LNFP-V

Inspection of the IRMPD spectra indicates that the four isomers are differentiated due to the presence of ions derived from sequential fragmentation. The spectrum for deprotonated LNFP-I displays only a single loss of Hex, whereas the spectra for deprotonated LNFP-II and III display a second loss of Hex. The next sequential fragments observed for LNFP-II and III differ and are due to the loss of Hex ($Z_{3\alpha}/C_2$) or Fuc ($Z_{3\beta}/C_2$), respectively. The overall sequence of losses is consistent with the final loss

being identified as the monosaccharide unit that is linked to the GlcNAc for each of these isomers (Gal for LNFP-II and Fuc for LNFP-III), indicating that loss of the terminal 1→3 linked monosaccharides is a much more facile loss than the loss of the terminal 1→4 linked monosaccharides. The IRMPD spectrum for LNFP-V is unique in that there are two types of cleavages involving Fuc; the first being the loss of Fuc ($Z_{1\beta}$) and another the loss of Fuc in conjunction with a loss of Hex ($C_{3\alpha}$). Examination of the LNFP structures suggests that the first losses from the non-reducing end generally occur as a Z-type cleavage and losses from the reducing end occur as a C-type cleavage. Unfortunately, for each isomer there is a lack of a significant amount of information for sequencing the backbone and Fuc position. In addition, the sequential losses are limited to one to three monosaccharide units, thus restricting the sequence coverage. Overall, the CAD and IRMPD spectra of the deprotonated oligosaccharides display losses that cannot be immediately identified as occurring from the reducing or non-reducing end of the oligosaccharides. Additionally, some ions (e.g., 348 Da and 364 Da in Figure 6-2, f and g, respectively) cannot be confidently identified as being a result of a sequential loss or an internal loss (e.g., "D-type loss"). Even with the correct identification of losses, it would require several stages of dissociation to completely characterize the oligosaccharides. In general, neither the negative ion mode CAD nor IRMPD spectra not provide enough information to sequence these isomers with confidence.

6.4.1.2 CAD and IRMPD of Sodium-Cationized Oligosaccharides

Due to the unsatisfactory structural characterization of the deprotonated oligosaccharides, the CAD and IRMPD spectra of the sodium-cationized oligosaccharides were obtained for comparison. In the positive ion mode, sodium-cationized complexes were formed almost exclusively over the protonated species, and thus they were used for the analyses. The types of losses observed for the sodium

complexes were similar to those observed for the deprotonated oligosaccharides (Figure 6-3). The residue losses observed for all isomers are tabulated in Table 6-2. The CAD spectra are all highlighted by a predominant loss of Fuc, rendering these spectra uninformative.

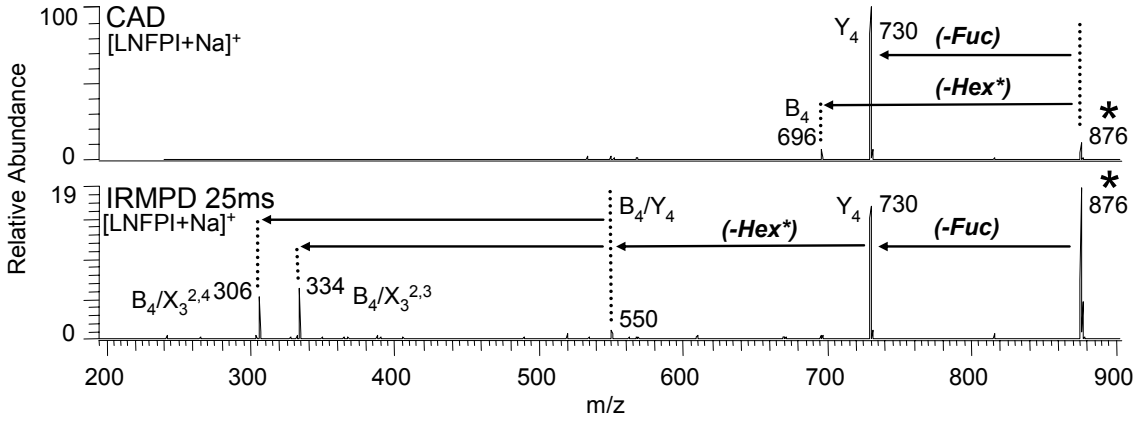

Figure 6-3. CAD and IRMPD spectra of sodiated LNFPI in the positive ion mode: a) CAD, b) IRMPD.

The IRMPD spectra are highlighted by a loss of Fuc followed by a sequential loss of Hex*, the asterisk indicating the inclusion of the intersaccharide oxygen in the neutral loss. Following the Hex* loss, the LNFP-I isomer undergoes cross-ring cleavages of the type $X_3^{2,4}$ and $X_3^{2,3}$, using the nomenclature of Domon and Costello [60], while the other isomers undergo an additional Hex loss. Inspection of the data summarized in Table 6-2 reveals why tandem mass spectrometric analysis of the sodium-cationized oligosaccharides suffers from the same general limitation as that observed for the deprotonated oligosaccharides in that there is limited structural or sequence information provided in any of the spectra. Since losses observed in the spectra cannot be immediately identified as occurring from the reducing or non-reducing end of the oligosaccharides, it is difficult to obtain confident sequence data. It would require

several stages of dissociation for more complete structural information which is unfeasible with the low ion populations obtained for the sodium-cationized oligosaccharides. Since neither the CAD nor the IRMPD spectra of the underivatized LNFPs yielded diagnostic fragment ions or sufficient sequencing information for the isomers, the boronic acid derivatization strategy was explored next.

6.4.1.3 Derivatized LNFP Oligosaccharides

We envisioned a special boronic acid derivatization reagent that would react efficiently with the oligosaccharides and would incorporate a strong IR chromophore. The IR-active boronic acid (IRABA) shown in Scheme 6-1 was designed to meet these criteria. The strategically placed nitrogen atom adjacent to the boronic acid functionality accelerates the derivatization reaction [58]. Without the nitrogen atom, the reaction with oligosaccharides proceeds with low efficiency. The phosphonate group provides an excellent IR chromophore at 10.6 um. Simple addition of the IRABA ligand to the oligosaccharide solutions results in formation of two covalent bonds between the boronic acid and the oligosaccharides in conjunction with two water losses. An example of this type of reaction for Glc is detailed in Scheme 6-1. Typical ESI mass spectra for the IRABA-derivatized LNFP-I reaction mixture are depicted in Figure 6-4 in both the negative and positive ion modes.

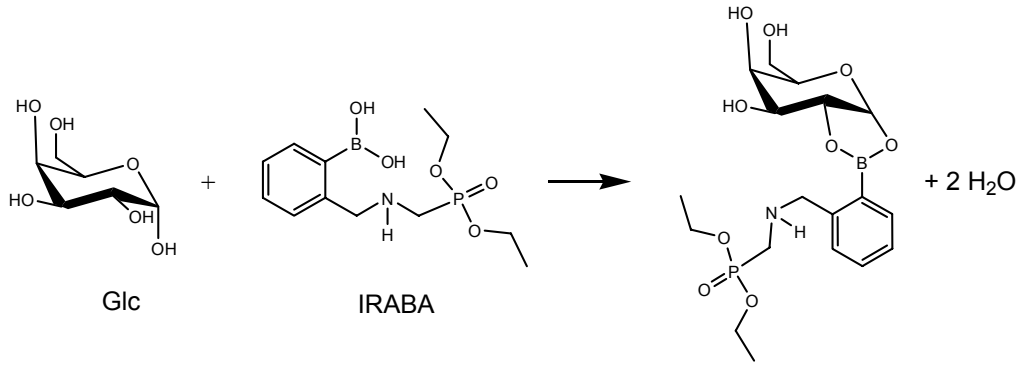

Scheme 6-1. Example reaction of IRABA with glucose (Glc).

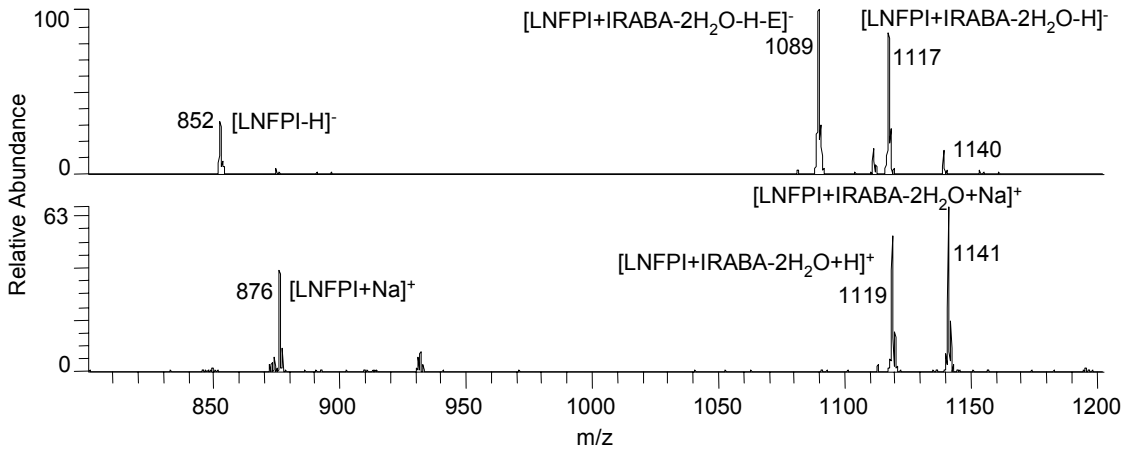

Figure 6-4. Full scan spectra of solutions of LNFPI after derivatization with the IRABA: a) negative ion mode, b) positive ion mode. 'E' indicates the loss of ethene.

In the negative ESI mode, the abundances of the IRABA-derivative is greater than that of the deprotonated oligosaccharide. In addition, there is a product attributed to the derivatized oligosaccharide with a loss of 28 Da, corresponding to a loss of ethylene from the diethylphosphonate functionality. In the positive ESI mass spectra, the IRABA-derivatized and sodium-cationized oligosaccharides are observed. Yields of the derivatized products are high, and sample clean-up is unnecessary. Following successful formation of the derivatized oligosaccharides, the diagnostic value of the fragmentation patterns obtained by CAD or IRMPD was evaluated.

6.4.1.4 CAD and IRMPD of Derivatized Oligosaccharides

The CAD and IRMPD data for the IRABA-derivatized LNFPs in the negative ion mode were collected by activation of the [LNFPI+IRABA-2H_2O-H]$^-$ species, and the resulting spectral data tabulated in Table 6-3. While the fragment ions in the IRMPD spectra of the underivatized oligosaccharides are a result of cleavages from both the reducing and non-reducing ends of the oligosaccharides, the most prominent fragment

ions in the IRMPD spectra of the derivatized analogs are a result of cleavages from the non-reducing end, particularly in the IRMPD spectra.

The CAD spectra for the derivatized LNFPs of the type $[LNFP+IRABA-2H_2O+H]^+$ are shown in Figure 6-5, and the complete series of data is tabulated in Table 6-3. The data suggests that there are two general dissociation pathways: the most prominent one from sequential losses from the non-reducing end of the oligosaccharides (a result of Y-type cleavages) and the other entailing losses from the reducing end (a result of B-type cleavages). In addition, there are also losses of the entire phosphonate moiety from the precursor ions, and these are indicated with a '●' in the spectra. The first general type of pathway is defined by sequential losses from the non-reducing end of the oligosaccharides (losses highlighted in bold type) and correspond to a loss of Fuc and a combined loss of Hex and HexNAc for the LNFPs. The persistent combined loss of Hex and HexNAc suggests that cleavage at the non-reducing end of the GlcNAc is not a facile process.

The LNFP-V isomer, with the Fuc attached to the reducing Glc, is differentiated from the other three by the initial loss of combined Hex and HexNAc which is observed as a prominent fragment ion of m/z 754 Da in the spectrum. Since the Fuc moiety associated with LNFP-I is the terminal saccharide at the non-reducing end, an initial loss of Hex,HexNAc could only occur via an internal loss, a type of cleavage not observed with the oligosaccharides studied using our derivatization strategy. For the LNFP-II and III isomers, both the Gal and Fuc are attached to the GlcNAc which also makes this fragment much less likely. The second general pathway observed in Figure 6-5 involves the combined loss of Hex, Hex*. Since fragmentation occurs from both the reducing and non-reducing ends, in most cases there is no indication from which end the sequential residue losses stem. Hex Hex* loss is consistent for all of the other compounds and arises

from cleavage at the reducing end of the oligosaccharide. In addition, the spectral data suggests that the inclusion of the oxygen atom in the fragments in this type of pathway is characteristic for losses initiated from the reducing end of the oligosaccharides for the IRABA-derivatized species.

Table 6-3. IRABA Derivatized LNFP Oligosaccharide Fragment Ion Abundances

[LNFP + IRABA - $2H_2O$ - H]$^-$ CAD	**C_4, C_3**	**C_3**							
LNFP-I	60	-							
LNFP-II	79	-							
LNFP-III	50	-							
LNFP-V	-	86							
[LNFP + IRABA - $2H_2O$ - H]$^-$ IRMPD	**C_4, C_3**	**C_2**	**$C_{3\alpha}$**						
LNFP-I	42	3	-						
LNFP-II	30	1	-						
LNFP-III	17	-	-						
LNFP-V	-	-	45						
[LNFP + IRABA - $2H_2O$ + H]$^+$ CAD	**Y_4,$Y_{3\beta}$,$Y_{1\beta}$**	**Y_3**	**B_3,B_2**	**$Y_{2\alpha}$**	**B_2**	**Y_2**	**Y_2,$Y_{2\alpha}$/$Y_{1\beta}$**	**B_1**	**Y_0**
LNFP-I	13	-	55	-	4	-	21	-	-
LNFP-II	18	-	43	-	4	-	31	-	-
LNFP-III	31	-	52	-	2	-	10	-	-
LNFP-V	47	-		15	29	-	3	-	-
[LNFP + IRABA - $2H_2O$ + H]$^+$ IRMPD	**Y_4,$Y_{3\beta}$,$Y_{1\beta}$**	**Y_3**	**B_3,B_2**	**$Y_{2\alpha}$**	**B_2**	**Y_2**	**Y_1**	**B_1**	**Y_0**
LNFP-I	4	6	-	-	3	20	10	8	17
LNFP-II	6	-	2	-	7	25	14	5	8
LNFP-III	12	-	2	-	5	23	10	2	17
LNFP-V	15	-	-	5	3	17	17	6	13

* as a percentage of total sequence and parent ion abundances,
+/- 5%

While these CAD spectra do include some diagnostic structural information and allow limited isomer differentiation, the sequence coverage of the oligosaccharides is minimal. It may be possible to obtain more structural information by performing further stages of CAD; however, multiple stages are frequently not feasible since the ion

populations for oligosaccharides are generally not sufficient for these experiments. For these reasons, IRMPD was employed so that the sequential fragmentation that is commonly promoted by the non-resonant nature of IR photoactivation may be exploited for characterization of the oligosaccharides.

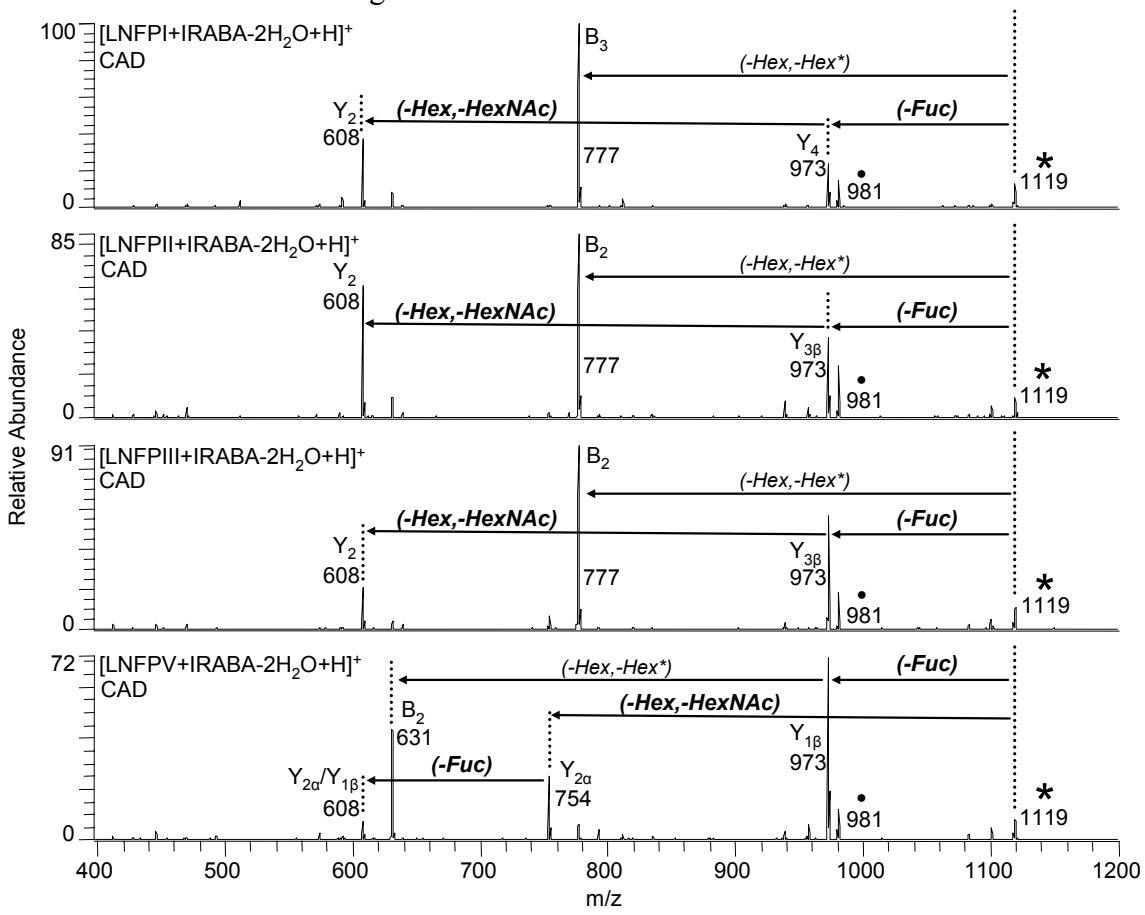

Figure 6-5. Positive ion mode CAD spectra of oligosaccharides after derivatization with IRABA: a) $[LNFPI+IRABA-2H_2O+H]^+$, b) $[LNFPII+IRABA-2H_2O+H]^+$, c) $[LNFPIII+IRABA-2H_2O+H]^+$, d) $[LNFPV+IRABA-2H_2O+H]^+$. Fragments ions that stem from loss of a phosphonate moiety are indicated with a '•'.

The IRMPD spectra for the IRABA derivatized LNFPs are depicted in Figure 6-6, and the entire series of mass spectral data is tabulated in Table 6-3. As with the CAD spectra, there are two general fragmentation pathways observed. The most prominent

pathway (bold type) results from sequential cleavages from the non-reducing end of the oligosaccharides. The secondary pathway results from cleavages that begin at the reducing end of the oligosaccharides, and the series of losses include the intersaccharide oxygen atom that is indicative of cleavages from the reducing end of the IRABA derivatized oligosaccharides.

In addition to the same losses observed in the CAD spectra, the IRMPD spectra also reveal ions that have undergone subsequent dissociation. These secondary IRMPD events are responsible for the two additional Hex losses observed for all of the LNFPs in Figure 6-6 (-Gal, 446 Da and -Glc, 284 Da). As a result, there is complete sequence coverage for each of the LNFPs. In addition, the diagnostic pathway for the LNFP-V is present (initial loss of Gal + GlcNAc) along with a diagnostic ion for the LNFP-I isomer that was not observed in the CAD spectra (Y_3). It is surmised that this ion is due to sequential fragmentation of the fragment ion at 973 Da due to the initial loss of Fuc. However, there is still not a single diagnostic ion that differentiates the LNFP-II and III isomers. These two isomers only differ in the reversed linkage positions of their non-reducing terminal Fuc and Gal moieties.

The primary fragmentation pathway (i.e. the sequence of losses initiated from the non-reducing end) is the key to reliable sequencing of the oligosaccharides. Since the fragments that arise from this pathway only stem from the non-reducing end of the oligosaccharide, the resulting sequential losses (masses of individual residues) map out the structure of the oligosaccharides. In contrast, the secondary pathways include cleavages from both ends of the oligosaccharides and therefore do not reliably map the structures.

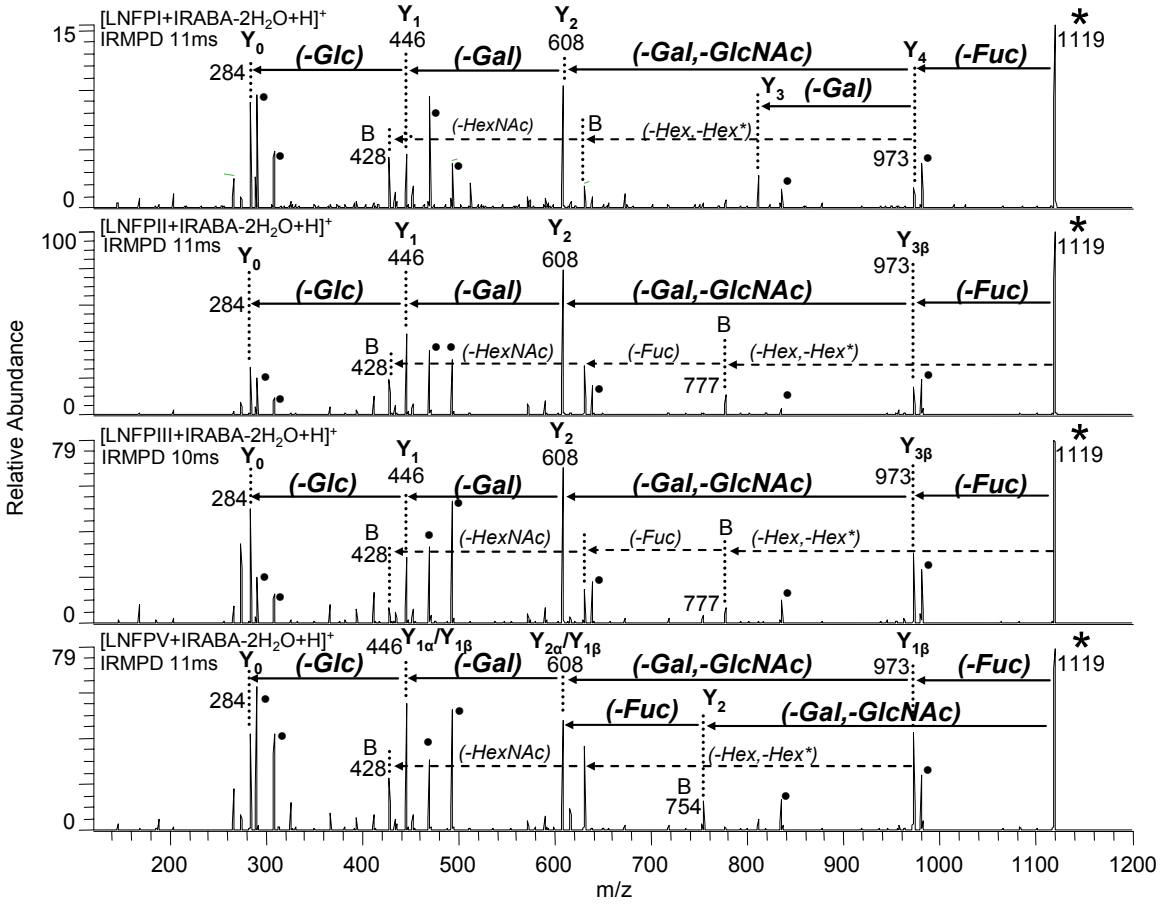

Figure 6-6. IRMPD spectra of LNFP oligosaccharides after derivatization with IRABA: a) $[LNFPI+IRABA-2H_2O+H]^+$, b) $[LNFPII+IRABA-2H_2O+H]^+$, c) $[LNFPIII+IRABA-2H_2O+H]^+$, d) $[LNFPV+IRABA-2H_2O+H]^+$. Fragments ions that stem from loss of a phosphonate moiety are indicated with a '•'.

This primary fragmentation pathway is observed only when the oligosaccharides are derivatized. Without derivatization, there are mixtures of losses that define the different types of secondary pathways with losses occurring from both the reducing and non-reducing ends of the oligosaccharides. Therefore, derivatization coupled with IRMPD has proven to be an excellent technique for sequencing the LNFPs in one activation event.

6.4.1.5 Site of Derivatization

The nature of the neutral losses related to the primary fragmentation pathway in the IRMPD spectra suggests that the IRABA is attached to the reducing sugar. Since the reducing sugar is the most reactive and may have both the alpha and beta configuration, it may bear the cis-diol functionality that readily reacts with boronic acids. The existence of the secondary pathway suggests that there is at least one other site of derivatization. Since the first losses in the secondary pathway include two Hex and Fuc, it is surmised that the secondary site of attachment is at one of the Gal moieties that also possess the cis-diol functionality.

To further elucidate the site of attachment, the reducing end of the LNFP-II isomer was reduced with sodium borohydride. The reduction converts the aldehyde of the reducing sugar to an alcohol forming an alditol. After the reduction reaction, the mixture was cleaned up using a Carbograph SPE cartridge, dried and rediluted prior to ESI-MS analysis. The resulting ESI mass spectra of the reaction product indicates complete conversion to the alditol since there is a prominent ion at m/z 878 corresponding to [LNFP-II(alditol) + Na]$^+$. In contrast, the ESI mass spectra of the oligosaccharide after the reduction reaction did not display an ion due to any unreduced species. The alditol form of LNFP-II was then reacted with the IRABA ligand, and no IRABA derivatization products were observed in the spectra, thus indicating that LNFP-II in the reduced form did not react with the IRABA reagent. Given these results, it is surmised that the IRABA reacts primarily at the reducing sugar and that any other sites of derivatization are minor products.

6.4.2 LNDFH Oligosaccharides

Since the derivatization of the LNFP series with the IRABA ligand followed by IRMPD was such an effective structural characterization strategy, the method was

expanded to another series of oligosaccharides, the LNDFH series shown in Figure 6-1. The IRMPD spectra of these IRABA derivatized oligosaccharides indicate that they dissociate by the same two pathways that were observed for the LNFP series (Figure 6-7). This data for the underivatized species is tabulated in Table 6-4 and the derivatized species in Table 6-5. As with the LNFP series, the primary fragmentation pathway consists of cleavages of one type that take place sequentially from the non-reducing to the reducing end.

The primary fragmentation pathway provides detailed sequence information for the LNDFH oligosaccharides with the exception of the two isomers that only differ in their reversed Gal and Fuc linkages to the central GlcNAc (Ia and Ib). Following the loss of terminal or branching Fuc moieties, fragmentation of the backbone for each of the isomers from the non-reducing end starts with the combined Gal-GlcNAc losses followed by two sequential Hex losses (Gal and Glc). Further, it is evident from the IRMPD spectra of LNDFH-Ia and Ib that there is a Fuc attached to both the non-reducing terminal Gal and the GlcNAc since there is an initial Fuc loss followed by a combined Fuc-Gal-GlcNAc loss. This result further confirms the sequential nature of the losses that correspond to the primary pathway. Other possible alternative sequences of these oligosaccharides, Fuc-(Fuc)-HexNAc-Hex- or Fuc-HexNAc-(Fuc)-Hex-, are discounted because in each of the IRMPD spectra throughout this chapter there has been a key intersaccharide cleavage at the reducing end of GlcNAc that would yield characteristic ions for Fuc-(Fuc)-HexNAc and Fuc-HexNAc, respectively. These fragments ions are not observed in the IRMPD mass spectra, thus discrediting these alternative sequences. Therefore the two Fuc must reside on the non-reducing ends Gal and GlcNAc.

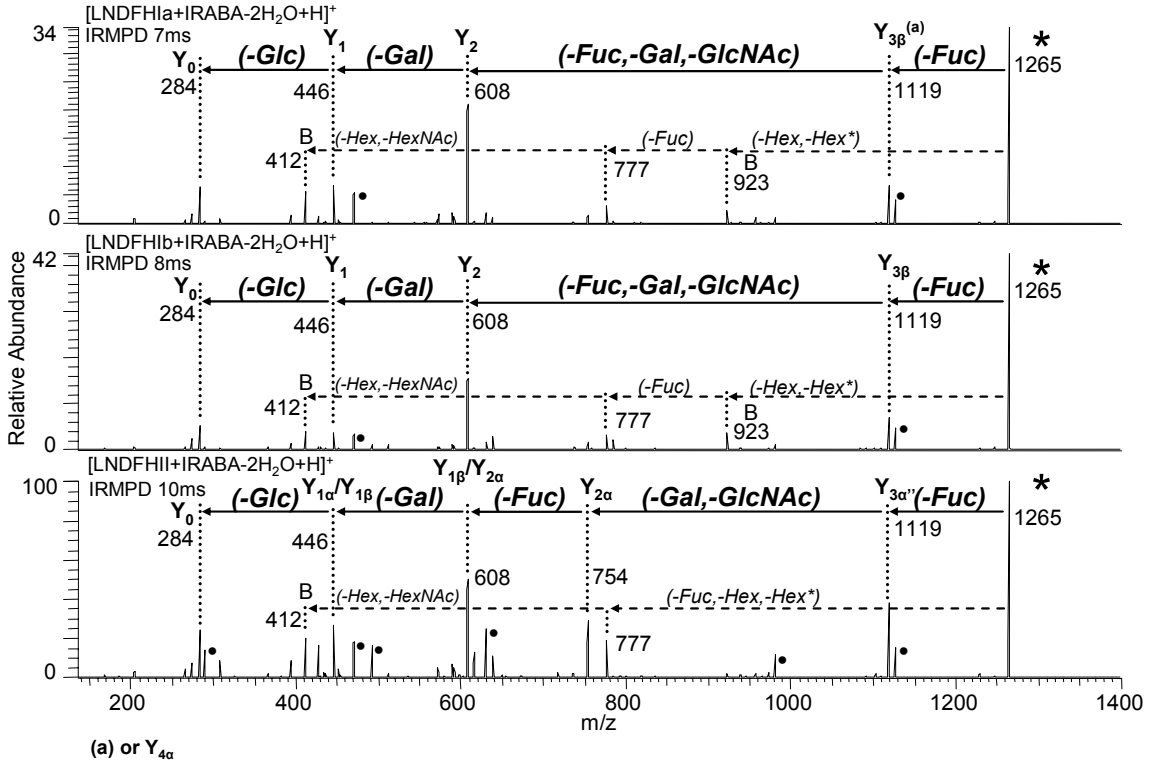

Figure 6-7. IRMPD spectra of LNDFH oligosaccharides after derivatization with IRABA: a) $[LNDFHIa+IRABA-2H_2O+H]^+$, b) $[LNDFHIb+IRABA-2H_2O+H]^+$, c) $[LNDFHII+IRABA-2H_2O+H]^+$. Fragments ions that stem from loss of a phosphonate moiety are indicated with a '•'.

The difference in the IRMPD spectrum for the LNDFH-II isomer is a result of one Fuc having a different position. Since the initial Fuc loss precedes the Gal-GlcNAc combined loss, it is evident that this Fuc resides on either the Gal or GlcNAc. However, if the Fuc residue were attached to the terminal Gal, one would expect an ion of m/z 957 that corresponds to a loss of Gal following the loss of Fuc. The LNFP-I isomer has this type of Fuc-Gal linkage and the corresponding fragment ion was observed in its IRMPD spectrum (Figure 6-6, m/z 811). Therefore the initial Fuc loss must be attached to the GlcNAc. With only two Hex left on the backbone, the remaining Fuc must be attached to one or the other. Since this Fuc loss precedes the loss of both of these Hex moieties, it

could be attached to either one. If the sequence continued beyond these two Hex moieties, there may be more fragment ions observed that would make it possible to pinpoint the precise location of the remaining Fuc.

Table 6-4. Underivatized LNDFH Oligosaccharide Fragment Ion Abundances

$(M - H)^-$ CAD	**C_4, C_3**		
LNDFH-Ia	88		
LNDFH-Ib	86		
LNDFH-II	90		
$(M - H)^-$ IRMPD	**C_4, C_3**		
LNDFH-Ia	92		
LNDFH-Ib	97		
LNDFH-II	86		
$(M + Na)^+$ CAD	**$Y_{3\beta}$, $Y_{3\alpha''}$**		
LNDFH-Ia	91		
LNDFH-Ib	91		
LNDFH-II	91		
$(M + Na)^+$ IRMPD	**$Y_{3\beta}$, $Y_{3\alpha''}$**	**$Y_{3\beta}/Y_{4\alpha}$, $Y_{3\alpha''}/Y_{1\beta}$**	**$Y_{3\beta}/Z3_{\alpha}$, $Y_{3\alpha''}/B_3$**
LNDFH-Ia	32	14	7
LNDFH-Ib	28	19	3
LNDFH-II	43	17	5

* as a percentage of total sequence and parent ion abundances, +/- 5%

6.4.3 DSLNT Oligosaccharide

The IRABA derivatization strategy was further extended to an acidic hexasaccharide, disialyllacto-N-tetraose (DSLNT), shown in Figure 6-1. As observed with the previous oligosaccharide series, the principal fragments are a series that arise from the backbone from the non-reducing to reducing end of the oligosaccharide (Figure

6-8). Following the loss of the two Sia moieties, a combined loss of Gal-GlcNAc resulting from cleavage at the reducing end of GlcNAc indicates the sequence Sia-Gal-(Sia)-GlcNAc. Subsequent losses reveal the completion of the sequence, Gal-Glc. The successful sequencing of this oligosaccharide indicates that the method may be further applied to larger and different types of oligosaccharides.

Table 6-5. IRABA Derivatized LNDFH Oligosaccharide Fragment Ion

[LNDFH + IRABA - $2H_2O$ - H]$^-$ CAD	**C_4**	**$Z_{1\beta}$**					
LNDFH-Ia	86	-					
LNDFH-Ib	80	-					
LNDFH-II	-	96					
[LNDFH + IRABA - $2H_2O$ - H]$^-$ IRMPD	**C_4**	**$C_4/Y_{3\beta}/Y_{3\alpha}$**	**$Y_{3\alpha'}/Y_{3\alpha''}$**				
LNDFH-Ia	17	40	-				
LNDFH-Ib	12	49	-				
LNDFH-II	-	-	56				
[LNDFH + IRABA - $2H_2O$ + H]$^+$ CAD	**$Y_{3\beta}$, $Y_{3\alpha''}$**	**B_3**	**B_2, $B_3/Y_{3\beta}$**	**$Y_{2\alpha}$**	**Y_2, $Y_{1\beta}/Y_{2\alpha}$**		
LNDFH-Ia	31	35	8	-	24		
LNDFH-Ib	34	44	4	-	11		
LNDFH-II	29	-	23	24	5		
[LNDFH + IRABA - $2H_2O$ + H]$^+$ IRMPD	**$Y_{3\beta}$, $Y_{3\alpha''}$**	**B_3**	**B_2, $B_3/Y_{3\beta}$**	**$Y_{2\alpha}$**	**Y_2, $Y_{1\beta}/Y_{2\alpha}$**	**Y_1, $Y_{1\alpha}/Y_{1\beta}$**	**Y_0**
LNDFH-Ia	8	3	10		61	19	19
LNDFH-Ib	16	6	6		19	6	13
LNDFH-II	39		7	29	17	9	8

* as a percentage of total sequence and parent ion abundances, +/- 5%

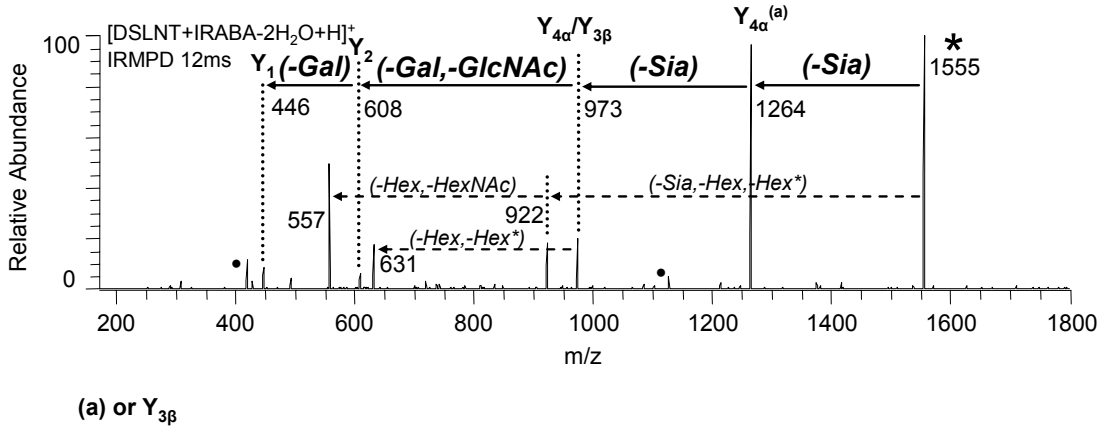

Figure 6-8. IRMPD spectrum of DSLNT after derivatization with IRABA. Fragments ions that stem from loss of a phosphonate moiety are indicated with a '•'.

6.5 CONCLUSIONS

The sequencing of oligosaccharides has been simplified by the use of IRMPD in a QIT. This was accomplished with the use of a boronic acid derivatizing reagent that was also functionalized with an IR-active phosphonate group to facilitate the photon absorption process. The oligosaccharides underwent modification by simple addition of the IRABA with reaction times of ~ 1 min and did not require sample cleanup prior to analysis by ESI-MS. The oligosaccharide products dissociated with high efficiency upon IR irradiation, and the degree of secondary fragmentation may be controlled by adjusting the irradiation time. The resulting IRMPD mass spectra display a characteristic primary fragmentation pathway resulting from cleavage from only the non-reducing ends, thereby simplifying the determination of oligosaccharide sequence. As a result, the method should be generally applicable to the sequencing of even larger oligosaccharides.

6.6 REFERENCES

1. Varki, A. *Glycobiology* **1993**, *3*, 97-130.

2. Linhardt, R. J.; Toida, T. *Accounts of Chemical Research* **2004**, *37*, 431-438.

3. Fannon, M.; Forsten, K. E.; Nugent, M. A. *Biochemistry* **2000**, *39*, 1434-1445.

4. Wu, Z. L.; Zhang, L.; Yabe, T.; Kuberan, B.; Beeler, D. L.; Love, A.; Rosenberg, R. D. *J. of Biol. Chem.* **2003**, *278*, 17121-17129.

5. Dwek, R. A. *Chemical Reviews* **1996**, *96*, 683-720.

6. Kukuruzinska, M. A.; Lennon, K. *Crit. Rev. Oral. Biol. Med.* **1998**, *9*, 415-448.

7. Helenus, A.; Aebi, M. *Science* **2001**, *291*, 2364-2369.

8. Varki, A.; Cummings, R.; Esko, J.; Freeze, H.; Hart, G.; Marth, J. *Essentials of Glycobiology*, First ed.; Cold Spring Harbor Laboratory Press: Cold Spring Harbor, NY, 1999.

9. Gorelik, E.; Galili, U.; Raz, A. *Cancer and Metastasis Reviews* **2001**, *20*, 245-277.

10. Dennis, J. W.; Granovsky, M.; Warren, C. E. *Biochimica et Biophysica Acta* **1999**, *1473*, 21-34.

11. Rebbaa, A.; Chou, P. M.; Vucic, I.; Mirkin, B. L.; Tomita, T.; Bremer, E. G. *Clinical Cancer Research* **1999**, *5*, 3661-3668.

12. Suzuki, Y.; Suzuki, M.; Ito, E.; Ishii, H.; Miseki, K.; Suzuki, A. *Glycoconjugate Journal* **2005**, *22*, 427-431.

13. Yamagaki, T.; Ishizuka, Y.; Kawabata, S.; Nakanishi, H. *Rapid Comm. in Mass Spectrom.* **1997**, *11*, 527-531.

14. Harvey, D. J. *Mass Spectrom. Rev.* **1999**, *18*, 349-451.

15. Zaia, J. *Mass Spectrom. Rev.* **2004**, *23*, 161-227.

16. Lancaster, K. S.; An, H. J.; Li, B.; Lebrilla, C. B. *Anal. Chem.* **2006**, *78*, 4990-4997.

17. Penn, S. G.; Cancilla, M. T.; Lebrilla, C. B. *Anal. Chem.* **1996**, *68*, 2331-2339.

18. Park, Y.; Lebrilla, C. B. *Mass Spectrom. Rev.* **2005**, *24*, 232-264.

19. Pfenninger, A.; Karas, M.; Finke, B.; Stahl, B. *J. Am. Soc. Mass Spectrom.* **2002**, *13*, 1331-1340.

20. Pfenninger, A.; Karas, M.; Finke, B.; Stahl, B. *J. Am. Soc. Mass Spectrom.* **2002**, *13*, 1341-1348.

21. Chai, W.; Piskarev, V.; Lawson, A. M. *Anal. Chem.y* **2001**, *73*, 651-657.

22. Weiskopf, A. S.; Vouros, P.; Harvey, D. J. *Anal. Chem.* **1998**, *70*, 4441-4447.

23. Konig, S.; Leary, J. A. *J. Am. Soc. Mass Spectrom.* **1998**, *9*, 1125-1134.

24. Leavell, M. D.; Leary, J. A. *J. Am. Soc. Mass Spectrom.* **2001**, *12*, 528-536.

25. Ashline, D. J.; Lapadula, A. J.; Liu, Y.-H.; Lin, M.; Grace, M.; Pramanik, B.; Reinhold, V. N. *Anal. Chem.* **2007**, *79*, 3830-3842.

26. Adamson, J. T.; Hakansson, K. *Anal. Chem.* **2007**, *Article ASAP*.

27. Wolff, J. J.; Amster, I. J.; Chi, L.; Linhardt, R. J. *J. Am. Soc. Mass Spectrom.* **2007**, *18*, 234-244.

28. Devakumar, A.; Mechref, Y.; Kang, P.; Novotny, M. V.; Reilly, J. P. *Rapid Comm. Mass Spectrom.* **2007**, *21*, 1452-1460.

29. Goldberg, D.; Bern, M.; Li, B. S.; Lebrilla, C. B. *J. Prot. Res.* **2006**, *5*, 1429-1434.

30. Fukui, K.; Takada, Y.; Sumiyoshi, T.; Imai, T.; Takahashi, K. *J. Phys. Chem. B* **2006**, *110*, 16111-16116.

31. Zhang, J.; Schubothe, K.; Li, B.; Russell, S.; Lebrilla, C. B. *Anal. Chem.* **2005**, *77*, 208-214.

32. Shi, S.; Hendrickson, C. L.; Marshall, A. G.; Siegel, M. M.; Kong, F.; Carter, G. T. *J. American Soc. Mass Spectrom.* **1999**, *10*, 1285-1290.

33. Xie, Y.; Lebrilla, C. B. *Anal. Chem.* **2003**, *75*, 1590-1598.

34. Pikulski, M.; Wilson, J. J.; Aguilar, A.; Brodbelt, J. S. *Anal. Chem.* **2006**, *78*, 8512-8517.

35. Wilson, J. J. B., J.S. *Anal. Chem.* **2006**, *78*, 6855-6862.

36. Crowe, M. C.; Brodbelt, J. S.; Goolsby, B. J.; Hergenrother, P. *J. Am. Soc. Mass Spectrom..,* **2002**, *13*, 630-649.

37. Crowe, M. C.; Brodbelt, J. S. *J. Am. Soc. Mass Spectrom.* **2004**, *15*, 1581-1592.

38. Crowe, M. C.; Brodbelt, J. S. *Anal. Chem.* **2005**, *77*, 5726-5734.

39. Goolsby, B. J.; Brodbelt, J. S. *J. Mass Spectrom.* **1998**, *33*, 705-712.

40. Goolsby, B. J.; Brodbelt, J. S. *J. Mass Spectrom.* **2000**, *35*, 1011-1024.

41. Goolsby, B. J.; Brodbelt, J. S. *Anal. Chem.* **2001**, *73*, 1270-1276.

42. Keller, K. M.; Brodbelt, J. S. *Anal. Biochem.* **2004**, *326*, 200-210.

43. Vartanian, V. H.; Goolsby, B.; Brodbelt, J. S. *J. Am. Soc. Mass Spectrom.***1998**, *9*, 1089-1098.

44. Shen, J.; Brodbelt, J. S. *Analyst* **2000**, *125*, 641-650.

45. Racine, A. H.; Payne, A. H.; Remes, P. M.; Glish, G. L. *Anal. Chem.* **2006**, *78*, 4609-4614.

46. Payne, A. H.; Glish, G. L. *Anal. Chem.* **2001**, *73*, 3542-3548.

47. Hashimoto, Y.; Hasegawa, H.; Yoshinari, K.; Waki, I. *Anal. Chem.* **2003**, *75*, 420-425.

48. Boue, S. M.; Stephenson, J. L.; Yost, R. A. *Rapid Comm. Mass Spectrom.* **2000**, *14*, 1391-1397.

49. Hashimoto, Y.; Hasegawa, H.; Waki, L. *Rapid Comm. Mass Spectrom.* **2004**, *18*, 2255-2259.

50. Morelle, W.; Faid, V.; Michalski, J.-C. *Rapid Comm. Mass Spectrom.* **2004**, *18*, 2451-2464.

51. Viseux, N.; de Hoffmann, E.; Domon, B. *Anal. Chem.* **1998**, *70*, 4951-4959.

52. Harvey, D. J. *J. Am. Soc. Mass Spectrom.* **2000**, *11*, 900-915.

53. Cheng, H.-L.; Pai, P.-J.; Her, G.-R. *J. Am. Soc. Mass Spectrom.* **2007**, *18*, 248-259.

54. Young, M. K.; Williams, D. *Rapid Comm. Mass Spectrom.* **2000**, *14*, 2083-2091.

55. Yang, H.-J.; Chen, Y.-Z. *J. Carbohydr. Chem.* **1993**, *12*, 39-48.

56. Chen, H.; Cotte-Rodriguez, I.; Cooks, R. G. *Chemical Communications* **2006**, 597-599.

57. Wong, A. W.; Cancilla, M. T.; Voss, L. R.; Lebrilla, C. B. *Anal. Chem.* **1999**, *71*, 205-211.

58. Zhu, L.; Shabbir, S. H.; Gray, M.; Lynch, V.; Sorey, S.; Anslyn, E. V. *J. Am. Chem. Soc.* **2006**, *128*, 1222-1232.

59. Zhu, L.; Anslyn, E. V. *J. Am. Chem. Soc.* **2004**, *126*, 3676-3677.

60. Domon, B.; Costello, C. E. *Glycoconjugate Journal* **1988**, *5*, 397-409.

Chapter 7: Synthesis

To complete the studies presented in the previous chapters, several different compounds were synthesized. These included a series of pyridyl ligands with electron-withdrawing substituents added to modulate their metal binding affinities. Five ligands were synthesized with bromine as the electron-withdrawing group, namely 4,4'-dibromo-2,2'-bipyridine, 4,4'-bis(bromomethyl)-2,2'-bipyridine, 5,6-dibromo-1,10-phenanthroline, 3,5,6-tribromo-1,10-phenanthroline and 3,5,6,8-tetrabromo-1,10-phenanthroline. In addition, pyridyl ligands with phosphonate groups incorporated to make them IR-active chelating agents were also synthesized. These included 4,4-(diethylphosphonate)-2,2'-bipyridine and 4,4'-bis(diethylmethylphosphonate)-2,2'-bipyridine. A derivatizing reagent for oligosaccharides was also synthesized. The 1-(N-(ortho-diethylmethylphosphonate))aminoethylbenzene boronic acid also incorporated a phosphonate group to yield an IR-active species.

7.1 BROMINATED PYRIDYL LIGANDS

The advantages of using a metal complexation strategy with neutral pyridyl ligands for the analysis of several groups of flavonoids was presented in Chapters 1 and 2. Because of the limited commercial availability of pyridyl ligands, it was not possible to purchase a set of ligands with electron-withdrawing substituents that would enable a logical systematic study (e.g., only differed in the number and type of substituents present on the ligands). Therefore, a set was synthesized using bromine atoms as the electron-withdrawing substituents to accomplish the study presented in Chapter 2. These included two bromine-substituted 2,2'-bipyridines and three bromine-substituted 1,10-phenanthrolines.

7.1.1 4,4'-Dibromo-2,2'-bipyridine

4,4-Dibromo-2,2'-bipyridine **5** was synthesized from 2,2'-bipyridine **1** based on a literature procedure[1, 2] and this is presented in Scheme 7-1. To obtain the 4-substituted pyridine, a well known nitration procedure was used followed by a nucleophilic aromatic substitution. The resulting brominated bipyridine-N-oxide **4** was then reduced to the bipyridine **5** using phosphorus tribromide.

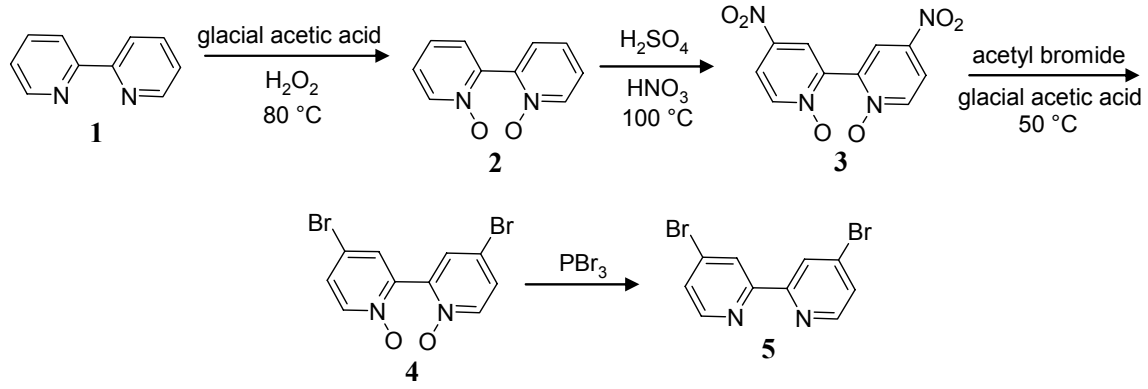

Scheme 7-1. Synthesis of 4,4'-dibromo-2,2'-bipyridine.

2,2'-bipyridine **1** (30.1 g, 193 mmol) was transferred to a round bottom flask and glacial acetic acid (125 mL, 2.19 mol) was added with stirring. The solution was heated to 80 °C and 30% H_2O_2 was added dropwise (96 mL, 974 mmol). The solution was stirred for two hours at 80 °C and another aliquot of 30% H_2O_2 was added dropwise (82 mL, 832 mmol). The resulting solution was stirred for ~24 hours at 80 °C. The solvents were then removed by rotary evaporation and the solids were recrystallized from H_2O and dried to yield 18.7 g (99 mmol) 2,2'-bipyridine-N,N-dioxide **2** in 51% yield.

2,2'-bipyridine-N,N-dioxide **2** (18.7 g, 99 mmol) was transferred to a round bottom flask and fuming sulfuric acid was added (35 mL, 377 mmol). The resulting solution was heated to 100 °C and fuming nitric acid (45 mL, 1.1 mol) was added. The

resulting solution was allowed to react for 7 hours. The solution was cooled to room temperature and poured onto ice, forming a yellow precipitate. The 4,4'-dinitro-2,2'-bipyridine-N,N-dioxide **3** precipitate was filtered, washed with water and dried to yield 7.2 g (25.9 mmol) 4,4'-dinitro-2,2'-bipyridine-N,N-dioxide **3** in 26% yield.

4,4'-dinitro-2,2'-bipyridine-N,N-dioxide (7.2 g, 25.9 mmol) was transferred to a round bottom flask and glacial acetic acid (60 mL, 1.05 mol) was added and the flask and condenser were purged with argon. The solution was heated to 50 °C and acetyl bromide (40 mL, 540 mmol) was added dropwise with stirring. The solution was refluxed for ~12 hours. The solution was then cooled to room temperature and poured onto ice. The solution was then brought to ~pH 12 using potassium carbonate and a precipitate formed. The 4,4'-dibromo-2,2'-bipyridine-N,N-dioxide **4** precipitate was then filtered and washed with water. The precipitate was then dried to yield 5.01 g (14.6 mmol) 4,4'-dibromo-2,2'-bipyridine-N,N-dioxide **4** in 56% yield.

4,4'-dibromo-2,2'-bipyridine-N,N-dioxide **4** (5.01 g, 14.6 mmol) was transferred to a round bottom flask. A condenser was added and the system was purged with argon. Phosphorus tribromide (15 mL, 155 mmol) was added and the resulting mixture was refluxed for ~12 hours. The solution was then brought to room temperature and poured onto ice. The solution was then brought to ~pH 12 using potassium carbonate. The resulting solution was then extracted with 50 mL of $CHCl_3$ five times. The combined organic layers were then dried using sodium sulfate, filtered, and the solvent was removed using rotary evaporation. The solids were then purified on silica gel using $CHCl_3$ and CH_3OH to yield 3.73 g (12 mmol) 4,4'-dibromo-2,2-bypridine **5** in 82% yield. ^1H NMR (CD_3Cl_3) δ = 7.509 (2H, dd, J = 5.2 Hz, 1.6 Hz), 8.486 (2H, d, J = 5.2 Hz), 8.608 (2H, d, J = 1.6 Hz).

7.1.2 4,4'-Bis(bromomethyl)-2,2'-bipyridine

4,4-Bis(bromomethyl)-2,2'-bipyridine **8** was synthesized from 4,4'-dimethyl-2,2'-bipyridine **6** based on a literature procedure[3] and this is presented in Scheme 7-2. The bromomethyl pyridine was obtained via activation and substitution of a 4-methyl pyridine. The benzylic anion was formed by deprotonation with a strong base and trapping with a silyl protecting group. The TMS-protected compound was deprotected with cesium fluoride and brominated with a mild brominating agent.

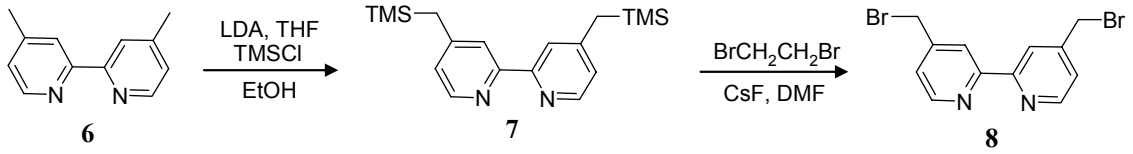

Scheme 7-2. Synthesis of 4,4'-bis(bromomethyl)-2,2'-bipyridine.

A solution of 4,4'-dimethyl-2,2'-bipyridine **6** (0.51 g, 2.77 mmol) was dissolved in THF (13 mL) under a nitrogen atmosphere in a round bottom flask. A two-necked round bottom flask with a nitrogen inlet was charged with THF (9 mL) and diisopropylamine (1 mL). The reaction mixture was then cooled to -78 °C and butyllithium (1.7 M in hexanes, 3.6 mL) was added. The reaction mixture was then stirred at -78 °C for 10 mins., warmed to 0 °C and stirred for 10 mins., and cooled back to -78 °C. The previously prepared 4,4'-dimethyl-2,2-bipyridine **6** solution in THF was then added via cannula to the cold lithium diisopropylamide (LDA) solution. The mixture turned black and was stirred at -78 °C for 1 hr. Chlorotrimethylsilane (TMSCl, 0.885 mL, 7 mmol) was then rapidly added to the reaction mixture via syringe. In ~1 s the reaction mixture turned pale green and the reaction was quenched by the rapid addition of ethanol (1 mL). The cold reaction mixture was then poured into a separatory

funnel containing saturated sodium bicarbonate (20 mL) and was warmed to ~25 °C. The mixture was then extracted with dichloromethane (3 X 30 mL). The combined organic fractions were then shaken with brine (~20 mL) and then dried over sodium sulfate. The mixture was then filtered and the solvent removed by rotary evaporation. The remaining solid was then dried to yield 0.701 g (2.13 mmol) 4,4'-bis[(trimethylsilyl)methyl]-2,2'-bipyridine **7** in 77% yield.

4,4'-bis[(trimethylsilyl)methyl]-2,2'-bipyridine **7** (0.361 g, 1.1 mmol) was transferred to a two-necked round bottom flask. Anhydrous cesium fluoride was added (0.68 g, 4.48 mmol). The flask was then flushed with nitrogen and hexabromoethane (0.55 mL, ~4 mmol) was added via syringe. N,N-dimethylformamide (5 mL) was added via syringe and the reaction mixture was stirred for 3 hours at room temperature, monitored by TLC on silica (EtOAc:hexanes, 1:4). The reaction mixture was then transferred to a separatory funnel containing 10 mL water and 10 mL EtOAc and was extracted with EtOAc (3 X 10 mL). The organic fractions were combined and shaken with brine and dried over sodium sulfate. The crude product mixture was then filtered and the solvent was removed by rotary evaporation. The crude product mixture was then dried overnight under vacuum and then purified by flash chromatography using deactivated silica gel (EtOAc: hexanes, 3:2) and yielded 0.269 g (0.79 mmol) in 72% yield. ^{1}H NMR (CD_3Cl_3) δ = 7.507 (2H, d, J = 8 Hz), 7.671 (2H, t, J = 7.6 Hz, 8Hz), 8.378 (2H, d, J = 7.6 Hz).

7.1.3 Bromo-1,10-phenanthrolines

5,6-dibromo-1,10-phenanthroline **10**, 3,5,6-tribromo-1,10-phenanthroline **11** and 3,5,6,8-tetrabromo-1,10-phenanthroline **12** were synthesized from 1,10-phenanthroline **9** based on a literature procedure[4] and this is presented in Scheme 7-3. The bromo substituted 1,10-phenanthrolines were synthesized by electrophilic aromatic substitution

with bromine. As expected, a mixture of multiple bromination products were obtained but several were separated by multiple recrystallization steps.

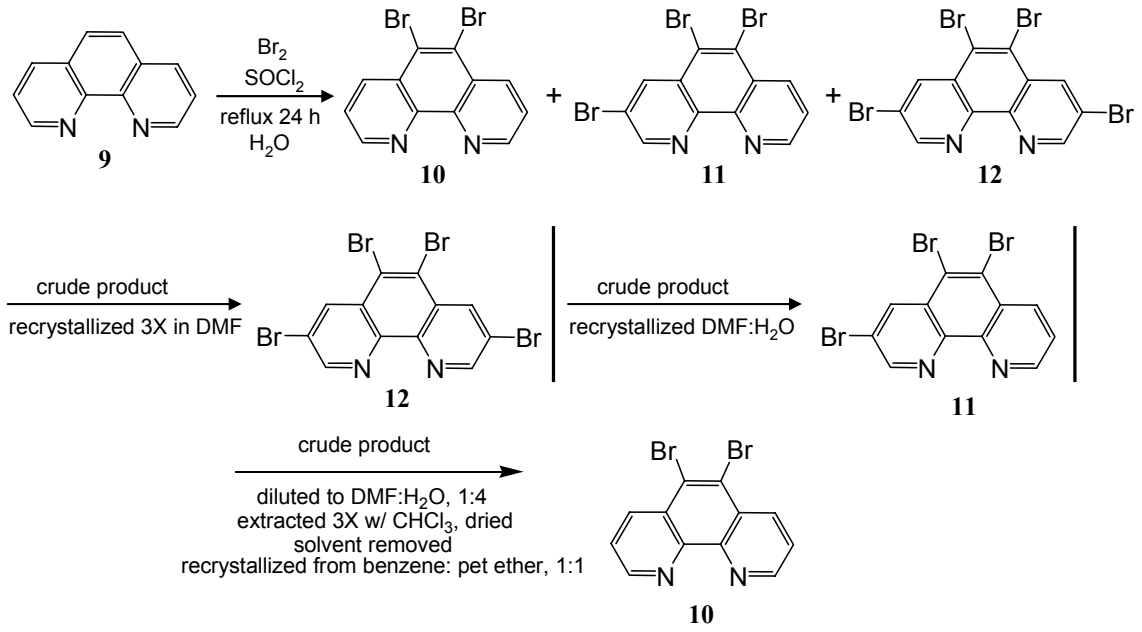

Scheme 7-3. Synthesis of bromo-1,10-phenanthrolines.

1,10-phenanthroline **9** (2.125 g, 11.8 mmol) was transferred to a round bottom flask that was equipped with a condenser. Thionyl chloride (100 mL, 1.37 mol) was then added and the 1,10-phenanthroline **9** dissolved on heating. Bromine (3 mL, 58 mmol) was then added and the reaction mixture was refluxed at 95 °C for 24 hours. The excess thionyl chloride and bromine were then removed under vacuum. Water (200 mL) was then added to the residue and it was neutralized with ammonium hydroxide. The mixture was then filtered and dried under vacuum to yield 4.7 g of crude product. By selective crystallizations and precipitations the three bromophenanthrolines were separated as outlined in the next three sections.

7.1.3.1 3,5,6,8-Tetrabromo-1,10-phenanthroline

The crude product (4.7 g) was dissolved in N,N-dimethylformamide (400 mL) on heating to 150 °C. Upon cooling, a precipitate formed that was filtered and recrystallized twice more from N,N-dimethylformamide. The precipitate was filtered and dried in an oven at 100 °C for one hour and overnight under vacuum to yield 1.76 g 3,5,6,8-tetrabromo-1,10-phenanthroline **12**. ^{1}H NMR (CD_3Cl_3) δ = 8.920 (2H, d, J = 2.2 Hz), 9.190 (2H, d, J = 2 Hz).

7.1.3.2 3,5,6-Tribromo-1,10-phenanthroline

The filtrate of the above separation was diluted with an equal volume of water (675 mL). A precipitate formed, was filtered and then recrystallized from N,N-dimethylformamide:water, 1:1. The precipitate was filtered and dried overnight under vacuum to yield 1.57 g 3,5,6-tribromo-1,10-phenanthroline **11**. ^{1}H NMR (CD_3Cl_3) δ = 7.748 (1H, dd, J = 8.8 Hz, 4.2 Hz), 8.765 (1H, dd, J = 8.8 Hz, 1.6Hz), 8.928 (1H, d, J = 2 Hz), 9.201 (2H, m).

7.1.3.3 5,6-Dibromo-1,10-phenanthroline

The filtrate of the above separation was diluted with water (3.2 L) and extracted one liter at a time with chloroform (3 X 100 mL). The organic layers were combined and dried with sodium sulfate and filtered. The chloroform was then removed by rotary evaporation and excess N,N-dimethylformamide removed by vacuum distillation. The residue was recrystallized from petroleum ether:benzene, 1:1, filtered and dried to yield 0.73 g 5,6-dibromo-1,10-phenanthroline **10**. ^{1}H NMR (CD_3Cl_3) δ = 7.740 (2H, dd, J = 8.4 Hz, 8.0 Hz), 8.782 (2H, dd, J = 8.8 Hz, 1.2Hz), 9.226 (2H, dd, J = 4.4 Hz, 1.2 Hz).

7.2 PHOSPHONATED PYRIDYL LIGANDS

As detailed in Chapters 5 and 6, the presence of a phosphate or phosphonate group greatly increases an ion's absorptivity upong IR irradiation. For this reason, the metal complexation technique presented in Chapters 1 and 2 was exploited as a means of adding a phosphonate group to analytes, ultimately to make them more amenable to IRMPD. The phosphonate groups were covalently attached to the auxiliary ligands thereby permitting addition of the phosphonate group without covalent modification to the analyte. The synthesis of these ligands is presented in this section.

7.2.1 4,4-(diethylphosphonate)-2,2'-bipyridine

4,4-(diethylphosphonate)-2,2'-bipyridine **13** was synthesized from 4,4'-dibromo-2,2'-bipyridine **5** (section 7.1.1) based on a literature procedure[5, 6] (Scheme 7-4). The 4,4-dibromo-2,2'-bipyridine **5** was converted to the phosphonate via a palladium coupling with diethyl phosphite (DEPH).

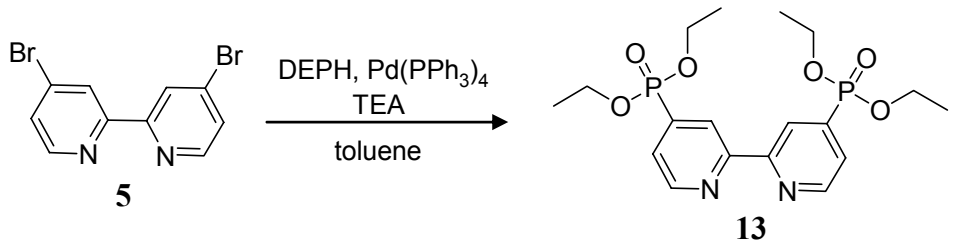

5 **13**

Scheme 7-4. Synthesis of 4,4-(diethylphosphonate)-2,2'-bipyridine.

4,4'-dibromo-2,2-bypridine **5** (0.43 g, 1.37 mmol) and tetrakis (triphenylphosphine) Palladium(0) (0.32 g, 0.27 mmol) were transferred to a round bottom flask equipped with a condenser and the system was flushed with argon and the remaining additions were made under the protection of argon. Dry toluene (5 mL) was then added via syringe with stirring. Diethyl phosphite (0.5 mL, 3.8 mmol) and

triethylamine (0.55 mL, 3.8 mmol) were then added via syringe. The reaction mixture was heated under argon protection and then refluxed for 4 hours. The reaction mixture was then cooled to room temperature and diethyl ether was added to precipitate triethylamine hydrobromide formed during the reaction. The mixture was then filtered and the solvent removed using rotary evaporation. The crude product was purified by flash chromatography on silica gel with $CHCl_3$:CH_3OH to yield 0.1868 g (0.44 mmol) 4,4-(diethylphosphonate)-2,2'-bipyridine **13** in 32% yield. ^{1}H NMR (CD_3OD) δ = 1.29 (12H, t), 4.13 (8H, m), 7.69 (2H, ddd), 8.68 (2H, d), 8.81 (2H, t).

7.2.2 4,4'-bis(diethylmethylphosphonate)-2,2'-bipyridine

4,4'-bis(diethylmethylphosphonate)-2,2'-bipyridine **14** was synthesized from 4,4-bis(bromomethyl)-2,2'-bipyridine (Section 7.1.2) based on a literature procedure[7, 8] and this is presented in Scheme 7-5. The phosphonate was synthesized from the 4,4-bis(bromomethyl)-2,2'-bipyridine **8** using the Arbuzov reaction. In this reaction the phosphorus does an SN2 substitution of the bromide. The bromide then attacks the carbon of one of the ethoxy groups via SN2 forming bromoethane and the desired product.

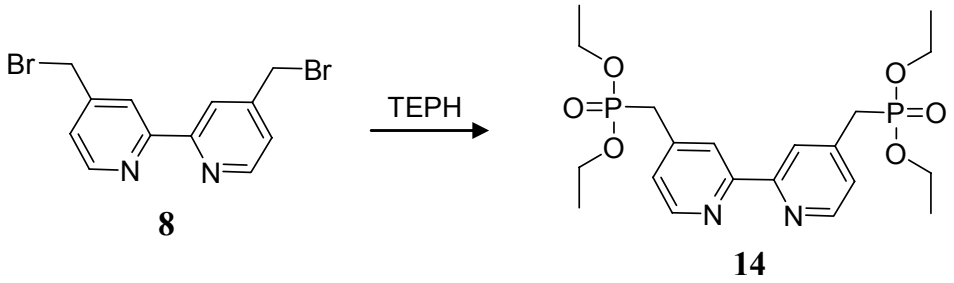

8 **14**

Scheme 7-5. Synthesis of 4,4'-bis(diethylmethylphosphonate)-2,2'-bipyridine.

4,4-bis(bromomethyl)-2,2'-bipyridine **8** (2.294 g, 0.87 mmol) was transferred to a round bottom flask and triethylphosphite (TEPH, 3 mL, 17 mmol) was added. The reaction mixture was stirred and refluxed for five hours. The mixture was then cooled to room temperature and the excess triethylphosphite was removed by vacuum distillation. The crude product was purified by flash chromatography on silica gel with EtOAc:CH_3OH to yield 0.0736 g (0.16 mmol) 4,4-(diethylphosphonate)-2,2'-bipyridine **14** in 18% yield. ^{1}H NMR (CD_3OD) δ = 1.29 (12H, t), 3.23 (4H, d), 4.16 (8H, q), 7.34 (2H, m), 8.41 (2H, m), 8.68 (2H, d).

7.3 PHOSPHONATED BORONIC ACID DERIVATIZING REAGENT

In Chapter 6, a study that uses a derivatization technique that exploits the reaction between boronic acids and cis diols was described. The phosphonate group was added to oligosaccharides via the reaction between a novel phosphonated boronic acid chemical derivatization reagent and a diol functionality on the reducing end monosaccharide. The synthesis of the phosphonated boronic acid is presented in this section.

7.3.1 1-(N-(ortho-diethylmethylphosphonate))aminoethylbenzene

1-(N-(ortho-diethylmethylphosphonate))aminoethylbenzene **18** was synthesized from 2-formylphenylboronic acid **15** and diethyl(aminomethyl)phosphonate oxalate **16** based on a literature procedure[9] and this is presented in Scheme 7-6. The boronic acid product was obtained by condensation of the aldehyde of the boronic acid with the amino phosphonate. This gave the imine which was subsequently reduced to the amine using sodium borohydride without the need for protection of the boronic acid.

2-formylphenylboronic acid **15** (0.589 g, 3.9 mmol) was dissolved in anhydrous CH_3OH under argon protection. N,N-diisopropylethylamine (Hunig's base, 2.74 mL, 16 mmol) was added followed by diethyl(aminomethyl)phosphonate oxalate **16** (1.011 g, 3.9

mmol) and the solution was stirred for 16 hours before $NaBH_4$ (0.11 g, 3.9 mmol) was added slowly. The solution was stirred at room temperature for 1 hour, followed by addition of another batch of $NaBH_4$. One hour later, the solvent was removed by rotary evaporation and the residue was diluted with CH_2Cl_2. The precipitate was removed with vacuum filtration, with the filtrate subsequently concentrated. An aliquot of the residue (0.30 g) was purified by flash chromatography on neutral alumina (2-5% NH_3-saturated CH_3OH in CH_2Cl_2) and dried to yield 0.1632 g 1-(N-(ortho-diethylmethylphosphonate))aminoethylbenzene **18**. ^1H NMR (400 MHz, CD_3OD) δ 1.39 (t, J=7.04, 6H, CH3) δ 3.23 (d, J=11.6, 2H CH's) δ 4.17 (s, 2H CH's) δ 4.20-4.26 (m, 4H CH's) δ 7.15-7.43 (m, 4H CH's). ^{13}C NMR(CD_3OD): = 16.8, 42.2, 43.4, 56.2, 64.4, 124.1, 127.9, 128.7, 131.4, 142.9. HRMS: calcd. $(M + Na)^+$ 324.1148, found 324.1135.

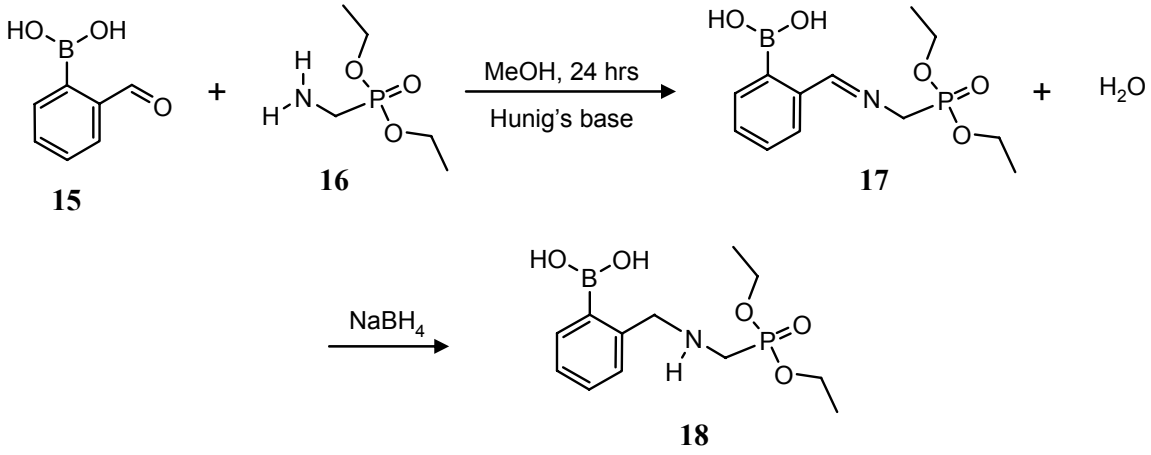

Scheme 7-6. Synthesis of 1-(N-(ortho-diethylmethylphosphonate))aminoethylbenzene IR-Active Boronic Acid (IRABA)

7.4 REFERENCES

1. Carlson, B.; Phelan, G. D.; Kim, J. H.; Jen, A. K. Y.; Dalton, L. R. *Abstracts of Papers - American Chemical Society* **2004**, *227*, U1314-U1314.

2. Maerker, G. C. *J. Am. Chem. Soc.* **1958**, *80*, 2745-2748.

3. Smith, A. P.; Lamba, J. J. S.; Fraser, C. L. *Org. Synth.* **2002**, *78*, 82-90.

4. Denes, V.; Chira, R. *J. Prakt. Chem.* **1978**, *320*, 172-175.

5. Montalti, M.; Wadhwa, S.; Kim, W. Y.; Kipp, R. A.; Schmehl, R. H. *Inorg. Chem.* **2000**, *39*, 76-84.

6. Penicaud, V.; Odobel, F.; Bujoli, B. *Tetrahedron Lett.* **1998**, *39*, 3689-3692.

7. Peng, Z. H.; Gharavi, A. R.; Yu, L. P. *J. Am. Chem. Soc.* **1997**, *119*, 4622-4632.

8. Will, G.; Boschloo, G.; Rao, S. N.; Fitzmaurice, D. *J. Phys. Chem. B* **1999**, *103*, 8067-8079.

9. Zhu, L.; Anslyn, E. V. *J. Am. Chem. Soc.* **2004**, *126*, 3676-3677.

Chapter 8: Conclusions

The characterization of glycosides and oligosaccharides is a challenging task since they are much more structurally complex than other biologically important molecules such as proteins and nucleic acids. In the work presented in this dissertation, several novel methods for the analysis of glycosides and glycans in a quadrupole ion trap (QIT) mass spectrometer have been presented. The methods involve activation using two different techniques known as collisionally activated dissociation (CAD) and infrared multiphoton dissociation (IRMPD). Unique chemical methods such as metal complexation in conjunction with the use of specifically tailored neutral auxiliary ligands and derivatization reagents were studied using CAD and IRMPD to increase the understanding of how more structural information may be obtained using QIT mass spectrometry.

In Chapter 3, the structures of flavonoid diglycoside isomers were elucidated using CAD, primarily for characterization of the carbohydrate portion of the molecules. The CAD spectra of the protonated and deprotonated spectra were compared for their utility in isomer differentiation. Due to the unsatisfactory results, a metal complexation strategy that also uses a neutral auxiliary ligand was introduced. By addition of a metal salt and a suitable neutral auxiliary ligand to flavonoids in solution complexes of the type $[M(II)\ (flavonoid\text{-}H)\ ligand]^+$ were formed which, upon CAD, resulted in more distinctive fragmentation patterns. Since most of the fragments observed involved cleavages within the flavonoid molecules and not simple losses of the auxiliary ligands, it was concluded that the binding affinities of the flavonoid and auxiliary ligands to the metal are similar. Pyridyl ligands that incorporate different electron-releasing substituents such as 4,4'-dimethyl-2,2'-bipyridine and 4,7-diphenyl-1,10-phenanthroline

were compared and the CAD spectra often varied depending on the ligand used. Based on these results, it was concluded that the fragment ions observed may be tuned by using ligands with different electron-releasing substituents thereby altering the metal binding affinity of the ligand.

The types of ligands used in the metal complexation strategy were further expanded in Chapter 4. In this work, the metal binding affinities of the auxiliary ligands and therefore the resulting CAD spectra were modified by incorporation of electron-withdrawing substituents into the ligands instead of electron-releasing substituents. Because of the limited commercial availability of pyridyl ligands with electron-withdrawing substituents, it was not possible to purchase a set of ligands with electron-withdrawing substituents that would enable a logical systematic study (e.g., only differed in the number and type of substituents present on the ligands). Therefore, a set was synthesized with bromine atoms as the electron-withdrawing substituents. The CAD spectra of a series of flavonoid diglycosides using the metal complexation strategy with five different brominated pyridyl ligands were compared. The fragmentation pathways observed in these spectra were even more varied than the series of spectra collected using electron-releasing substituents (Chapter 3). A direct correlation was made between the types of fragments observed and the metal binding affinity of the ligands in solution. It was concluded that the variations in the metal/ligand binding energies influence the energetics of dissociation pathways and also affect the preferred metal coordination sites in the flavonoid complexes. It was further determined that the ligand also has an impact on the way the disaccharide moiety of the flavonoid interacts with the metal since the addition of bromo substituents changes the steric environment of the auxiliary ligands, which may influence the conformations of the complexes and thus the degree of interaction of the disaccharide group with the metal center.

In Chapter 5, the flavonoid metal complexation strategy was used as a means of incorporating an IR-active group, a phosphonate moiety, into the flavonoid metal complexes as a substituent on the auxiliary ligand. This study was not only an approach to increase the efficiency of IRMPD in the QIT for the analysis of flavonoids, but also as a general method to incorporate the IR-active phosphonate moiety into an analyte complex without necessitating covalent modification. Two phosphonated pyridyl ligands were synthesized, one in which the phosphonate moiety is attached directly to the aromatic rings and one in which the phosphonate groups are removed from the aromatic rings by one methylene group. As compared with the IRMPD spectra of the flavonoid complexes without phosphonated substituents on the auxiliary ligands, it was concluded that the dissociation efficiency of the flavonoids complexes containing the phosphonated auxiliary ligands was greatly increased. It was additionally determined, based on the irradiation times used and the degree of fragmentation observed, that the phosphonate groups removed from the aromatic ring by one methylene group underwent dissociation more efficiently than when the phosphonate groups were attached directly to the aromatic ring, indicating more efficient IR absorption for the former. This finding was further supported by Fourier transform infrared absorption attenuated total reflectance (FTIR-ATR) that indicated that the high IRMPD efficiencies stem from the very large IR absorptivities of the IR-active ligands.

In the study presented in Chapter 6, the IR-active phosphonate moiety was incorporated into a boronic acid resulting in a novel IR-active boronic acid (IRABA) derivatizing reagent that was used for the structural analysis of oligosaccharides using IRMPD. The IRABA reacted readily with oligosaccharides and this resulted in a simplified method for determining the sequence and branching of oligosaccharides. The IRABA reagent was designed to both enhance the efficiency of the derivatization reaction

and to facilitate the photon absorption process. Based on the IRMPD spectra, it was revealed that oligosaccharide fragments are formed from primarily one type of diagnostic cleavage, thus making sequencing straightforward. It was further concluded that the presence of sequential fragment ions, a phenomenon of IRMPD, permit the comprehensive sequencing of the oligosaccharides studied in a single stage of activation.

In summary, four different methods for altering the energetics of activation and the types of fragments observed were presented. It was shown that a metal complexation strategy including neutral auxiliary ligands alters the types of fragments observed for flavonoid isomers upon dissociation. It was also illustrated that the substituents residing on the ligands alter the metal binding affinity and as a result the types and abundances of fragment ions observed. The benefits of IRMPD in a QIT were also shown in two studies. For example, it was shown how incorporation of IR-active phosphonate groups into ligands results in increased photon absorption efficiencies by the complexes. This strategy was extended to a derivatization reagent that was used for the analysis of oligosaccharides using IRMPD in a QIT.

This dissertation provides a framework for several future avenues of research that build on the results presented herein or expand into new areas. For example, the research that involves the metal complexation of flavonoid diglycosides has opened up a new means for identification of carbohydrate moieties that is valuable particularly when there is limited sample available and this method may be applied to other classes of glycosides. By using this metal complexation strategy with IR-active ligands, a method of making analytes more susceptible to IRMPD without covalent modification was introduced that may be applied to different classes of compounds. The derivatization technique that was developed for the analysis of oligosaccharides has exciting implications for more complete sequencing of larger oligosaccharides since the information is obtained in one

stage of activation and is not reliant upon a substantial ion population surviving several stages of collisional activation. This technique may be used for the sequence characterization of N-linked glycans in a quadrupole ion trap with minimal sample consumption. Each of the studies has resulted in a novel method that will substantially increase the structural information obtained in future studies using quadrupole ion trap mass spectrometry.

Vita

Michael Pikulski was born on June 29, 1969 in Silver Spring, Maryland. He received his B.S. in Chemistry from The University of Texas at San Antonio. He worked in industry at DPT Laboratories and Advanced Bio Surfaces, both in San Antonio, Texas. He then received his M.S. in Chemistry from The University of Texas at San Antonio with his thesis topic in electrochemistry.

Permanent address: 114 E. 31st St. #307, Austin, TX 78705

This dissertation was typed by the author.